ISBN 978-82-471-3082-7 (printed ver.)
ISBN 978-82-471-3083-4 (electronic ver.)
ISSN 1503-8181

Doctoral Thesis
Matthew Carl Homola

Doctoral theses at NTNU, 2011:259

Matthew Carl Homola

Atmospheric icing on wind turbines

Modeling and consequences for energy production

NTNU
Norwegian University of
Science and Technology

Doctoral theses at NTNU, 2011:259
NTNU

NTNU
Norwegian University of
Science and Technology
Thesis for the degree of
philosophiae doctor
Faculty of Information Technology, Mathematics, and
Electrical Engineering
Department of Engineering Cybernetics

NTNU
Norwegian University of
Science and Technology

Matthew Carl Homola

Atmospheric icing on wind turbines

Modeling and consequences for energy production

Thesis for the degree of philosophiae doctor

Trondheim, September 2011

Norwegian University of
Science and Technology
Faculty of Information Technology, Mathematics, and Electrical Engineering
Department of Engineering Cybernetics

NTNU
Norwegian University of Science and Technology

Thesis for the degree of philosophiae doctor

Faculty of Information Technology, Mathematics, and Electrical Engineering
Department of Engineering Cybernetics

ISBN 978-82-471-3082-7 (printed ver.)
ISBN 978-82-471-3083-4 (electronic ver.)
ISSN 1503-8181
ITK report 2011-8-W
Doctoral Theses at NTNU, 2011:259

Printed by Tapir Uttrykk

Atmospheric icing on wind turbines:

modeling and consequences for energy production

Matthew Carl Homola

A Dissertation Submitted in Partial Fulfillment of
the Requirements for the

Philosophiae Doctor Degree (PhD)

Department of Engineering Cybernetics
Norwegian University of Science and Technology

2011

Abstract

The work presented in this thesis presents new knowledge about the effects of atmospheric icing on wind turbines. The main contributions of this thesis are in the following areas:

- Monitoring and description of the effect of ice accretions on the power production of the wind turbines at Nygårdsfjell wind park. Information on icing was collected with icing sensors and webcameras, and thereafter the effects were analyzed. Power production data were analyzed for power losses and compared with two other wind parks which experience icing.

- Analyses by numerical modeling to determine the effect on ice accretion resulting from changes in turbine size, droplet size, location along blade, and ambient temperature. The numerical modeling was performed using two different ice accretion solvers; a panel method based solver, TURBICE, and a CFD based solver, FENSAP-ICE. The calculated ice shapes were found to be relatively smaller for larger wind turbines, which for similar shapes reduces their aerodynamic significance. On the other hand the results indicated that ice accretion on larger turbines occurs with a higher temperature difference relative to ambient than for smaller turbines and in some conditions ice shapes were found to be dissimilar for different sized turbines. The different shapes could then have a greater aerodynamic penalty than would have been formed for a smaller turbine.

- Analyses by numerical modeling to determine the effect on aerodynamics of the ice shapes resulting from the above examinations. The CFD solver FLUENT was used to determine the lift and drag coefficients of iced and uniced airfoils. These were then converted to a torque coefficient and for dry rime icing the results indicated that smaller turbines had a larger performance penalty due to ice shapes. Horn shaped glaze ice shapes resulting from warmer conditions were found to give greater performance penalties than the more streamlined rime shapes.

- Calculation of power production losses due to ice accretions on a wind turbine. The BEM method was used together with calculated lift and drag data for an iced blade to calculate performance losses due to icing on a rotor. Allowing the turbine to operate at its design tip speed ratio also when iced, reduced the power loss due to the icing from 27% to 24% for operation in region 2.

The likelihood of the modeled results was confirmed through comparison to measured performance of actual wind turbines during icing events.

The results of this thesis have been presented at international conferences, or published in international journals.

Preface and acknowledgements

This thesis is submitted in partial fulfillment of the requirements for the Philosophiae Doctor Degree (PhD) at the Norwegian University of Science and Technology (NTNU). The reported work is a result of my doctoral studies from September 2006 to September 2010 at Narvik University College. The research has been financially supported by the Norwegian Ministry of Education and Research, and by Nordkraft AS.

I am grateful for the support of my advisor Professor Per Johan Nicklasson for helping to initiate this work and for advice and support underway. Without his encouragement to consider a doctoral degree after finishing my M.Sc. I would not have been able to enjoy the results of increased insight resulting from rigorous study of a problem. I am also grateful for the assistance of my other two advisors Professor Per Arne Sundsbø and Associate Professor Amund Skavhaug who have given both motivation and encouragement along the way.

Thank you to all of my co-authors, especially Dr. Muhammad S. Virk at Narvik University College. Working with him gave an extra motivation near the end of my studies. A special "Kiitos" to VTT, for the opportunity to have a research period at the facility in Helsinki, and to Tomas Wallenius and Dr. Lasse Makkonen who made my research period at the VTT facility in Helsinki quite fruitful and who have also provided good and interesting discussions.

Many others have assisted in various ways to the completion of this work and naming them all would not be possible. Nevertheless I mention some. My colleagues at Narvik University College have helped in many ways. Thank you to Dr. Guy Mauseth, Dr. Kevin Chow, and Dr. Klas Pettersson for interesting on- and off-topic discussions. Thank you to Dr. Tore Wiik for helping arrange the funding for this work. Thank you to Nordkraft AS for allowing access to Nygårdsfjell wind park and its data as well as for supporting the work financially.

Thank you to my family both here in Narvik and in Brush Prairie. Without their support underway it would have been difficult to maintain progress. The largest thank you is reserved for my wife Birgit who brought me to Norway and has been patient with the long days involved in the doctoral work.

Narvik, March 22, 2011
Matthew Carl Homola

Happy is the man that findeth wisdom, and the man that getteth understanding. For the merchandise of it is better than the merchandise of silver, and the gain thereof than fine gold.
Proverbs 3:13-14 (KJV)

Contents

List of Figures

Nomenclature

This lists the most commonly used abbreviations and symbols in this thesis, but is not exhaustive and omits some symbols which are unique to specific chapters.

Symbols

α	[deg]	angle of attack, the angle between the relative velocity of the airflow and the centerline of the airfoil.
β	[deg]	air inflow angle
γ	[K/km]	lapse rate
Γ	[K/km]	dry adiabatic lapse rate, 9.8 [K/km]
λ		tip speed ratio
λ_r		local speed ratio
ρ	[kg/m^3]	density
a		axial induction factor
a'		tangential induction factor
A	[m^3]	cross sectional area
c	[m]	chord length
C_d		drag coefficient
C_l		lift coefficient
C_p	[J/(kg K)]	specific heat capacity at constant pressure
C_y		torque coefficient
F_y	[N]	in-plane force
H	[m]	height
p	[Pa]	air pressure
r	[m]	radius along the blade
R	[m]	radius of the blade
T	[°C]	temperature
U	[m/s]	air velocity
v	[m/s]	relative velocity
w	[g/m^3]	liquid water content
z	[m]	elevation change

Abbreviations

AOA	Angle of attack
BEM	Blade element momentum
CFD	Computational fluid dynamics
LWC	Liquid water content
mas	meters above sealevel
MVD	Median volume diameter
RH	Relative humidity

Chapter 1

Introduction

The organization of this chapter is to first describe the background for the work at Narvik University College, then briefly describe why wind power is an important subject, review the previous work on the icing problem for wind turbines, describe the contributions of this thesis, list the resulting publications, and finally give an outline for the remainder of the thesis.

1.1 Background

Previous work at Narvik University College had been done in modeling of drifting snow and icing of ships, as well as with sensors. This gave a good background for studying atmospheric icing and its effects on wind turbines. In addition, Nordkraft AS, through its subsidiary Nordkraft Vind AS, was in the process of erecting three wind turbines near Narvik, in an area where they would be subject to icing each winter. They were interested in having more information about icing and its effects on wind turbines and generously supported this research. One of the turbines in the park was made available for research purposes and all operational data on the turbines was also made available. At the start of this work there was little interest from turbine manufacturers in the issue of icing so it was fortunate to have the support of Nordkraft AS. It should be noted that contact was initially established with Narvik Energi AS, which later (2009) changed its name to Nordkraft AS. Nordkraft AS is used throughout this work for consistency.

As in all such work there were limitations on what could be attempted. Limitations on funding and available time meant that not all possible sensor types or options, nor unlimited variations in icing parameters could be explored. Some of these limitations and the choices resulting from them are described further in the relevant chapters. Mechanical loads, and ice shedding were found to be outside the scope of this work and so are only described in the review section.

1.2 Wind power

In recent years the interest in renewable energy production has grown as the disadvantages associated with the burning of fossil fuels have become better known.

The power of the wind has been harnessed by mankind for millenia. Nonetheless it is only recently that wind power has become more mainstream, being mainly used now to generate electricity, with the main value attributed to the wind generation being the value of the saved fuel costs [2]. Wind power is an excellent source of renewable energy in areas with sufficient wind resources since wind power has relatively few and well known negative consequences. As such wind power has experienced tremendous growth on-shore in recent years, and off-shore it is expected that similar growth will take place. This growth has caused wind power plants to be installed in areas which are periodically subject to atmospheric icing and this icing has been found to have negative consequences for the wind power plants.

1.3 Review of previous work related to the icing problem

Icing has been a problem related to wind power since the first sailor who encountered sea spray icing recognized the danger of iced rigging. In modern times icing is also a problem for wind power, though largely in a different manner.

To understand the difficulties for wind power it is most helpful to look at the experiences from aircraft icing as well as power line and communication mast icing.

Unfortunately for wind power, the properties of both of the previous two groups with icing related issues are combined. Wind turbine blades have similar relative velocities and ice collection to aircraft, which are higher than for stationary objects. In addition, wind turbines are physically bound to their location, once erected, and can not choose to maneuver around an icing storm or event, as an aircraft may. Wind turbines are also subject to the effects of orographic lifting, terrain lifting, of air parcels which causes a much higher liquid water content over hilltops than are experienced for surrounding areas.

Wind power plants are increasingly being planned and built in areas where they are periodically subject to atmospheric icing. Many Arctic and Alpine regions have good wind resources, but icing on wind turbines has been recognized as a hinderance to the development of wind power in these regions. This icing, while being a danger to people in the vicinity of the turbine [3] and increasing fatigue loads on the turbine [4], also tends to degrade the aerodynamic performance of the blades resulting in potentially large power losses [5, 6]. The amount of energy production lost due to icing is an area of large uncertainty and this uncertainty a potential wind power investor must be paid for through a higher expected rate of return. The result is reduced investment due to the uncertainty. A better method for estimating the effects of ice on power production of wind turbines is one of the specified objectives of the International Energy Agency (IEA) Annex XIX: Wind Energy in Cold Climates [7].

Atmospheric icing causes power losses for wind turbines, due to instrument or controller errors caused by icing, and due to ice accumulations disrupting the blade (airfoil) aerodynamics.

1.3.1 The consequences of icing on wind turbines

There are a range of effects on wind turbine operation resulting from ice accretions, and the discussion of this section is not meant to be exhaustive, but to present a

range of the results of icing and previous work. The following have been described in the literature, but other effects may also occur.

Complete stop due to icing

When icing is severe, it often results in the complete stop of the wind turbine. This can happen through several different ways. One is that the aerodynamics of the blade become so disrupted that the turbine is not rotated by the force of the wind. Another is that the imbalance causes the vibration alarm in the turbine to trip, thereby stopping the turbine. A third is that the difference between the expected rotor torque, based on the wind speed measurement, exceeds a preprogrammed level, causing an alarm and automatic stop.

An example illustrating how a wind turbine can be completely stopped by icing, with resulting loss of all possible production was described by Ronsten [5]. The performance of the Äppelbo wind turbine in Sweden was described, where the 900 kW NEG Micon wind turbine, was stopped by icing for over seven weeks in the winter of 2002-2003.

There has been at least one period each winter at Nygårdsfjell wind park where the turbines have been completely stopped by icing, though usually only for one or two days.

Disruption of aerodynamics

Disruption of aerodynamics can cause a reduction in power production. As shown by Jasinski et al. [6] and Dahlqvist [8] the onset of ice accretion causes an increase in surface roughness which leads to an increase in the drag coefficient and corresponding reduction in power production. Continued growth of rime ice causes a continuing increase in the drag coefficient and reduction in power production, as can be seen in Figure 1.1[1] from Seifert and Richert [9].

The effect of an icing event on an airfoil is generally an altered airfoil shape, resulting in reduction in lift coefficient (C_l) and increase in drag coefficient (C_d) [10]. The result of these changes for a wind turbine can be seen in that the in-plane (rotating) force,

$$F_y = (C_l \cos\beta - C_d \sin\beta)\,\frac{1}{2}\rho v^2 c(r)\,, \quad \text{[N]} \tag{1.1}$$

is reduced both from the decrease in C_l and the increase in C_d. The air density is ρ [kg/m^3], v [m/s] is the air velocity relative to a point on the rotating blade, β is the inflow angle of the relative air velocity and c [m] is the chord length at radius r. The changes in these forces are illustrated in Figure 1.2.

On the other hand, when the rotating force decreases, this causes a reduction in the axial induction factor which again results in the angle of attack increasing compared to the plain blade and thereby partly compensating for the lower C_l.

Potapczuk and Al-Khalil [11] has shown that the change in the drag coefficient is dependent on the ice accretion temperature.

[1] All reprinted figures in this thesis are reprinted with the permission of the copyright owners.

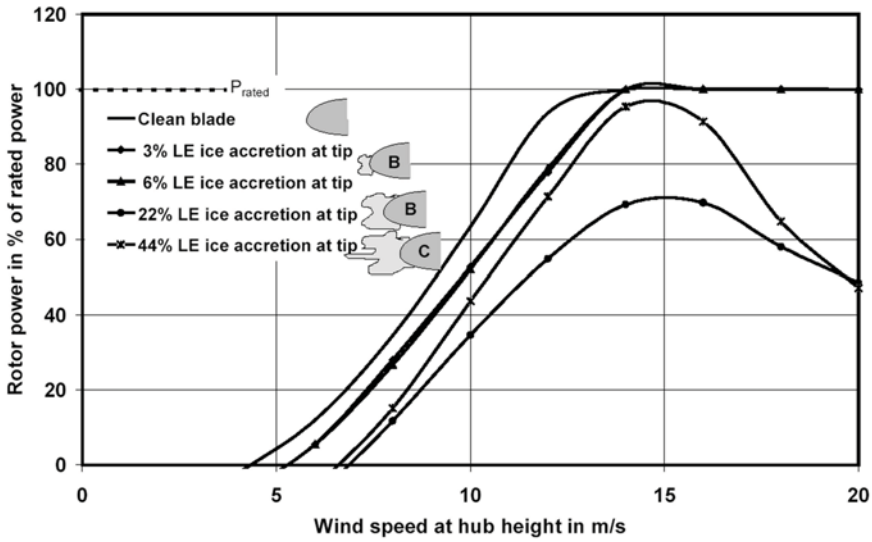

Figure 1.1: Calculated power curve for a pitch controlled fictitious turbine with different types of ice accretion [9].

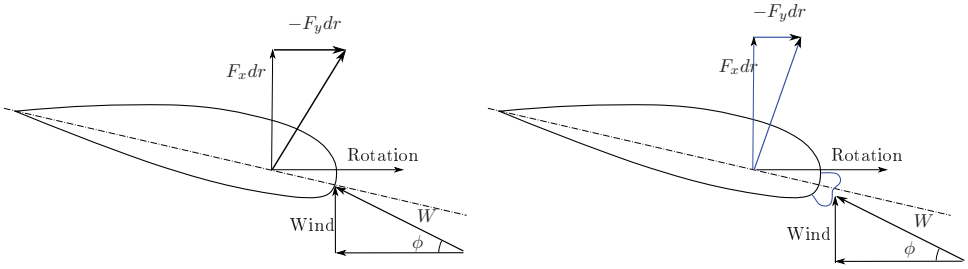

Figure 1.2: Airfoil without and with ice illustrating reduced torque when ice is present.

Reduction in power production due to icing was calculated to be up to 19% for a pitch controlled turbine with heavy rime by Kimura et al. [12]. Power losses of up to 50% with the wind turbine still operating have been observed at Nygårdsfjell wind park during an icing event.

Some work has been done to estimate wind turbine power losses due to icing [6, 13, 14, 12, 15], but recent results may have shown less performance reduction than earlier studies would have indicated [16]. Unfortunately the above studies are of turbines with differing design strategies and sizes and are therefore difficult to compare directly with each other. One possible cause may be the dependence of icing on the geometry of the object accreting ice.

Overloading due to delayed stall

Overloading due to delayed stall has primarily been discussed as a problem for stall regulated turbines Jasinski et al. [6]. But, thrust overloading can occur on pitch controlled turbines as well. This can occur when the added drag of the ice prevents the turbine from reaching rated power. In this case, the turbine operates at a higher angle of attack than normal, and if stall does not occur, the combination of torque and drag can perhaps overload some portion of the wind turbine.

Increased fatigue due to imbalance

Differences between the ice accretions on the blades of a wind turbine cause imbalance in the rotor. This imbalance can be both mass and aerodynamic imbalances.

Operation of a wind turbine with an imbalance causes an increase in the loads imposed on many of the components of the turbine. Though the extreme loads are already covered when design for the loss of a blade is calculated, the fatigue loads will cause a shortening of the lifetime for the components [4]. Figure 1.3 shows how the bending loads of the tower increase dramatically when there is a mass imbalance of the rotor, such as can occur with ice. Unbalanced aerodynamics of the wind turbine rotor can also occur with combinations of ice accretion and shedding. This aerodynamic imbalance causes the same type of operational imbalance as a mass imbalance.

Ice shedding

The pieces of ice shed from wind turbines can be quite large, and are definitely not insignificant, as can be seen in Figure 1.4. Though no reports of personal harm due to ice shedding from wind turbines have been found, the number of wind parks and turbines are increasing and it can be assumed that something will occur eventually if preventive measures are not implemented. Though the risks are greatest for service personnel who must approach the wind turbine, others can be at risk when the wind turbine is located near a road or recreation area.

The possible distances for thrown ice have been roughly estimated by Tammelin et al. [17] as follows:

$$d = 1.5\,(D + H) \tag{1.2}$$

Where d [m] is the possible distance ice can be thrown, D [m] is the diameter of the rotor and H [m] is the height of the nacelle. This equation can only be considered a rough estimate, but gives a general idea of the area which is at risk for ice throw.

Instrument icing

Icing of instruments can also be a problem for wind turbines. Probably the worst consequence of iced instruments would be that the controller would not shut down the turbine during extreme winds if the wind sensor was iced, potentially leading to catastrophic failure.

The effects of icing on anemometers has been studied [18] and it has also been shown in an icing wind tunnel that as ice builds up on an unheated anemometer,

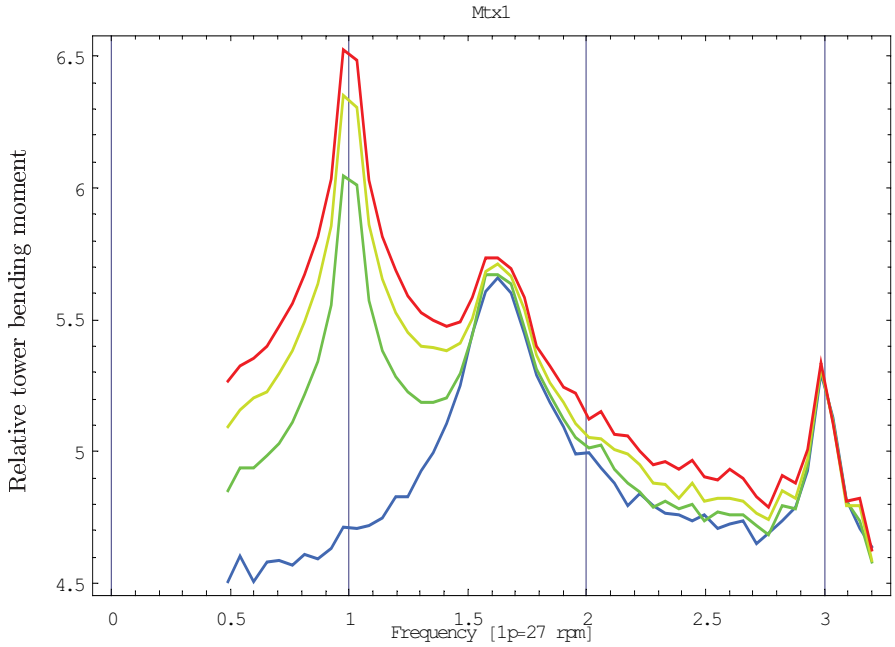

Figure 1.3: FFT of tower bottom showing increase in load, for different simulated mass imbalances. Blue is 0 kg imbalance, green is 25 kg, yellow is 50 kg and red is 75 kg imbalance [4].

the reported wind speed becomes lower and lower [19]. This is a result of the accreted ice increasing the drag of the cups and slowing their rotation. Such a slowed rotation condition can persist long after the icing event has passed for an unheated anemometer.

Figure 1.4: Piece of ice shed from a turbine at Nygårdsfjell wind park.

1.3.2 Previously reported experiences with icing on wind turbines

Experiences with wind turbines in icing conditions have not been as well reported as could be wished for, in regards to sharing experiences, but some experiences have been described in the literature.

Operational experience for a 150 kW stall regulated turbine installed near Whitehorse, Yukon in Canada, including detailed production data for seven years was described by Maissan [20]. This turbine was installed with leading edge heaters with a power of 1/4 watt per square inch. It initially had 6 inch wide heaters at the leading edge, but these were replaced with 12 inch wide heaters after three years to improve performance in very severe icing and very cold temperatures. Without heaters the icing builds up especially on the leading edge with thickness increasing towards the blade tips. Power production drops off dramatically when the blades are coated with rime ice, and without the leading edge heaters production can stop completely. During the third winter, when one of the blade heaters failed and operation continued without blade heaters, annual icing losses were estimated to about 20% of the production target. Maintaining electrical contact to the blade heaters on the tip brake sections of the blade was a problem during icing events. After three years operation the blades were coated with a black coating called StaClean which in addition to improved solar absorption, is also supposed to have a low ice adhesion. This coating seems to have improved performance in the following winters. In spite of the challenges from icing, the experiences with the turbine were good enough that a second turbine, a 600 kW pitch regulated machine was installed.

From the photographs in Maissan [20] it could also be seen a typical stepped

shape of the leading edge ice, where ice is accreting most rapidly at the tips, but is also breaking loose from the tips when a certain thickness is reached. This causes the thickest leading edge ice to form at some point near the middle of the blade span, where the ice has not broken off, while closer to the tips the ice has broken off and re-accreted several times. Similar patterns have been observed at Nygårdsfjell, as can be seen in Figure 1.5.

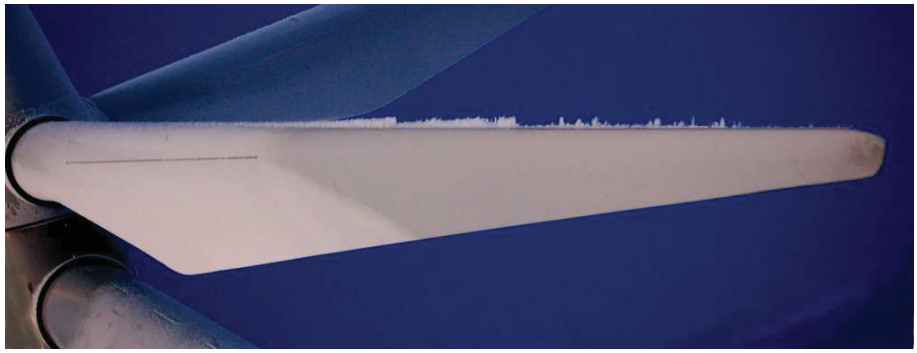

Figure 1.5: Blade icing at Nygårdsfjell showing stepped shape towards the tip.

Some experiences with icing were also reported by Westerlund [21]. This was also a test of some ice sensors and measurement of risk from ice casting from a 600 kW Vestas V44, a pitch controlled turbine type, near Härnösand in northern Sweden for parts of two winters. Included in the report was a detailed description of six significant icing events. Interestingly it was reported that almost no power losses could be detected for light icing periods, though it has been shown that the performance of an airfoil is significantly reduced with the introduction of surface roughness. On the other hand it was found power losses of up to 50% for moderate icing and they experienced no cases of severe icing. Reflective IceMarkers were installed along the blades and photographed with a flash to document ice thickness. These were visible until an ice thickness of approximately 0.5 mm, at which point the reflections were no longer visible. This photography method did not work during rain, snow or fog due to the flash being reflected by the particles or droplets in the air. This particulary occurred at the times when documentation was especially desired. A strategy to minimize the danger due to ice casting was night operation after periods of icing. This increased the chance that the ice accumulations would come off the blades during periods of time when skiers and others were less likely to be in the area. Operation of the turbine was seen to remove ice in three ways. First operation in milder air melted or loosened the ice. Second flexing of the blades due to wind gusts cracked loose ice on the outer portions of the blade. Third when the relative humidity was low ($<$80%) the induced wind over the ice surface resulting from operation eroded the ice (sublimation).

Icing events during one winter at Murdochville, in Canada were monitored and analysed for relevance for the nearby wind park [22]. Of the 18 events identified, eight of them were estimated to be of significance for wind turbines. No comparison with power production of the wind park was done in the paper.

1.3.3 Monitoring of icing

The best position for detection of icing on a wind turbine is on the wing itself, and as close to the tip as possible, for two reasons. The first reason is based on the physical process of icing as described in Chapter 2. The rate of ice accretion is directly related to the relative velocity of the supercooled water droplets, and it is at the wing tip that the highest velocity occurs. This means that monitoring ice accretion on a stationary object during site planning can underestimate the icing that an operating wind turbine will experience. The second reason is that the blade tips can experience icing due to low clouds even thought the nacelle is ice-free. Figure 1.6 shows a wind turbine operating with the nacelle just below the cloud base, but the blades sweeping up into the cloud. At Pori, in Finland, measurements showed the number of in-cloud icing periods at 84 m was six times the number of in-cloud icing periods at 62 m [23]. So icing should also be measured as close to the planned wind turbine locations as possible, and on as high of a mast as is possible, to best capture the conditions the wind turbines will be operating in.

Figure 1.6: Turbine in partial fog, illustrating that the blade tips can extend into a cloud while the nacelle is below the cloud base.

Monitoring of icing at a wind power site can take several forms. One method is to use wind speed measurements from an ice free anemometer together with the wind turbines power curve to generate an estimate for expected power production, which actual power production can then be compared with.

Installation of an ice detector in connection with other site measurements is recommended by Baring-Gould et al. [24], at any site where icing is expected to occur. This in spite of the admission that only few, if any, of the ice detectors are

well proven. The primary objective of an ice detector is to record the occurrence and intensity of icing events. Additionally, ice duration, density and accumulated mass may be important characteristics. A review of icing sensors for wind turbines was performed by Homola et al. [25], with no ideal sensors being identified there. Part of the reason for this is that there are a several reasons for using an ice detector. Ice occurrence, ice intensity and ice duration may well require three different sensors in order to adequately record all three.

To asses potential ice induced downtime, measurements of icing occurrence and intensity are recommended by Baring-Gould et al. [24], including monitoring the duration of ice on surfaces to estimate the potential economic impact if no anti- or de-icing technology is employed. It is necessary to have both knowledge of icing intensity and duration, as well as the wind resource during the icing duration to calculate potential energy losses.

The results of replies to a questionnaire regarding the type of icing and its duration was analyzed by Durstewich [26]. Nearly 100 replies during the two year period were analyzed and it was found that most of the icing events had a duration of three days or less, and only one event, of 20 day duration, that lasted longer than 10 days. No question was asked regarding power losses caused by the icing, but the majority of the responses that included wind speed showed a wind speed between 4 and 10 m/s. This speed is in the linear region of wind turbine operation where any increased blade roughness will reduce the power production.

Detection of icing has also been reviewed by Fikke et al. [27] and Parent and Ilinca [28], with the first providing descriptions of eight different sensors and their methods of operation. The latter described detection of icing

1.3.4 Icing modeling

Modeling of atmospheric icing on airfoils was first needed for aircraft but much of the work has relevance also for icing on wind turbine airfoils.

One of the codes which has been extensively verified for aircraft is LEWICE, a code developed by NASA [29]. The 2D version of the code used the inviscid panel method for flow field calculation, calculated particle trajectories based on the flow field and then computed ice accretion by computing a control volume energy balance. In order to include more accurate velocity effects near the airfoil surface and to include effects of compressibility, the inviscid panel method was replaced by an Euler/Navier-Stokes code. Calculation of ice accretion and airfoil performance degradation was performed using this LEWICE/NS code and compared with wind tunnel tests [11]. This work did not result in as good agreement for the ice shapes as previous work by Shin et al. [30], particularly for the glaze ice region. This work did show that the highest drag shapes were the horn shapes resulting from a "warmer" heat balance.

Another code which has been used mainly for wind turbines is the TURBICE code presented by Finstad and Makkonen [31]. The TURBICE model results have been verified through comparison with both icing wind tunnel experiments of aircraft wing sections and natural wind turbine icing, with good results for both rime and glaze conditions, [32], and TURBICE is used for part of the work in this thesis.

Power production losses resulting from icing were estimated by Kimura et al. [12]. The method used was determination of reduction of airfoil performance by 2D wind tunnel tests using mock icing shapes on an airfoil. The results of the performance tests were used together with existing meteorological data to estimate ice duration and energy production losses. They proposed a simple correction procedure for C_l and C_d curves based on whether the icing was glaze or rime type. Glaze ice was assumed to give no or only slight changes in C_l and C_d, while rime ice was assumed to reduce the maximum lift and stall angle, increase the drag and change stall characteristics. The estimated C_l and C_d curves are shown in Figure 1.7. None of the ice shapes analyzed were horn shapes. Ice type, intensity and duration were all estimated using meteorological data for wind velocity, temperature, visibility and solar radiation.

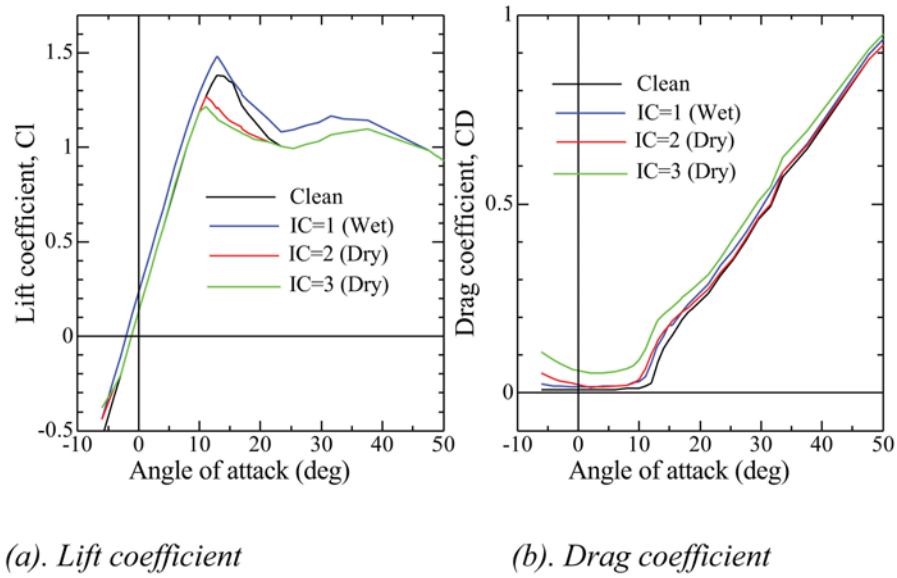

Figure 1.7: Estimated C_l and C_d curves for plain and iced cases [12].

Both wind tunnel tests and computer simulations were performed on an airfoil to determine performance changes resulting from icing by Jasinski et al. [6]. The airfoil changes were then used to estimate the effects of rime ice on the power production of a 14 m radius 450 kW turbine operated in both stall regulated and pitch regulated modes. The work showed that following a rime icing event, the lowest drag angle of attack became the angle at which the ice was accreted, due to the extended leading edge caused by the ice. The icing shapes were calculated for the 75% station along the blade, with the acknowledgement that ice accretion would be higher at the tip, but lower towards the root. Therefor the two effects were expected to tend to offset each other. The performance analysis for the pitch regulated turbine showed about 14% power loss for a smaller ice shape and 20% for a larger ice shape below rated power. Above rated power there was no power loss.

For the stall regulated turbine the results were quite different, with the smaller ice shape showing power losses of 15-20% over the entire operating range, but the larger ice shape resulting in a peak power production 16% higher than rated due to delayed stall.

1.3.5 Icing mitigation

Mitigation of the effects of icing is usually considered to have two strategies, either anti-icing, which means preventing ice from forming on the protected surface, or de-icing, which means removing the ice layer from the surface after formation.

A number of methods have been proposed and tested for prevention and removal of ice on wind turbine blades. Several of these approaches are detailed individually below.

Direct heating of the surface, either through the use of microwaves, or with electrical resistance heating is a relatively straight forward method. The JE-System of direct resistance heating has been shown to work effectively, but Kemijoki OY has stopped development of this system. LM Glasfiber has tested both microwave based systems and electrical resistance heating systems [33]. Their results showed positive results for the microwave system when surface absorbers were applied, but that further research was necessary. The resistance heating elements, or heating foil as it is called, functioned well, and was able to deice the blades both during operation, and in standstill conditions.

Painting the blades black has also been done to more effectively absorb solar radiation after a period of icing [20]. Indirect heating of the surface has been proposed and tested, where typically the inside of the blade is heated with warm air or a radiator and the heat is then transferred to the outer surface. Such a system was installed on an Enercon turbine in Switzerland [34], and though the experience with this system was limited, the initial results were promising, as can be seen in Figure 1.8 which shows power output being restored after a heating cycle.

Mechanical removal, as is done on the leading edges of aircraft wings appears to be a promising alternative [35], though further development is needed before a system for wind turbines is available. A system where the blades were flexible enough to crack loose the ice has also been proposed, as the flexing of the blades already is known to help shed ice. The disadvantage of trying to crack loose the ice is that thin layers of ice can adhere quite strongly to the blade, and are not necessarily brittle enough to crack loose from just vibration of the blade.

A surface treatment that prevented ice build up has been sought since it is known that without nucleation sites small water droplets can remain liquid at temperatures well below 0 °C. Even a coating that significantly reduced the adhesion strength should aid in spontaneous shedding of ice accretion. Several anti-icing coatings tested by Kimura et al. [36] appeared to have little effect, but later work with another coating has shown very promising results, with a 10-fold reduction of adhesion strength [37].

A system where the blade surface is protected by a layer of clean air was presented by Battisti [38]. This system uses an air flow from inside the blade, and rows of small holes near the leading and trailing edges to generate a layer of clean and, if necessary, heated air directly around the blade surface. This layer of air would

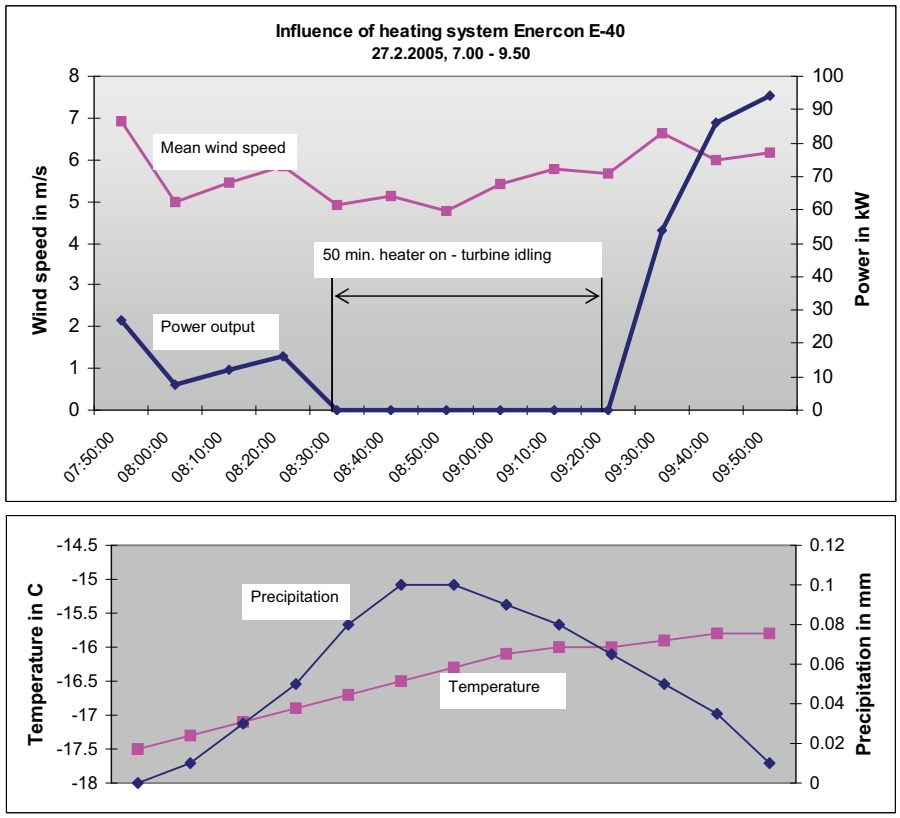

Figure 1.8: Restored power production after a heating cycle [34].

deflect the majority of water droplets in the air, and could melt the few droplets that managed to strike the surface.

1.4 Contributions of this thesis

The contributions of this work has been to extend the results and research regarding the effect of atmospheric icing on wind turbines, as follows:

- The effect of atmospheric icing on the power production of the turbines at Nygårdsfjell wind park was analyzed and compared with previously reported results. Improvements to icing monitoring were proposed and implemented and differences compared to previously reported experiences were discussed and explanations for the differences were suggested. It was found that icing related power losses at Nygårdsfjell were less than what earlier reported results from smaller turbines had found. One suggestion for this discrepancy was that differences in the size of the turbines could change the icing losses. The work

has been published in Homola et al. [16], Homola et al. [39], and Homola et al. [40] and is described in Chapter 3.

- The dependence of atmospheric icing on the wind turbine size, ambient temperature and droplet size was examined through numerical modeling. It was found that dry rime icing results in ice accretion that is relatively less both in terms of ice mass and ice thickness for larger turbines, confirming the proposed theory. Since the shapes were similar, this should also result in less aerodynamic disruption for larger turbines. It was found that larger turbines give a higher leading edge temperature during ice accretion which results in dissimilar ice shapes for different sized turbines when the heat balance of the ice accretion results in temperatures near the freezing point. Changes in ice accretion along the span of a large turbine blade were also investigated with the result that the ice accretion rate increases with distance from the hub, as previous work has shown. Some of this work is published in Wallenius et al. [41], Homola et al. [42], Homola et al. [43], Ronsten et al. [44], Homola et al. [45], and Homola et al. [46], while the remaining portions have been submitted for review. This work is described in Chapter 4.

- The effect of ice accretions on the aerodynamic characteristics of wind turbine blades was studied with the help of numerical modeling. It was confirmed that for dry rime icing, the relatively smaller ice shapes on larger turbines resulted in less degradation of the aerodynamic characteristics of those blade profiles. For the case of dissimilar ice shapes it was confirmed that the glaze ice, horn type shapes gave the greatest aerodynamic penalty. For the ice accretions calculated along the length of a large turbine blade, the resulting effect on the power production of the wind turbine was calculated and it was shown that changing the turbine controller could increase power production when there is ice on the blades. The calculated power losses resulting from the modeled icing event was then compared with measured power losses during icing events at Nygårdsfjell. Parts of the work in this area are published in Virk et al. [47], Homola et al. [48], and Homola et al. [49] while the remaining portions have been accepted for publication. This work is described in Chapter 5.

1.5 Publications resulting from this work

The following list contains the publications developed during the period of work presented in this thesis, including recently submitted manuscripts. For calculation of publication statistics the Norwegian Ministry of Education and Research awards publication points to universities and colleges based on the level of the publishing journal. In this system level 1 is a normal international peer-reviewed journal while level 2 is perceived as a higher level journal. Since the number of publication points affects the funding of the university or college, the journal level is considered an important indicator by some and therefore the level of each journal is included in the following list. Following the listing of each publication the main contributions of this author to each of the publications is briefly mentioned.

Journal publications

- Homola, M.C., T. Wallenius, L. Makkonen, P.J. Nicklasson and P.A. Sundsbø (2009) The relationship between chord length and rime icing on wind turbines. Wind Energy, http://dx.doi.org/10.1002/we.383, level 2.

  The contribution of this author was the idea for the work, portions of the modeling setup and execution, and data analysis.

- Virk, M.S., M.C. Homola and P.J. Nicklasson (2010) Effect of rime ice accretion on aerodynamic characteristics of wind turbine blade profiles. Wind Engineering, Vol. 34, No. 2, http://dx.doi.org/10.1260/0309-524X.34.2.207, level 1.

  The contribution of this author was some of the ideas for the work, calculation of torque coefficients, and analysis.

- Homola, M.C., M.S. Virk, T. Wallenius, P.J. Nicklasson and P.A. Sundsbø (2010) Effect of atmospheric temperature and droplet size variation on ice accretion of wind turbine blades. Journal of Wind Engineering and Industrial Aerodynamics, http://dx.doi.org/10.1016/j.jweia.2010.06.007, level 1.

  The contribution of this author was some of the ideas for the work, icing modeling setup, calculation of torque coefficient, and results analysis.

- Homola, M.C., T. Wallenius, L. Makkonen, P.J. Nicklasson and P.A. Sundsbø (2010) Turbine size and temperature dependence of icing on wind turbine blades. In press at Wind Engineering, level 1.

  The contribution of this author was the idea for the work, modeling setup, and data analysis.

- Homola, M.C., M.S. Virk, P.J. Nicklasson and P.A. Sundsbø (2011) Performance losses due to ice accretion for a 5 MW wind turbine. In press at Wind Energy, level 2.

  The contribution of this author was the idea for the work, BEM analysis, and calculation of power improvement.

Conference publications

- Homola, M.C., P.J. Nicklasson, P.A. Sundsbø and A.E. Holdø (2008). Experiences from icing at Nygårdsfjell wind park. European Wind Energy Conference 2008, Brussels, Belgium

  The contribution of this author was the idea for the work, design and installation of monitoring system, and data analysis.

- Wallenius, T., M.C. Homola, L. Makkonen and P.J. Nicklasson (2008). Relationship between chord length and rime icing on wind turbines; Winterwind 2008, Dec. 9-10, Norrköping, Sweden

  The contribution of this author was the idea for the work, portions of the modeling setup and execution, and data analysis.

- Homola, M.C., J. Byström, P.J. Nicklasson and P.A. Sundsbø (2008). A corrector for wind power estimation and its usage in estimating icing losses. Winterwind 2008, Norrköping, Sweden

  The contribution of this author was the idea for the work and the data analysis.

- Homola, M.C., T. Wallenius, L. Makkonen, G. Beeri, P.J. Nicklasson and P.A. Sundsbø (2008). Scaling of icing on wind turbines; Multiphysics 2008, Dec.10-12, Narvik, Norway

  The contribution of this author was the idea for the work, portions of the modeling setup and execution, and data analysis.

- Ronsten, G., S. Dierer, B.E. Nygaard, L. Makkonen, M. Homola (2009). Measures needed for the successful development of wind energy in icing climates, European Wind Energy Conference 2009, Marseille, France

  The contribution of this author was results from icing modeling and discussions on the paper.

- Homola, M.C., T. Wallenius, L. Makkonen, P.J. Nicklasson and P.A. Sundsbø (2009). The dependence of icing severity on chord length, European Wind Energy Conference 2009, Marseille, France

  The contribution of this author was the idea for the work, portions of the modeling setup and execution, and data analysis.

- Homola, M.C., G. Ronsten and P.J. Nicklasson (2009). Energy production losses due to iced blades and instruments at Nygårdsfjell, Sveg and Aapua, 13th International Workshop on Atmospheric Icing of Structures IWAIS 2009, Andermatt, Switzerland

  The contribution of this author was the idea for the work, and data analysis for Nygårdsfjell.

- Homola, M.C., P.J. Nicklasson and P.A. Sundsbø (2009). Two years of icing monitoring at Nygårdsfjell Wind Park, 13th International Workshop on Atmospheric Icing of Structures IWAIS 2009, Andermatt, Switzerland

  The contribution of this author was the idea for work, sensor system design and installation, data collection and analysis.

- Homola, M.C., M.S. Virk, P.J. Nicklasson and P.A. Sundsbø (2011) modeling of ice induced power losses and comparison with observations, Presented at Winterwind 2011, Umeå, Sweden

  The contribution of this author was the idea for the work, data collection and analysis.

Submitted publications

- Virk, M.S., M.C. Homola, P.J. Nicklasson (2010) Ice accretion on large wind turbine blades. Submitted to Journal of Wind Engineering and Industrial Aerodynamics, level 1.

  The contribution of this author was some of the ideas for the work and analysis.

1.6 Thesis outline

Outline of the rest of this thesis is as follows:

Chapter 2 gives a brief description of how and why atmospheric icing forms, beginning with the formation of supercooled cloud droplets and then how the droplets collide with and accrete on objects.

Chapter 3 describes how the effect of icing on the power production of the Nygårsdfjell wind park was monitored and analyzed.

Chapter 4 deals with the results of simulations analyzing the sensitivity of atmospheric icing to different parameters. Some of the parameters studied are turbine size, droplet size and ambient temperature during an icing event.

In **Chapter 5** the changes in the aerodynamics resulting from icing are described and the resulting effect on power production is calculated. The modeled changes in power production are then compared with measurements from actual icing events.

The final chapter, **Chapter 6**, brings together the conclusions of this work and makes suggestions for areas of further research.

Chapter 2

Icing physics

To understand how and why atmospheric icing occurs it is necessary to understand the governing physics. In this chapter the connection between icing and clouds is explained, thereafter the properties and formation of clouds and their constituent droplets are reviewed, the heat balance of the ice accretion process is described and finally some of the important factors for icing on wind turbines are discussed. This chapter is a review of the above topics for completeness of this work and much of the review is based on the work of Rogers and Yau [50].

2.1 Icing and clouds

Atmospheric icing is the term used to describe the accretion of ice on structures or objects. This accretion can take place either due to freezing precipitation or freezing fog. In Norway it is primarily freezing fog which causes ice accumulation on structures, and this occurs mainly on mountaintops. The reasons for this will be explained in this chapter through the mechanisms for cloud formation and ice formation. The physics involved in the formation of clouds are of interest when studying atmospheric icing, as it is the liquid water present in clouds that is primarily responsible for atmospheric icing and corresponding challenges.

Clouds are common over most inhabited areas on earth, and are actually large numbers of small water droplets or ice crystals suspended in the air and that together form what appears to be a solid mass. When clouds occur at ground level it is called fog. This means that in mountainous areas, a person in a valley might look up and say that it is cloudy, while a person on the mountain (if the clouds are low enough) would experience fog.

The general processes involved in the formation of clouds are commonly known. Water evaporates forming water vapor which rises until it cools and condenses. The multitude of condensed water droplets form clouds, which eventually leads to rain, thereby completing the water cycle from liquid, through vapor and clouds, back to liquid again.

2.2 Observed properties of clouds

The observed properties of clouds range in scale from the molecular level to the level of 100's of kilometers. Processes on the molecular level control the formation of each individual droplet, while processes on a macro scale steer cloud formations and weather patterns. Clouds are not a static entity, but are dynamic with constant interactions and exchanges between two or three of the phases of water;

- gas $\leftrightarrow$ liquid
- gas $\leftrightarrow$ solid
- liquid $\leftrightarrow$ solid

A cloud can also be viewed as a wave, where the extent of the cloud is the range wherein water condenses and outside of which the droplets evaporate. An example of this can be often seen when prevailing winds push air up a mountainside, as illustrated in Figure 2.1, where the individual water droplets are continuously moving upward while the cloud base does not move. This wavelike motion means that a cloud can propagate either faster or slower than the air that the cloud is in.

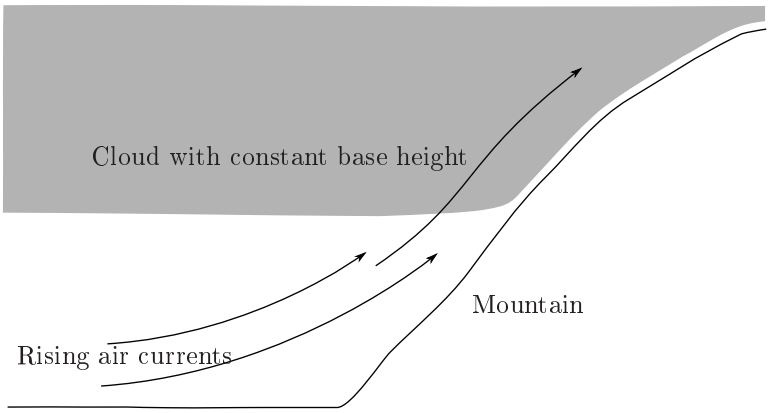

Figure 2.1: New droplets continuously form at the same level in the rising air current, making the cloud base appear stationary.

In spite of their solid appearance, clouds have actually very little water in them. Typical water content for a cloud can be from 0.1 to 1 g/m^3 which means that the mass of water is usually less than 0.1% of the mass of air. This small mass of water is spread over many droplets giving a very large surface area.

Clouds can contain both updrafts and downdrafts. Typically clouds are caused by a rising body of air, but if a parcel of cold dry air penetrates the cloud from the top due to turbulence or some other movement and mixes with some of the cloud droplets, this can cause evaporation of some of the droplets which cools the air further and accelerates the downward motion. The acceleration is determined by the temperature of the entrained pocket of air, which can be calculated as follows.

$$\frac{d}{dt}(T_p - T) = -E(T_p - T) - E\frac{L\mu}{c_p} - (\Gamma - \gamma_c)\frac{dz}{dt} \tag{2.1}$$

Where T[°C] is the cloud temperature, $E = (1/m)(dm/dt)$ is the rate of entrainment, T_p[°C] is the temperature of the parcel, Γ[K/km] is the dry adiabatic lapse rate (rate of warming for the sinking dry air), γ_c[K/km] is the lapse rate of the cloud, L is the heat of vaporization for water, μ is the mixing ratio of the condensed water and c_p is the specific heat of dry air at constant pressure.

2.3 Cloud formation and growth

Clouds proceed through several phases during their growth. Some of the processes involved are described in this section, first rising air and atmospheric stability then the mixing of air at different levels. Finally clouds either have droplet formation or ice crystal formation, and often a transition from one to the other during their lifespan. A brief discussion of the physics of droplet motion is included as well.

2.3.1 Rising air and atmospheric stability

The formation of clouds is caused by rising air. Rising air can be driven by several mechanisms. Firstly, prevailing winds can press the air against mountains, thereby causing it to be driven upward. Secondly, frontal lifting can occur when two weather fronts meet. The warm front will be pressed up by the cold front. Thirdly, heating of an air parcel relative to the surrounding air will cause it to rise due to its increased buoyancy. An example is when air is heated near the surface such that when a small parcel of air is displaced to a higher elevation it is then lighter than the surrounding air and its upward motion will accelerate.

The ambient temperature lapse rate (rate at which the temperature falls off with increased elevation) is called γ and is defined as follows.

$$-\left(\frac{\delta T}{\delta z}\right) = \gamma \tag{2.2}$$

This temperature lapse rate describes how air at higher elevations is typically cooler than at lower elevations. Rising air cools approximately following the ideal gas law because the ambient pressure decreases with altitude and thereby the air expands, causing cooling. The rate of cooling can be calculated based on the decrease in pressure by:

$$\left(\frac{T}{T_0}\right) = \left(\frac{p}{p_0}\right)^k \tag{2.3}$$

where $k = (c_p - c_v)/c_p$.

When conditions as described in the third type of rising air occur, it is called an unstable atmosphere. This type of unstable atmosphere has a lapse rate greater than the dry adiabatic lapse rate, Γ, which is approximately 9.8 K/km. In the opposite situation, with a lapse rate less than Γ, a parcel of air displaced to a higher elevation will be cooler than its surroundings, and will tend to return to its original elevation.

2.3.2 Air mixing

Air from different elevations and areas of the cloud mix due to turbulence, leading to some of the observed properties of clouds. When a parcel of air rises, there must be an equal amount of air that sinks somewhere else to replace the rising air. Both the rising air and the sinking air will mix with their surrounding air at their boundaries. Since the temperature / saturation vapor pressure curve is concave upward, it is possible for two unsaturated quantities of air to be supersaturated when mixed. An example of this is when breath condenses on a cold day and is illustrated in Figure 2.2, where (T_1, e_1) and (T_2, e_2) are the vapor pressure and temperature of the two unsaturated air parcels, (T, e) is the point which would be reached based on relative mixing and (T', e') is the actual mixed point. Vapor has condensed until saturation was reached, and the condensation caused some heating of the mixture. The saturation vapor pressure curve, e_s, is also shown.

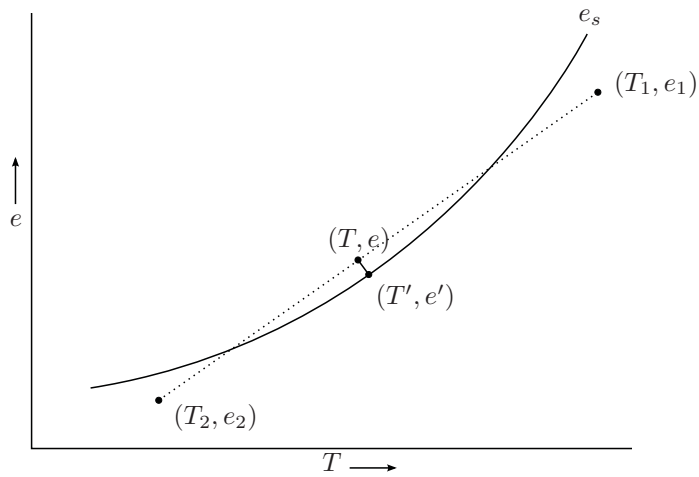

Figure 2.2: Mixing of two unsaturated air samples leading to supersaturation and condensation. After Rogers and Yau [50]

2.3.3 Droplet formation and growth

Clouds consist of small water droplets, or ice crystals. The process leading to cloud formation is usually that air rises and cools due to expansion until the air becomes supersaturated. Air can also be cooled leading to supersaturation by mixing with colder air, as described in the previous section.

The process by which condensing water becomes raindrops is as follows. Initial water droplets form that are extremely small and until the droplet sizes reach their critical size they are classified as stable, growing and shrinking with the amount of supersaturation of the atmosphere. When the droplets reach a size greater than

critical they become unstable, and will continue to grow as long as the value of super saturation is sufficient.

Droplets can grow both by continuing condensation, and by collisions and coalescence with other droplets. For condensation to continue, additional water vapor must be made available. This can occur through continued cooling of the air parcel by continued ascent and expansion. Alternatively, mixing with a moister air parcel could also make more water available.

Collisions and coalescence are not statistically significant until the droplet reaches a minimum size. For the smallest cloud droplets, the amount of free space between droplets is relatively large so it is not likely that the droplets will be on collision courses. In addition, not all droplets on collision courses collide. This is due to the fact that the airflow around a droplet is disturbed by the presence of the droplet and thereby the droplets can follow the airstream around each other. Additionally, very small droplets follow the velocity of the airstream quite closely due to their short relaxation time (Equation 2.6). Thereby all droplets have nearly synchronized movements together with the airstream, and the opportunity for collisions is low.

2.3.4 Condensation nuclei

In perfectly pure water vapor or air cooling could continue until supersaturation of several hundred percent before homogenous condensation occurred. But, in normal atmosphere there are large numbers of small particles called condensation nuclei which allow heterogeneous condensation at lower levels of supersaturation. These condensation nuclei are hygroscopic and some of them are active above the dew point. This means that their surfaces may be wetted even at less than 100% relative humidity. These particles with some amount of water attached at less than 100% relative humidity are what cause haze during warm and humid periods. One example of how wetting can occur is if the condensation nucleus is a salt. When the salt dissolves in water, the vapor pressure of the solute is lower than that of pure water, thereby enabling liquid water to be formed at less than 100% relative humidity.

Air does not normally reach high levels of supersaturation because the large numbers of nuclei cause many small droplets to form and begin to grow as soon as supersaturation is reached. The growth of these droplets reduces the amount of water vapor present and limits the level of supersaturation to 2-3% [50].

2.3.5 Formation of supercooled droplets

Supercooled droplets are the cause of atmospheric icing and form due to several reasons. The first is that homogenous nucleation of small water droplets does not occur until the temperature is about -40 °C. Homogenous nucleation occurs when the random motions of the water molecules causes some of them to align in the crystal form, thereby providing an ice nucleation point. Due to the small size of the water droplets in clouds, the surface free energy causing cohesion of the droplet is relatively large, and hinders the expansion that occurs with ice formation. The larger the volume of water present, the less supercooling is necessary to initiate

homogenous nucleation. Water droplets of 5 µm freeze spontaneously at about -40 °C.

Since ice in clouds usually forms at higher temperatures than -40 °C it can be deduced that homogenous nucleation is not the primary method of ice formation. Nucleation occurs at higher temperatures if an ice nuclei is present. If the number of active ice nuclei in the atmosphere was as high as the number of condensation nuclei, than supercooled cloud droplets would seldom occur. But, at about -20 °C, the number of ice nuclei is estimated to be about a factor of 10^7 lower than the total number of particles in the air, and a factor of 10^5 lower than the number of condensation nuclei [50]. At colder temperatures the number of active ice nuclei increases exponentially. This relatively low number of ice nuclei means that at temperatures between -20 and 0 °C clouds often form as supercooled water droplets instead of ice.

2.3.6 Ice crystal formation and growth

Formation of ice crystals can occur through several different processes. The first is if water vapor deposits directly on a nuclei. The second is if condensation first occurs followed by freezing when the temperature falls. Thirdly, a water droplet can freeze by impacting a nuclei.

The formation of ice crystals is not assured even if the temperature is below freezing because the number of ice nuclei in the atmosphere is much lower than the number of condensation nuclei. In addition ice nuclei are not active at temperatures above freezing, and some are not active until the temperature falls to below -9 °C.

When ice crystals first form in a cloud of supercooled water droplets, they will begin to grow due to deposition at the expense of the water droplets, which will evaporate to maintain the supersaturation. This occurs because ice has a lower vapor pressure than water. The atmosphere therefor has a higher supersaturation in relation to the ice particles than in relation to the water droplets.

2.4 Droplet motion

In Figure 2.3 a larger droplet is shown overtaking a smaller. The smaller droplet may or may not be swept aside with the airstream, as mentioned previously. The collision efficiency, probability that a droplet with radius r will collide with a droplet of radius R, has been calculated by various authors, several of which are summarized by Rogers and Yau [50].

Equations of motion for the x and y coordinates for water droplets are as follows.

$$\frac{dV_x}{dt} = \frac{1}{\tau}(U_x - V_x) \tag{2.4}$$

$$\frac{dV_y}{dt} = \frac{1}{\tau}(U_y - V_y) \tag{2.5}$$

The velocity of the droplet is V, the velocity of the air is U and the droplet relaxation time, τ is defined as:

$$\tau = \frac{2r^2\rho}{9\mu} \tag{2.6}$$

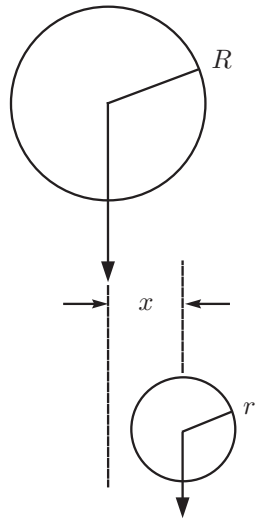

Figure 2.3: Droplet collision geometry. After Rogers and Yau [50]

Where the droplet radius is r, ρ is the droplet density and μ is the air viscosity.

For a small cloud droplet, with a radius of 5 µm, τ is calculated to be 0.31 ms, which means that the droplet responds very quickly to changes in the wind velocity. For a gust acceleration of 2 m/s^2, the droplet will move 0.6 mm relative to the air in one second.

2.5 Example: Condensing water

Clouds are made up of small water droplets or ice particles. To illustrate what occurs an example was contrived using typical data for Nygårdsfjell. The example describes how air that is cooled will become supersaturated and how the amount of liquid water in the cooled air can be calculated.

Air from Narvik is blown in the fjord and then up the mountains to Nygårdsfjell. For a typical winter storm with southwest winds, the temperature may be +2 °C and 80% relative humidity (RH). Assuming this air undergoes an adiabatic expansion as it moves up to Nygårdsfjell at 420 mas and that the adiabatic lapse rate is stable at 9.8 K/km. The following shows the calculation of the resulting liquid water content (LWC) at Nygårdsfjell.

$$RH = f = \frac{e}{e_s} \tag{2.7}$$

$$e = f e_s = 0.80 \cdot 706\,\mathrm{Pa} = 564.8\,\mathrm{Pa} \tag{2.8}$$

Due to the increase in altitude, there is a corresponding drop in temperature of 4.11 K, to -2.11 °C, which gives a new saturation vapor pressure of 531.295 Pa

(interpolated from Rogers and Yau [50, table 2.1]).

$$T_2 = T_1 + \Gamma(z_1 - z_2) = 2\,^\circ\mathrm{C} + \frac{0.98\,\mathrm{K}}{100\,\mathrm{m}}(0\,\mathrm{m} - 420\,\mathrm{m}) = 4.11\,^\circ\mathrm{C} \tag{2.9}$$

Since the initial vapor pressure is higher than the saturation vapor pressure at the final temperature, some supersaturation has occurred. Assuming the availability of sufficient, activated, condensation nuclei, the liquid water content of the air can be calculated as follows. First find the air pressure at the higher elevation,

$$p_2 = p_1 \sqrt[k]{\frac{T_2}{T_1}} = 100\,\mathrm{kPa}\ \sqrt[0.286]{\frac{268.89\,\mathrm{K}}{275\,\mathrm{K}}} = 99.359\,\mathrm{kPa} \tag{2.10}$$

then calculate the amount of water vapor present per kg of dry air at the initial condition,

$$w_1 = \varepsilon\frac{e_1}{p_1 - e_1} = 0.622\frac{564.8\,\mathrm{Pa}}{100000\,\mathrm{Pa} - 564.8\,\mathrm{Pa}} = 3.533\,\mathrm{g/kg} \tag{2.11}$$

Calculate the water vapor present at the final conditions.

$$w_2 = 0.622\frac{531.295\,\mathrm{Pa}}{99359\,\mathrm{Pa} - 531.2958\,\mathrm{Pa}} = 3.344\,\mathrm{g/kg} \tag{2.12}$$

Subtract the two to find the amount of water vapor that has condensed during the process, which we here assume has gone entirely over to liquid water. This is called the Liquid Water Content, LWC of the air.

$$LWC_2 = w_1 - w_2 = 0.189\,\mathrm{g/kg} \tag{2.13}$$

This liquid water forms droplets which can then freeze on impact, thereby causing icing. Not taken into consideration in the above calculation is the heating of the air caused by condensing water vapor. In this example it does not have a large effect, but for a larger lifting height the error could be significant by not taking it into account. When in a cloud the lapse rate is closer to 6 K/km, instead of 9.8 K/km.

This LWC of 0.189 g/kg can not be directly used to calculate the rate of icing of an object because icing is also dependent on the droplet size spectrum, wind velocity and object geometry.

2.6 Orographic lifting and LWC

It can be seen from the previous section that the greater the lifted height of an air parcel and the greater the cooling the parcel experiences, the higher the liquid water content will become. This results in higher liquid water content over hills and ridges, where the air has just been lifted, than what could be expected at the same elevation above level terrain. It was shown in Makkonen and Ahti [51] that icing correlates more strongly with elevation in relation to surrounding terrain than with elevation relative to sea level and that icing on the summit of a hill is more severe than on the slope of a mountain at the same elevation. This phenomenon has also been clearly illustrated with recent work in modeling which shows a higher concentration of liquid water above a hilltop [52], as can be seen in Figure 2.4.

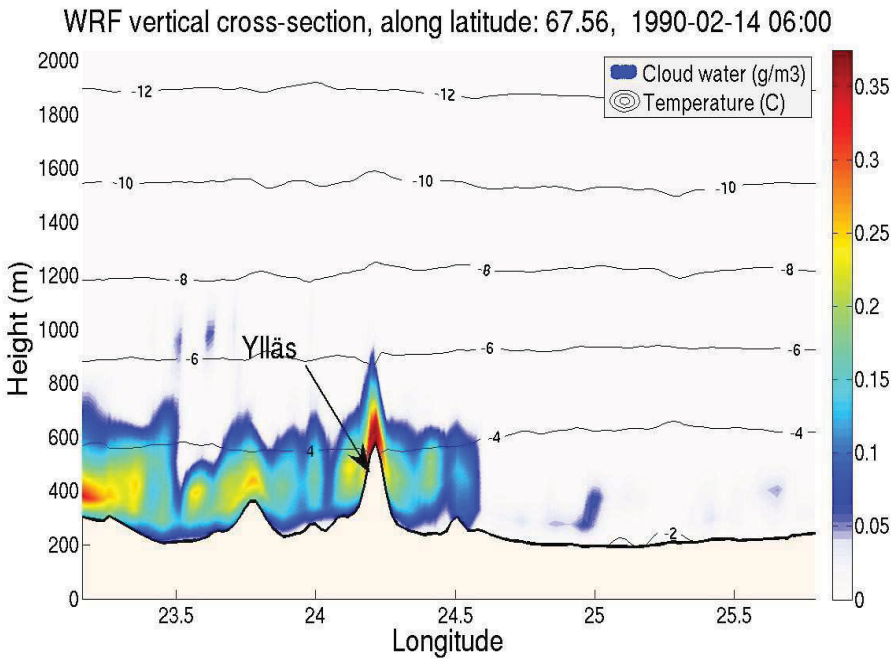

Figure 2.4: Liquid water concentration is much higher above the hilltop than at surrounding locations [52].

2.7 Atmospheric icing

Atmospheric icing is the term used to describe the build up (accretion) of ice on surfaces exposed to supercooled cloud droplets. Atmospheric icing also includes ice formed from freezing rain or snow, but the formation from supercooled cloud droplets is the main source of problems for aircraft, wind turbines, transmission towers and the like.

Atmospheric icing occurs when supercooled cloud droplets come in contact with a surface which provides a crystallization site. The type of ice formed is dependent on the thermal balance of the surface. The terms in the thermal balance equation are, energy released by the freezing droplets, heat capacity of the forming ice/water layer, kinetic energy of incoming droplets, evaporation, radiation, convection, conduction, and friction caused by the airflow.

If the amount of supercooling is large, or the heating flux due to freezing is small, the droplets freeze almost instantly upon reaching the surface. This causes a light and weak ice with a relatively large amount of trapped air called light rime. If the heating flux is higher or cooling less, then the droplets will freeze slightly slower and less air will be trapped. This denser and stronger ice is called hard rime. If the heat flux and cooling is such that a layer of liquid water is always present on the surface, then clear ice called glaze is formed. The equation for heat flux is described by Equation (2.14) [53] and is illustrated in Figure 2.5.

$$Q_f + Q_{adh} + Q_{kin} = Q_{ss} + Q_{sub/evap} + Q_{cd} + Q_{cv} + Q_{rad} \tag{2.14}$$

The terms in the equation are, Q_f, heat of freezing, from the freezing of the supercooled water droplets, Q_{adh}, adiabatic heating is from the friction within the boundary layer, Q_{kin} is the kinetic heating from the water droplets, Q_{ss} is the sensible heat of the water to the freezing temperature, $Q_{sub/evap}$ is the heat of sublimation or evaporation, Q_{cd} is the heat loss due to conduction into the surface, Q_{cv} is the convective heat loss due to airflow over the surface, Q_{rad} is the radiative heat loss from the surface. The main terms are the heat of freezing, and the heat losses due to convection, and sublimation/evaporation.

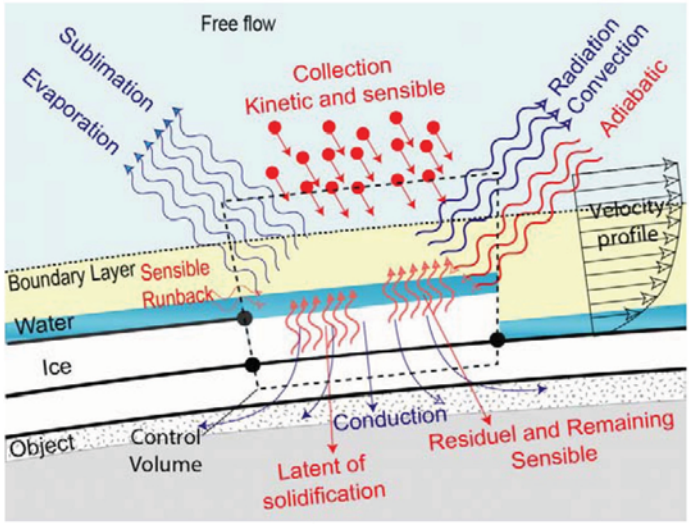

Figure 2.5: Icing heat balance [53].

A physical model of icing is described by equation (2.15), as detailed by Makkonen [54, p.53] and in ISO 12494 [55].

$$\frac{dM}{dt} = \alpha_1 \cdot \alpha_2 \cdot \alpha_3 \cdot w \cdot v \cdot A\,, \quad \left[\frac{\text{kg}}{\text{s}}\right] \tag{2.15}$$

Where A [m^2] is the cross sectional area of the object with respect to the direction of the particle velocity vector, w [kg/m^3] is the mass concentration of the particles, v [m/s] is the relative velocity of the particles and the α_1, α_2 and α_3 terms are correction factors with values in the range 0.0 - 1.0.

The collection efficiency (or collision efficiency), α_1, represents the flux density of particles striking the surface in relation to the maximum possible. The sticking efficiency, α_2, represents the ratio of the flux density of particles sticking to the surface to the flux density of the particles striking the surface. The accretion efficiency, α_3, represents the rate at which ice builds up on the surface in relation to the flux density of particles sticking to the surface.

The collection efficiency, α_1, for an airfoil is always less than 1.0 since particles trajectories will be deflected by the air stream, and thereby be deflected from striking the surface. Figure 2.6 illustrates this point, and also makes it clear that large droplets are collected more efficiently than small droplets. Another important point regarding the collection efficiency is that smaller objects are generally more efficient collectors than large objects. This is due to the fact that with small objects the streamlines in front of the object will have a shorter radius when flowing around the object, which makes it more difficult for the water droplets to follow the airflow, due to their mass and velocity. This means that relatively more droplets will strike the surface than in the case of a larger object, where the droplets will be diverted from the surface by the flow of air. This means that two different objects can have entirely different rates of ice accretion, even under the same conditions.

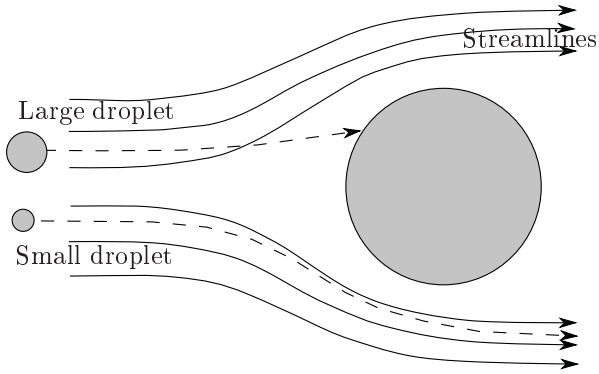

Figure 2.6: Collection efficiencies for large and small droplets. After ISO 12494 [55].

The sticking efficiency accounts for the fact that some particles, upon striking the surface, may bounce off again without sticking. If the accretion efficiency is under 1, it means that some portion of the particles sticking to the surface are melting and running off. In the case of dry rime icing this term is 1.

2.8 Summary

As a summary, some of the factors described in this chapter that are important for studying atmospheric icing of wind power plants are discussed. This especially means ice formation on the blades which disturbs the aerodynamic performance of the wind turbines.

The most important factors described in this chapter seem to be droplet motion and the physics of collision. Without collision of the droplets with the turbine blades, no icing can occur. In addition the geometry and relative wind speed varies along the length of the blade meaning that icing can occur on one portion of the blade but not on another, or that different types of icing can occur on different areas of the blade at the same time.

The review of the physical processes involved in cloud formation and icing presented in this chapter allow a better understanding of why icing of different types

occurs, as illustrated with the following example. Figure 2.7 shows two pictures of glaze ice fallen from a turbine blade at the Nygårdsfjell wind park.

Figure 2.7: Glaze icing from a wind turbine blade.

Examination of meteorological records at the time of ice formation showed that it was a fresh westerly breeze, -1 to 0 °C. It can also be seen from the small radius of curvature of the inside of the ice profile that the ice formed on the leading edge of the blade, near the tip. Since the turbine was also operating at this time, it means that the ice was built up with a relative wind speed of about 70 m/s. At the same time rime accumulations were seen near the blade roots (Figure 2.8). This means that the higher wind speeds at the blade tips caused both a larger water flux onto the blade and higher kinetic heating, thereby maintaining the wet conditions (warmer conditions) necessary for glaze ice. At the blade root, lower wind speeds allowed the droplets to freeze as they struck the blade resulting in rime.

A third important factor for studying icing is consideration of what type of data is necessary to input into an icing model. Ideally it would be possible to enter directly all of the variables in the equations describing icing. But, several of the parameters are not readily or usually measured, thereby causing much greater uncertainty. Two of the most important parameters are LWC and MVD. Neither of these two parameters is commonly measured in the field. The droplet size (MVD) directly affects droplet motion and whether or not a collision occurs. In addition, the droplet size affects the type of icing that forms since the collision efficiency directly effects the heat balance of the surface. Larger droplets with their higher collision efficiency cause a warmer surface and are therebye more likely to result in glaze, while small droplets with their lower collision efficiency result in a cooler surface and perhaps soft rime. In addition even though the average heat balance can be such that soft rime would be expected, the impacting of large droplets is more like discrete events, whereas small droplets easier can be reflected by their average. The average heat balance does not reflect that the impact of a large droplet causes a large addition of heat of fusion, such that it can take some time before the average temperature at that location is again reached.

The lack of known conditions during icing events means that even for a perfect

Figure 2.8: Rime icing on a wind turbine blade indicated by the ring and arrow.

icing model it is not possible to duplicate exactly an icing event and accurately estimating icing of structures is difficult. But one positive result of icing is that the type and amount of icing formed can be used together with an icing model to estimate what the LWC and MVD were during an icing event [56].

Chapter 3

Icing monitoring

Monitoring of icing can take different forms, from monitoring the standard deviation of a wind vane measurement to cameras recording the visual conditions. The organization of this chapter is to first discuss the reasons for icing monitoring, describe briefly Nygårdsfjell wind park, and then present results and analysis of the effect of icing on the power production at Nygårdsfjell wind park during two phases of monitoring there. The final section discusses calculation of energy losses due to icing from Nygårdsfjell wind park and compares with two other wind parks.

3.1 Reasons to monitor

Ice accretion on wind turbines is a significant issue and therefor information on icing is needed both before and after a wind park is constructed. The two main phases when monitoring is needed are the planning phase and the operating phase. The planning phase comprises the period from a potential wind site is selected for evaluation, through measuring and evaluating the wind resource and potential income for the project as well as determining the cost for building the project. After the planning phase comes the building phase and finally the operating phase during which the economic return on investment is attempted to be maximized while avoiding injury or harm to people or property. The use of icing monitoring during the planning and operating phases is discussed in more detail in the following subsections.

3.1.1 Planning phase

During planning it is necessary to obtain an estimate of the expected energy production from the planned wind park to determine the project economy. Expected energy production is normally calculated by using an expected wind speed probability density function together with the wind turbines expected power curve. If icing is expected at the site then the power curve will be be reduced during the periods with icing and thereafter as long as the ice accretions persist on the turbine. One of the factors making the annual energy estimate a critical component is that any incorrect assumptions will affect the income stream for the entire lifetime of

the wind park, normally 20 years. As the energy production is the sole source of income for a wind park any deviations from the actual production are immediately apparent in the project's bottom line. The importance of an incorrect calculation of icing losses is illustrated in the following example. Assuming a planned return on investment of 10% for a wind park means that for each 1% of annual energy production lost to icing the project loses 10% of its expected profit and a 10% lower energy production than expected results in no profit for the project. Calculation of the icing losses for a site may justify installing a de- or anti-icing system on the wind turbines.

Knowledge of icing at a site during the planning phase is also important to know if wind measurement statistics have been disturbed by icing during the wind measuring campaign at the site. In the case that the wind measurements are reduced due to ice accretion on the wind sensors, and this is not corrected, a project that would actually be profitable may be discarded as being unprofitable due to the incorrectly measured wind.

Knowledge of icing is also needed to determine if measures to protect from falling ice or warn of the danger of falling ice should be included in the turbines construction. Finally, prolonged operation of a partially iced wind turbine may reduce its expected lifetime and consideration of this should also be included in the financial calculations.

The first issue described for the planning phase, namely what the affect of ice on the power production of wind turbines may be has been the major focus of this thesis.

3.1.2 Operating phase

Information on icing is also needed during operation. Firstly the safety of people in and around the wind park must be assured. Warnings are needed to indicate the risk of icing and it may be required to stop the turbines in the event of icing if the risk associated with ice cast is too great or to postpone planned visits to the site when it is known that ice cast may occur.

It may be desirable to be able to quantify the energy production losses due to icing separately from other losses. Quantifying the energy losses due to icing allow a continued analysis of the cost effectiveness of implementing an ice mitigation strategy.

Finally, operation of the turbine may be modified during icing conditions: anti-icing or de-icing systems may be activated or the turbine controller may switch modes to optimize operation in an iced condition. One option may be to operate such that loads on the blades or other components are reduced and another may be to increase the iced efficiency by adjusting operation. A modification to increase the iced efficiency of a wind turbine is discussed in section 5.3.

3.2 Description of Nygårdsfjell wind park

The Nygårdsfjell wind park is located in Narvik, Norway (60°30′ N) in the mountains near the Swedish border. Therefore it was seen as a candidate for research

regarding icing of wind turbines already during the planning phase and contact between the wind power developer, Nordkraft Vind, and Narvik University College was initiated.

During the fall of 2005 three 2.3 MW Siemens wind turbines (SWT-2.3-93) were installed. The turbine foundations are at about 420 m.a.s. and with 80 m towers have a nacelle height of about 500 m.a.s. They are variable speed with power output controlled by pitch regulation. The tip chord is 0.8 m and the root chord is 3.5 m. The aerodynamic profiles used are not published by Siemens, only the data NACA 63.xxx and FFAxxx. Since the aerodynamic profiles of these turbines were not made available, the modeling work described later in this thesis had to make use of other turbine designs.

3.3 First measurement campaign (2005-2007)

After installation of the wind turbines at Nygårdsfjell documentation of the effects of icing on the production was needed. Icing sensors had been evaluated in previous work [25] where the optimum location for icing detection was deemed to be on the blade and as near the tip as possible due to the highest rate of accretion and highest elevation being reached at the blade tips. For the turbines at Nygårdsfjell this location was not possible to install at due to restrictions on what could be done on the blades. Neither was it possible to install a sensor at the upper elevations of the rotor. Installation of an icing sensor on a turbine nacelle has a variety of disadvantages, including those described by Homola et al. [25]: not reflecting the entire area swept by the rotor, having a different relative wind speed than the blade tips, and not recording ice shedding from the blades. But, due to the constraints described above this location was deemed the best possible at the time and the nacelle was selected as the installation location. Budget constraints also played a role and since HoloOptics, when contacted, was willing to supply a beta version of their optics based ice sensor for testing purposes it was chosen.

For monitoring the effects on energy production it is necessary to also evaluate the expected power production which requires information on the available wind resource. The IEC standard [57] specifies measuring the wind at hub height and upstream of the turbine. This was not practically possible for this work and so the wind speed as measured on the nacelle was used instead. Reasoning for this is described further in the Analysis portion of this section.

3.3.1 Measurement equipment

In the following the sensors used are briefly described.

Ice sensor

A HoloOptics T23 beta version ice sensor was installed in December 2005 and operated until the summer of 2006. The T23 ice sensor indicated ice already the day after being installed, and a photo was taken of the sensor while it was indicating, and with ice on the sensing surface. The ice sensor seemed to work well and indications on several occasions were corroborated by observations on site. However, this sensor

failed during the fall of 2006 and was not able to be replaced during the remainder of the test period.

Wind and power

The wind turbines were equipped with two anemometers on the nacelle; a KK-electronics with thermostat controlled heating element was set as the primary anemometer and an NRG IceFree3 was set as the secondary. The anemometer arrangement is shown in Figure 3.1, with the NRG IceFree instruments on the left side. The wind turbine log files include a range of data, including wind speed and

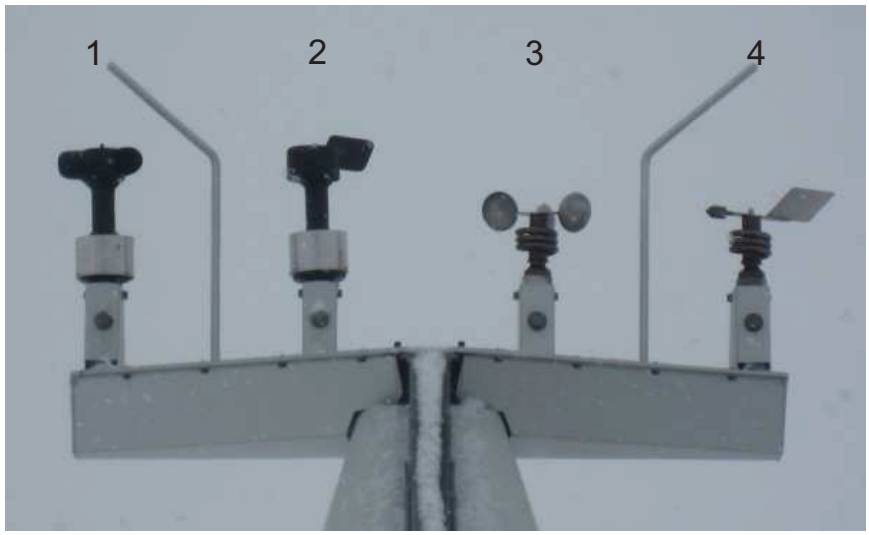

Figure 3.1: Anemometers and windvanes on the rear of the turbine nacelle. 1. NRG IceFree3 anemometer, 2. NRG IceFree3 windvane, 3. KK-electronics anemometer, and 4. KK-electronics windvane.

direction, ambient temperature, blade pitch, rotor rpm, and active power.

Weather station

A small weather station was installed in the wind park, which measures wind speed, direction, temperature and air pressure. The weather station was installed in 2006 for other purposes but the data was made available for this work and data was available for all of 2007.

3.3.2 Analysis

Analysis of the production data was done by processing the turbine log files together with the icing sensor and weather station logs. Data from the two prevailing wind directions were analyzed separately because the performance curves were quite

different for east and west winds. Filtering of the data was performed to remove corrupt data points, as well as periods when the turbines were not operating, or were starting or stopping. The 2006 data was then separated into three groups for easterly winds and three groups for westerly winds based on the recorded temperature and icing indications. The three groups were called warm, cold and ice, with criteria being, temperature above 3 °C, temperature at or below 0 °C with icing not indicated, and temperature at or below 0 °C with icing indicated, respectively. For 2007, the data was only grouped based on temperature with the two groups being warm (above 3 °C) and cold (0 °C or less).

Effect curves based on the nacelle anemometers for each of the groups of data were generated following the IEC standard 61400-12-1 [57]. It is not expected that the nacelle anemometers give accurate free-stream values of wind speed as specified in the IEC standard , but they should be sufficient for comparison between ice-free and icing periods as it has been shown that nacelle anemometers correlate well with upwind meteorological masts (though with some relationship) [58], and that they give a more precise measurement of the wind speed at the rotor plane [59]. The measured wind speed was corrected for changes in air density due to temperature and pressure changes, as specified in IEC standard, using the following procedure. First the air pressure at hub height (p), was calculated as

$$p = p_b \left[1 + \frac{\gamma}{T_b}(H - H_b)\right]^{\frac{-g}{\gamma R}} \quad [\text{Pa}], \tag{3.1}$$

where $\gamma = -6.5$ K km^{-1} is the temperature gradient, T is the temperature, H is the height, $g = -9.807$ m s^{-2} is acceleration due to gravity, $R = 287.1$ J K^{-1} kg^{-1} is the gas constant and the subscript $_b$ refers to the values at the point of measuring. Thereafter the air density (ρ) was found to be

$$\rho_{10\text{min}} = \frac{p_{10\text{min}}}{R \cdot T_{10\text{min}}} \quad \left[\frac{\text{kg}}{\text{m}^3}\right]. \tag{3.2}$$

Finally the normalized wind speed (V_n) was calculated as

$$V_n = V_{10\text{min}} \frac{\rho_{10\text{min}}}{\rho_0}^{1/3} \quad \left[\frac{\text{m}}{\text{s}}\right], \tag{3.3}$$

where $\rho_0 = 1.225$ kg m^{-3} is standard air density.

Figure 3.2 shows variations in the power curves for one direction of one of the turbines and Figure 3.2 shows the standard deviation of the data in each bin for the same power curves.

The curves were similar for the other turbines. In examining the standard deviation of power production for the turbines, it can be seen that the standard deviation was similar for the warm group in 2006 and for the warm group in 2007. In contrast, the standard deviation for the cold/icing group from 2007 was much larger than for the similar groups from 2006.

The power curves for the turbines show that on average they produced about the same when the icing sensor was indicating icing and when it was not. It

was expected that all icing would show a clear decrease in production, as has been indicated previously [6, 17, 13]. For 2007, the standard deviation of power production was larger during cold periods than during warm which presumably resulted from icing. This seems to indicate that the icing in 2007 was perhaps more severe than in 2006.

Some relatively short periods of underproduction that seem to be a result of icing were seen, one of these is described below and is shown in Figure 3.3. In the middle of a two day long period during which the icing sensor indicated icing continuously, the wind speed dropped to about 3 m/s and then increased. During the increase the power production was significantly below the normal curve, until the wind reached about 8 m/s, at which time the production jumped back up to the normal curve. It is theorized that this jump corresponds to spontaneous shedding of ice that had accumulated on the blades. This entire episode occurred during temperatures of -3 °C to -5 °C, so the possible shedding would not have been related to melting. The same type of response over the same period of time was seen on two of the turbines. The third turbine was stopped during this period, so no conclusions could be drawn about it.

It is interesting to notice that the "iced" power production for both turbines appears to very much the same during this time period until the jump occurs. This seems to indicate that the ice accumulation on both turbines was similar, and that with a wind speed of about 8 m/s, the wind loads began to cause the ice to be shed.

Data for one of the turbines was analyzed to determine the approximate amount of underproduction in 2007. The amount of lost production was calculated by checking each 10 minute average against the warm power curve. If the power produced was more than 1.5 times the warm standard deviation below the power curve, then that period was deemed underproduction. Thereafter the actual power production was subtracted from the expected power production based on the power curve and the resulting amount was added to the total. The total was found to be approximately 26 MWh, where more than half of the underproduction was from a two day icing event. Periods when the turbine was stopped due to icing are not included in the above, so the total power loss due to icing is larger than this.

The measurement of wind speed is critical to accurate power performance measurements. It was seen that the KK-electronics anemometer was underreporting the wind speed during some periods of icing, so all analysis was performed with the measurements from the NRG IceFree3 anemometers. Figure 3.4 shows how a plot of wind speed vs. power appears when an anemometer gives incorrect measurements of wind during icing periods.

Unfortunately, uncertainty regarding the performance of the anemometers increased after examining the 2007 data. It was found that both anemometers have periods when they clearly were not measuring the correct wind speed. Therefore some of the NRG data also had to be filtered out. Figure 3.5 shows data from the NRG anemometer that was filtered out of the dataset for determining the power curves. Some of the data points on or near the power curve came because they were between data points to the left of the power curve.

3.3.3 Discussion

Some possible reasons for the lack of correlation between indications of icing and production losses are discussed below.

Ice may be broken or shaken loose from the blades continuously during operation such that large accumulations do not typically occur. This seems a likely explanation based on the analysis of the data thus far. Production data indicates that ice can be shed quite effectively from the blades, with icing indication and underproduction followed by a jump in production up to the normal production levels. In contrast to what was reported of experience from Pori, Finland [60], the instances of lost production due to icing were most often at below rated speed. It seems that the turbine is perhaps shedding the ice more efficiently at higher speeds and is thereby able to generate at full power.

Another possibility is that there could be a low correlation between ice on the blades and ice on the sensor. One drawback of using a nacelle mounted anemometer is that ice may accumulate on the blades without accumulating on the sensor, or vice versa. It would have therefore been preferable to have a direct ice measurement on the blade, but this has practical difficulties which have been discussed previously [25]. It was observed that the periods when icing was not indicated also contains some times when the turbine operated with ice on the blades, when ice remained on the blades after an icing event was over. Though icing has been observed on the blades up to a few days after an icing event, it has only been observed near the blade root, so this is not thought to cause a large error.

The anemometer could be affected by ice about the same as the blades. If the anemometer used is underreporting the wind speed during the same periods that the blades are under producing, then loss of production may not be able to de discerned. Error of up to 60% due to icing on a cup anemometer with heating was reported by Fortin et al. [53]. However, NRG reports that they have increased the heating of the head for the IceFree3 as compared to the IceFree1 and 2 [61]. If the icing and melting of the rotor blades and the anemometer proceed along the same decreased production / measurement curve then no under or over production would be seen.

The larger dimension blades may collect less ice. Previous work has shown that a thicker surface is a less efficient ice collector than thinner surfaces [62] and therefore larger dimension blades should accrete relatively less ice during a similar icing encounter than thinner blades. Related to this, the icing may have been insufficient to cause the types of problems seen elsewhere. To determine this, a more in-depth monitoring of icing during the winter is necessary, preferably with an automatic camera that can allow the amounts of ice on the blades to be analyzed together with the production data.

In spite of the range of uncertainties surrounding this type of field data analysis, the fact that the expected correlation between indication of icing and loss of production could not be shown gives grounds to consider what could cause this type of response if the data is largely correct. One possibility is that instead of icing becoming more serious with increasing wind turbine dimensions, it may be that multi-megawatt pitch regulated wind turbines are less affected by icing than smaller stall regulated turbines. Several reasons this could be true are; a larger

chord and leading edge radius could be causing a lower collection efficiency, or the "gust slicing" effect on larger turbines may cause more rapid changes in the forces on the blade thereby shaking loose ice earlier.

3.3.4 Section summary

Monitoring of icing of the wind turbines at Nygårdsfjell with the HoloOptics T23 icing sensor was expected to show a clear correlation with loss of production, similar to the production losses due to icing reported elsewhere. Analysis from the first year does not show a clear correlation between indication of icing and loss of production in spite of a number of icing indications and a few incidents which show loss of production.

Minor differences between the effect curves for the icing and cold periods could be seen, and several periods of reduced production, likely due to icing, were identified during each of the years. During some of these periods large jumps in production levels were seen with almost no change in wind speed. This may be the result of ice shedding from the blades and thereby restoring their aerodynamic performance.

Low production losses in spite of icing often being indicated may indicate that larger multi-megawatt wind turbines are less susceptible to icing than smaller wind turbines. This could be due to lower collection efficiencies for the dimensionally larger blades. Alternatively, the icing periods were of too low intensity to affect production, though the icing sensor could detect them. The power production from 2007 showed a higher standard deviation than the data from 2006, which seems to indicate that 2006 had less intense icing than 2007.

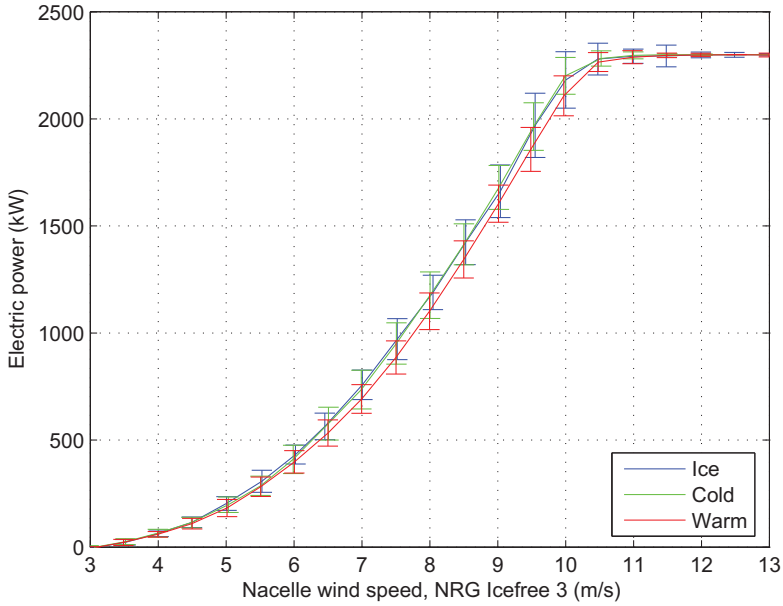

(a) Power curves, 2006.

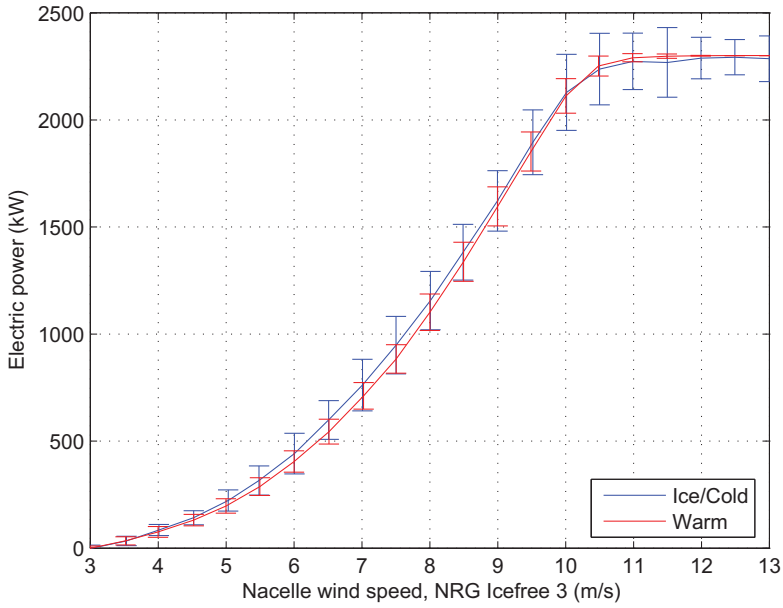

(b) Power curves, 2007.

Figure 3.2: Measured power curves, 2006 and 2007.

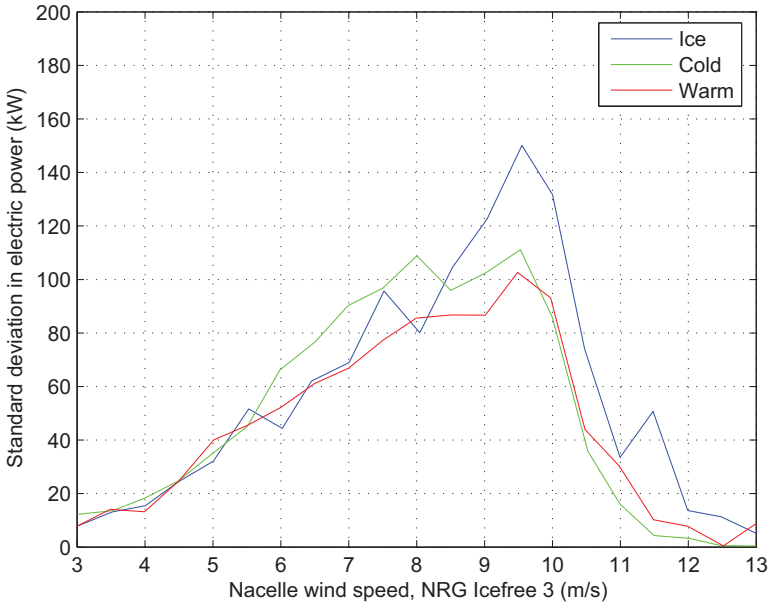

(c) Standard deviation, 2006.

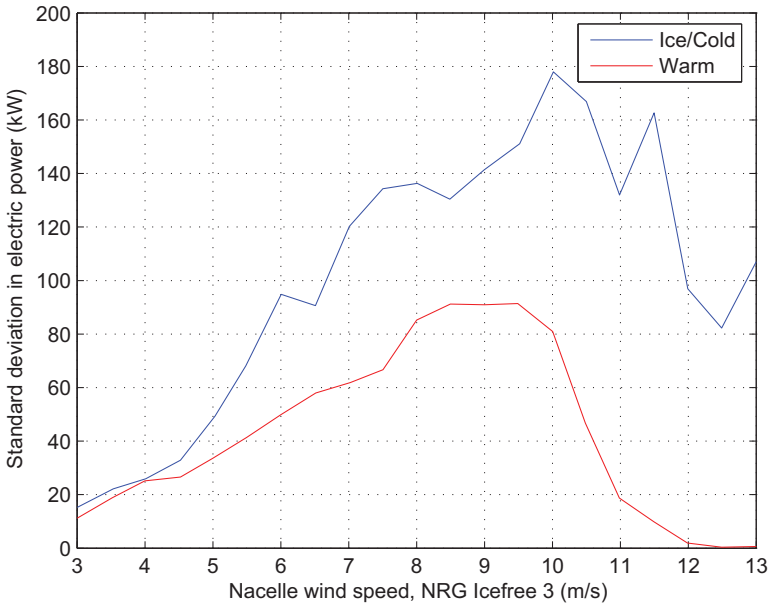

(d) Standard deviation, 2007.

Figure 3.2: Measured power standard deviation, 2006 and 2007.

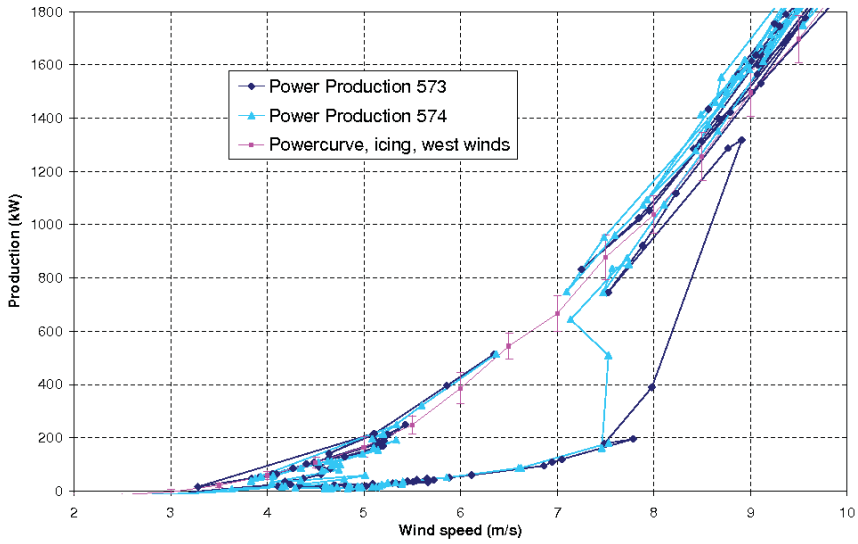

Figure 3.3: Production was below normal until wind speed of about 8 m/s, where production came back up to normal.

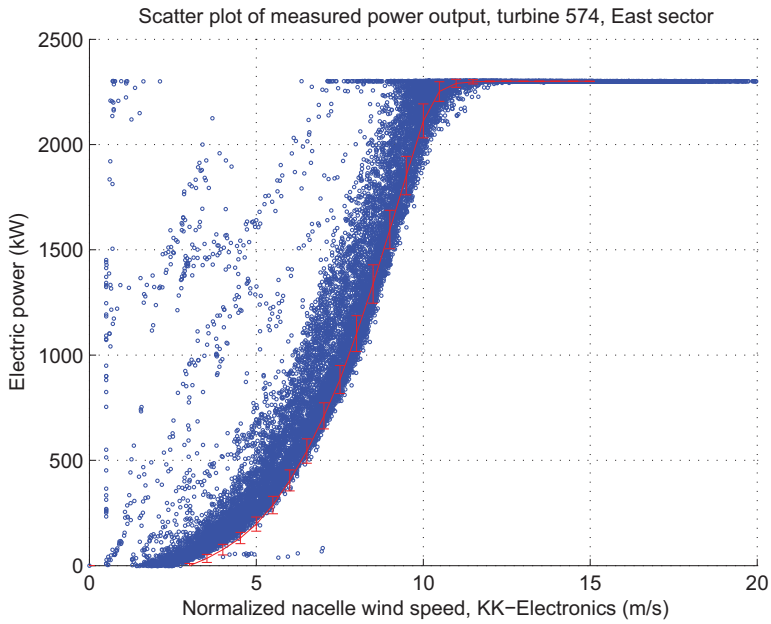

Figure 3.4: Example of power performance plot when an anemometer is periodically being slowed by icing.

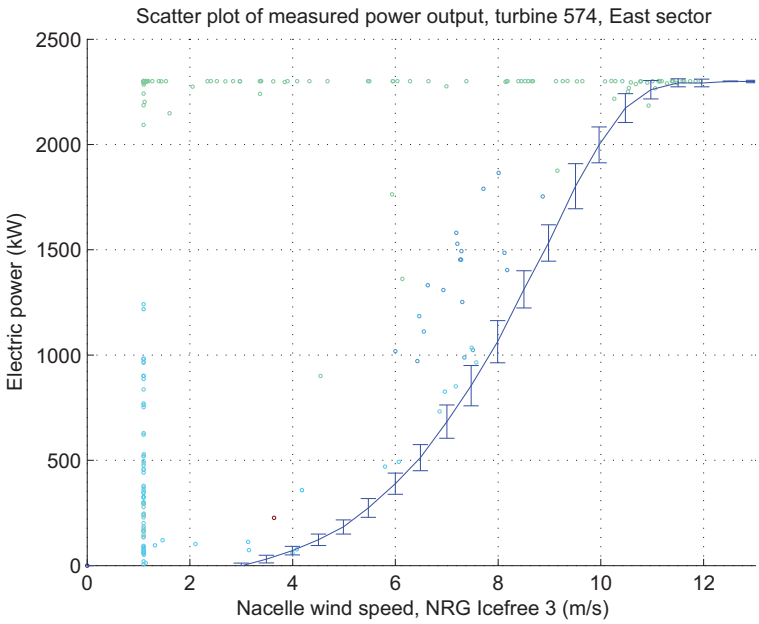

Figure 3.5: Data points that were removed due to underreported wind speed, probably resulting from the anemometer being affected by ice.

3.4 Second measurement campaign (2007-2009)

Following the first measurement campaign there remained many unsolved questions. One of these was to document more precisely the icing intensity and icing of the blades. In connection with this the installation of an improved HoloOptics sensor and cameras were performed for a second measurement campaign.

3.4.1 Measurement equipment

The additional equipment for monitoring icing that was installed is described in this section together with the normal wind turbine instruments which were used for icing evaluation.

Web cameras

Two web cameras were installed during the 2007-08 winter. The brand and type chosen was Mobotix M22-Sec [63]. This camera type has a range of built in functions that seemed to be suitable for this application. Some of these are; a weather proof housing, capability for a direct Ethernet connection, built in ftp function to transfer captured images to an ftp server, can store images to a shared folder on a computer on the local network, automatic motion detection function that can be used to trigger when pictures are taken and timer functions to take pictures at specified intervals. Camera one was fitted with a 43 mm lens and set to take pictures of the tail area (anemometers) every 15 minutes. Camera two was fitted with a 65 mm lens and set to take pictures of the blades every 10 minutes when motion was detected. Heat lamps were mounted on short booms to keep the cameras clear of ice during the winter. The operation of the heat lamps was simply that they were on all of the time. New bulbs were installed near the start of the icing season to ensure best possible operation during the winter. Figure 3.6 shows the cameras installed on the wind turbines warning-light boom. The camera was able to capture some images with icing clearly visible on the blades, and an example can be seen in Figure 3.7. This can be contrasted with the image of a clean blade as shown in Figure 3.8

Having adequate light for good quality pictures was a challenge, especially during the winter when the light period of each day is quite short and on the cloudy days when icing is of interest. Figure 3.9 illustrates the type of images from these kinds of periods. The camera automatically lengthens the image exposure time when there is less light, but this necessarily causes blurring of the moving blade. The motion detection seemed to be less reliable during darker periods, but as the image quality during such times was already too low for visual confirmation of icing that does not seem to be a major issue. This example illustrates why cameras are not a reliable type of ice detector, but the images can still give useful information as to the conditions at the site during periods of good visibility, particularly when combined with other types of sensor information. Fog or low clouds disturb visibility in addition to absorbing light and result in similarly poor image quality.

An additional challenge with the web cameras was in using the motion detection to capture images of the blades. The parameters were adjusted many times without resulting in consistent image captures of the blades. Finally it was found that the

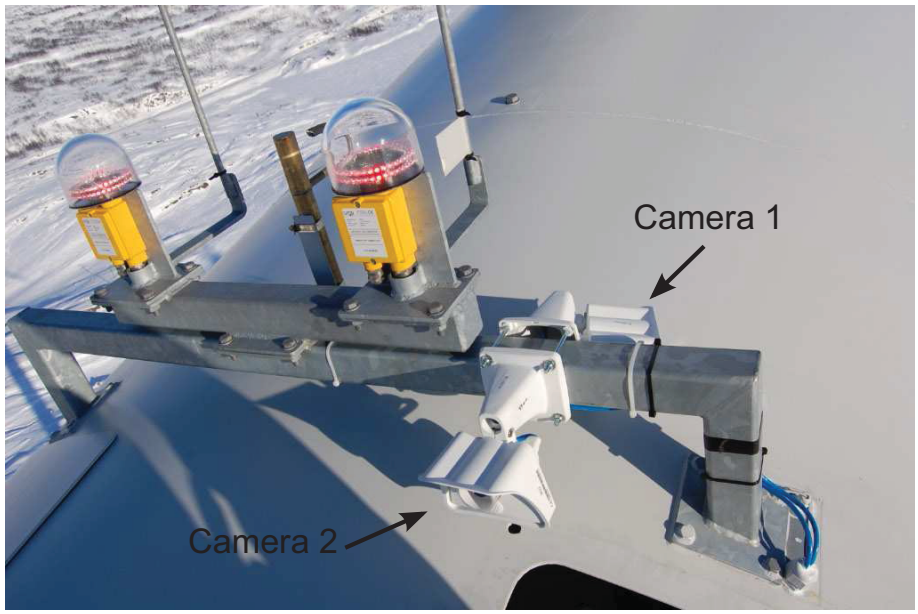

Figure 3.6: Web cameras mounted on light boom. Camera 1 captures images of the blades, while camera 2 captures images of the wind sensors installed on the rear of the nacelle.

camera has too low of a frame rate for the motion detection software to work properly, when the camera resolution is set to the maximum. The problem could be solved by either using a wider angle lens or lowering the resolution, but both options would result in poorer images of the blades. Ultimately it was decided to increase the number of pictures taken to get enough good images.

Ice Sensor

A HoloOptics icing sensor was installed on one of the turbines on the same light boom as the cameras. The installed sensor is shown in Figure 3.10.

Data acquisition was done with a direct connection to one of the pins on a serial port of a laptop computer, and a Labview script was written to read the status of the pin every three seconds and write it to a text file. This meant that the data files were larger than necessary, and perhaps it would have been better to only record the transitions between high and low. The laptop required a protective box to keep it warmer during the winter, so an insulated box with thermostat and a 60 W lamp for extra heating was constructed. This box also contained the power supply for the ice sensor.

The ice sensor setup had no method for testing for correct operation. Therefore it was necessary to visit the site periodically and manually block the beam to determine if the ice sensor was working properly.

The HoloOptics ice sensor used here only used the detection of the reflected light

Figure 3.7: Wet snow accretion imaged by web camera. This icing likely occurred when the turbine was stationary during a snowfall of near or slightly above freezing with a decrease in temperature following. The slightly orange hue along the left edge of the image results from the infrared heat lamp which keeps the camera lens ice-free.

beam to indicate ice or no-ice. This meant that rain can cause a false indication by disturbing the reflection. Therefore during data processing the temperature measurements from the wind turbine were used to ensure that only periods below 0.5 °C would be indicated as icing.

Wind and power measurements

Wind and power measurements were made through the wind turbines internal data acquisition system. For the winter of 2007-2008, the two anemometers used were NRG IceFree3 and KK-electronics with an extra radiant heating spiral. During the spring of 2008, the NRG anemometers were replaced with sonic anemometers.

All of the anemometers have had some difficulties during the winter, but the combination of the KK and sonic anemometers seems overall to perform more consistently in icing and cold conditions then the combination of KK and NRG IceFree3 anemometers had. It appears that turbine 573 in 07-08 had some problems, while 575 in 07-08 shows the least spread of any.

Figure 3.8: Clean blade imaged by web camera to illustrate contrast with the iced blade.

3.4.2 Analysis

The ice sensor data was processed to generate an average for each 10 minute period, to correspond with the 10 minute periods of the wind turbines data system. Thereafter the two datasets were combined and the combination of icing indication and power losses were plotted together.

Figure 3.11 shows the power production of one of the wind turbines from one year plotted against the highest of the two anemometers as blue dots. Periods when power production appears abnormally high, defined here as more than 115% of the expected or mean power for the bin, is called overproduction, and can be seen as a point above or to the left of the main band of data points. These correspond to a high power production relative to the recorded wind speed and may indicate that the anemometers are iced or otherwise not operating correctly. The red dots on the figures are the periods when the HoloOptics sensor indicated icing and the temperature was below 0.5 °C.

Similar figures were generated for the other turbines and years. Though the figures do not show a perfect correlation between over- or underproduction and icing indications, they do seem to show that icing indications occurred often during times with over- or underproduction. The calculated power losses from the wind turbines are described in section 3.5, together with the calculation of overproduction and underproduction. The correlation between an indication of icing and the turbine

Figure 3.9: Example of why cameras are an unreliable method of ice detection. Icing was indicated by the ice sensor at the time of this image, but lack of light makes image quality too low for confirmation.

operating in over- or underproduction was calculated for each year per turbine and is shown in Table 3.1. There it can be seen that the correlation is low, but slightly positive.

Table 3.1: Correlation between icing indication and over/under production for each year per turbine.

	573	574	575
2007-08	0.022	0.035	0.081
2008-09	0.127	0.041	0.046

3.4.3 Discussion

Monitoring wind turbine performance under icing conditions has a few challenges. Visibility is generally poor during icing conditions. Firstly because the icing itself results from water droplets in the air, fog, which reduce both visibility and light. Secondly daylight during the winter is much less than during the summer, especially with arctic sites such as Nygårdsfjell.

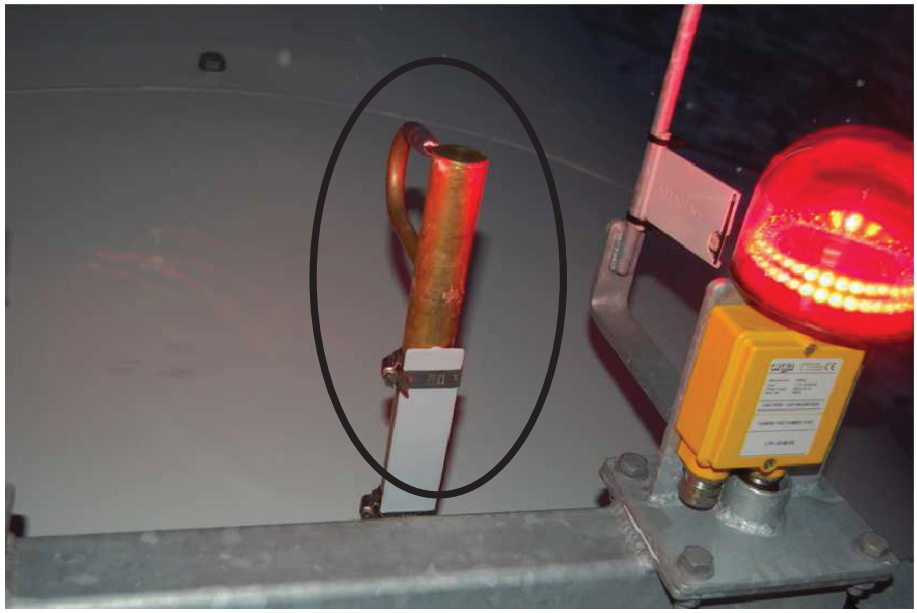

Figure 3.10: HoloOptics sensor, inside the ring, as installed on the light boom.

Neither the cameras or ice sensor come as ready kits for icing monitoring on wind turbines so a significant amount of time for planning and installing these items must be calculated for. One of the areas that took quite some time was the collecting and archiving of the data.

The HoloOptics icing sensor does not appear to indicate all of the periods when power production deviates from the normal for the measured wind speed, but this can have several reasons. First, the icing sensor has a different geometry than both the anemometers and the turbine blades. Therefore ice can accumulate more or less on the different geometries due to their different collection efficiencies and relative wind speeds [64]. Second, the turbine blades operate in a range of altitudes, so they can encounter icing independently of the nacelle [23]. Finally, icing has both an accumulation period and a duration. Since the ice sensor automatically de-ices, it is expected to only show icing during the accumulation period. Thereafter ice can persist and continue to disturb the wind turbine operation for some time after the ice accumulation is over.

Further work could examine the timing of icing indications and production errors to determine how much of the mismatch between the two is due to the persistence of ice after an icing event. Reliable anemometer operation is also critical to monitoring of a wind turbines performance and incorrect wind speeds are an issue at times here.

3.4.4 Section summary

Monitoring icing and its effects on wind turbines is not a trivial task. The experiences from Nygårdsfjell described in this section are that the low light and low

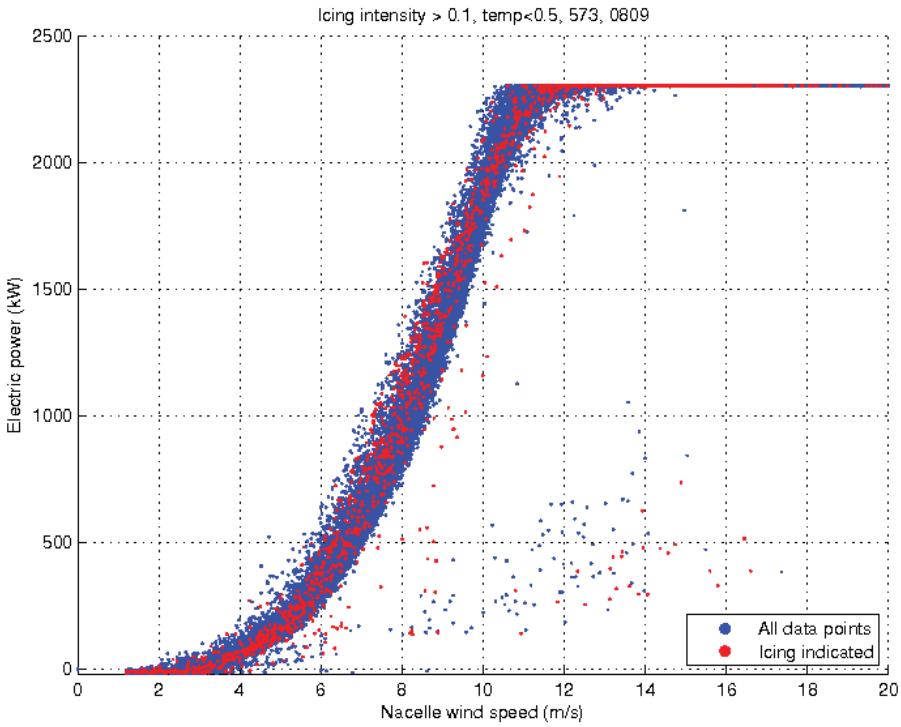

Figure 3.11: The turbine production data for turbine 573, in 2008-09 is shown in blue, and periods when icing was indicated by the HoloOptics sensor are shown in red

visibility during times of typical icing make it difficult to use cameras for visual confirmation of icing. The icing indications from the icing sensor used were only weakly correlated to periods when the wind turbine operation could be seen to be outside of the normal operational envelope. At least some of the lack of correlation can be understood by the anemometers not always operating correctly during icing conditions, and the differences in ice accretion on the different geometries.

3.5 Calculation of energy losses and comparison with other sites

Another of the questions raised after the first measurement campaign was to compare with data from other wind parks with multi-megawatt turbines. In this section estimates of energy production losses caused by iced blades and meteorological instruments are described for three wind power sites in Norway and Sweden. The turbine types were Vestas V90-2MW, Vestas V82-1.5MW and Siemens SWT-2.3-93. Analysis was performed with the same data processing for all of the three sites and energy losses are compared.

3.5.1 Introduction

In this section, both 10 minute and 1 hour data is used to estimate the losses due to iced-up wind turbine blades and sensors for three wind power sites in Norway and Sweden.

3.5.2 Site descriptions and analysis

The data analysis generally followed the form of first removing periods when the turbine was stopped, then generating expected power production curves based on the median of all operating data (including periods when the turbines were affected by ice) in 0.5 m/s bins. The median is used so as to give less weight to outliers. Thereafter a threshold of 85% of the expected power production was used to determine if the turbine was producing too little power for each time period, as was done in Ronsten [65]. During periods when the actual power production was less than the threshold, the difference between the expected power (from the power curve) and the actual power was counted as a power loss.

This method is expected to underestimate the actual power losses because of two reasons. The first being that using all data to generate the power curve may result in the curve being lower than it really should. The second is that power losses that are less than 15% are within the threshold and are not counted as power losses. The method can also underestimate power losses in certain conditions, if the anemometer is more affected by the icing than the power production, then the anemometer will record an incorrect low wind speed, thereby making it appear that the turbine is producing better than expected, even though the turbine may be producing less than it should due to the icing.

The sites were not specifically chosen because of any expected correlation or similarity in icing, but rather because all three sites had been found to have losses due to icing and during a meeting between parts involved at the three sites it was proposed to attempt to compare the measured losses in a systematic manner.

Nygårdsfjell

Nygårdsfjell windpark is an alpine arctic wind park which consists of three 2.3 MW pitch controlled Siemens wind turbines, in northern Norway as described in the beginning of this Chapter. Instrumentation consisted of standard wind turbine

instrumentation, an optics based icing sensor on the nacelle, and two web cameras monitoring the blades and the other instruments, as described in the previous section. Data analysis was performed for the two one year periods, May 1, 2007 - May 1, 2008 and May 1, 2008 - May 1, 2009.

During data analysis some slight modifications to the general procedure were made. Firstly, energy losses were only calculated for periods when the wind speed was greater than 5 m/s to avoid the nonlinearities associated with starting and stopping. Secondly, analysis of the data for the winter periods showed that the anemometers had many periods when they were clearly reporting a wind speed that was too low. So, only data from the summer period of May 1 - Oct. 1 with ambient temperature above +2 °C was used to generate the expected power curves. And, due to the problems with the anemometers, an area of "overproduction" was identified. This corresponds to periods when the anemometers are falsely giving too low of a value and thereby appear to be unrealistically good production. The threshold for this was set to 115% of expected power plus 50 kW for wind speeds above 3 m/s and above 0 kW below 3 m/s. The percentage of time that the turbine was operating in this overproduction region is shown in Table 3.2.

It can be seen from Table 3.2 that the energy losses during the 2008-09 winter were somewhat less than during the 2007-08 winter, and that in all but one case the energy losses are dominated by the winter component, indicating that low temperature related events are causing the losses. In all cases it can also be seen that there is a significant percentage of the winter period with overproduction indicated. Therefore the estimate of energy lost must be considered a conservative estimate. Finally, plots of the power production data from the turbines, with all data points plotted in blue, and the areas of over- and underproduction plotted in green and red respectively were generated. An example for one of the turbines is shown in Figure 3.12. These figures also illustrated that there were problems with the wind measurements during both winters.

Table 3.2: Production analysis results from Nygårdsfjell

	2007-2008			2008-2009		
Production [MWh]	573	574	575	573	574	575
Summer	2170	2040	2209	2277	2083	2234
Winter	4827	5054	4553	6085	5747	6025
Total	6934	7092	6762	8362	7830	8259
Losses, Summer	7	2	9	1	17	4
Losses, Winter	44	25	40	34	5	14
Losses, Total	51	28	48	35	21	19
Losses, Summer	0.3%	0.1%	0.4%	0.1%	0.8%	0.2%
Losses, Winter	0.9%	0.5%	0.9%	0.6%	0.1%	0.2%
Losses, Total	0.7%	0.4%	0.7%	0.4%	0.3%	0.2%
Time with Overproduction, Summer	0.7%	0.1%	0.0%	0.3%	0.3%	0.6%
Time with Overproduction, Winter	7.2%	2.1%	0.2%	4.2%	5.4%	4.1%

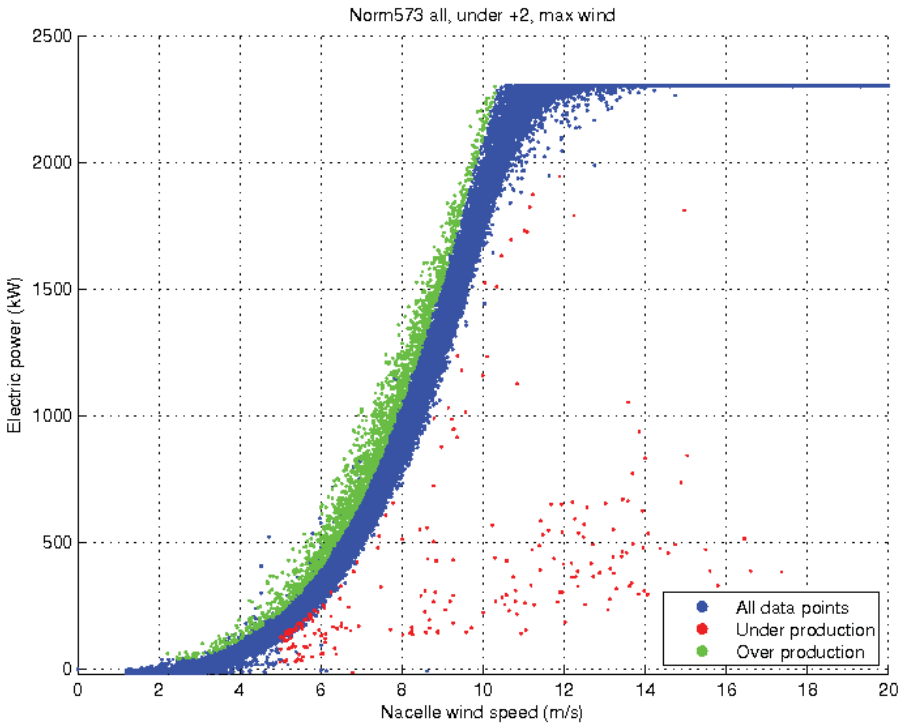

Figure 3.12: 10 minute production data from Turbine 573, 2008-09, at Nygårdsfjell showing all data in blue, overproduction in green and underproduction in red.

Some of the difference in the power data figures between the two winters is most likely due to the NRG IceFree3 anemometers, which were present during the 2007-08 winter, being replaced with sonic anemometers. It appears that the combination including the sonic anemometer gives results that appear consistent between the turbines.

The losses calculated here for Nygårdsfjell do not seem to be too large, with the average for all three turbines for both years being only 0.5%. Unfortunately the losses are probably somewhat higher than calculated due to the anemometer problems. Also, for Nygårdsfjell all stopped periods were also removed such that any unexpected stops caused by icing are not included in the above statistics.

Sveg

One-hour data from a Vestas V90-2MW at Svegström (Brickan) in the municipality of Härjedalen have been analyzed [66]. The available data include nacelle wind speed and power from the turbine, as well as meteorological data from the Swedish Meteorological and Hydrological Institute (SMHI). The influence of icing on power performance and energy production was of primary interest. The time period covered is 2007-12-11 to 2008-04-30.

The analysis of power performance data shows that icing of the Sveg wind turbine caused an energy production loss in the order of 5%, or 150 MWh out of totally 2.8 GWh, between 2007-12-11 and 2008-04-30. The energy production relative to the estimated production is shown in Figure 3.13, where five significant periods of lower production can be seen.

Aapua

The Aapua wind farm consists of seven V82-1.5 MW on Etu-Aapua, a hilltop in the Municipality of Övertorneå and was put into regular operation in September 2005.

It was well known by the owners that icing has significantly influenced the power performance of the Aapua wind farm. The magnitude of this effect had, however, not been investigated previously.

The wintertime energy production losses, based on the measured nacelle wind speed, were significantly higher compared to those during the summers, as can be seen in Table 3.3. More alarming, however, is the increase in downtime during the winters over the years due to a lower availability resulting in reduced energy production.

The average energy production loss, not including manual stops, is more than four times higher in the wintertime compared to those in the summertime. Winter is defined as T$<$+2 °C. All manual stops, a total of 205 days, are excluded, as are periods with missing data. The average energy production loss, based on actual production, was 27.9% in the wintertime (T$<$+2 °C) and 6.6% in the summertime (T$>$+2 °C).

Table 3.3: Energy production losses in Aapua during summer- and winter from October 1, 2005 - March 31, 2009.

Production [MWh]	Aapua 1	Aapua 2	Aapua 3	Aapua 4	Aapua 5	Aapua 6	Aapua 7	Total
Summer	8272	7390	5690	7620	5765	6933	7262	48932
Winter	6844	6799	7131	6641	4027	7170	7866	46478
Total	15116	14189	12821	14261	9793	14103	15128	95409
Losses, Summer	507	448	393	523	479	518	362	3230
Losses, Winter	1850	1308	1600	2157	1314	2286	2454	12968
Losses, Total	2356	1756	1993	2680	1793	2804	2816	16199
Losses, Summer	6.1%	6.1%	6.9%	6.9%	8.3%	7.5%	5.0%	6.6%
Losses, Winter	27.0%	19.2%	22.4%	32.5%	32.6%	31.9%	31.2%	27.9%
Losses, Total	15.6%	12.4%	15.5%	18.8%	18.3%	19.9%	18.6%	17.0%

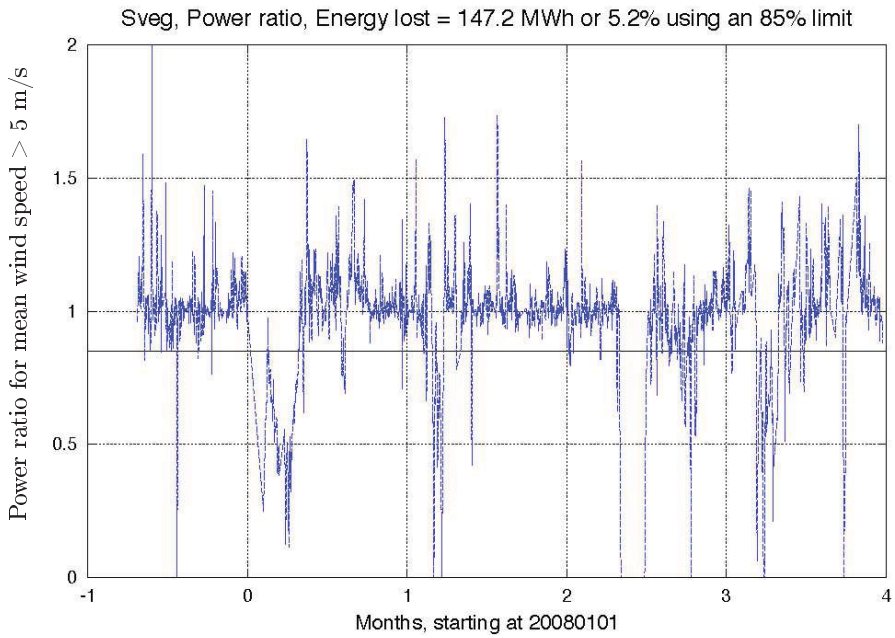

Figure 3.13: Five periods of icing. The energy production loss due to icing is estimated to be 5% during the period shown. The threshold shown is at 85%.

The method chosen, i.e. comparing the actual power for both summers and winters with the nominal power in each wind speed bin, enables the determination of when the power output is affected by low temperature related conditions. It is, based on a comparison of data from the summer time, assumed that icing, and not wakes, is causing this significant increase in losses.

In Ronsten [65], data for all turbines are missing during the start of the icing

seasons in 2006 and 2007. Data from missing periods are not included in the evaluation. The power performance for each turbine during winters and summers can also be seen in Figure 3.14. The increased spread in power performance data during the winters is obvious and significant.

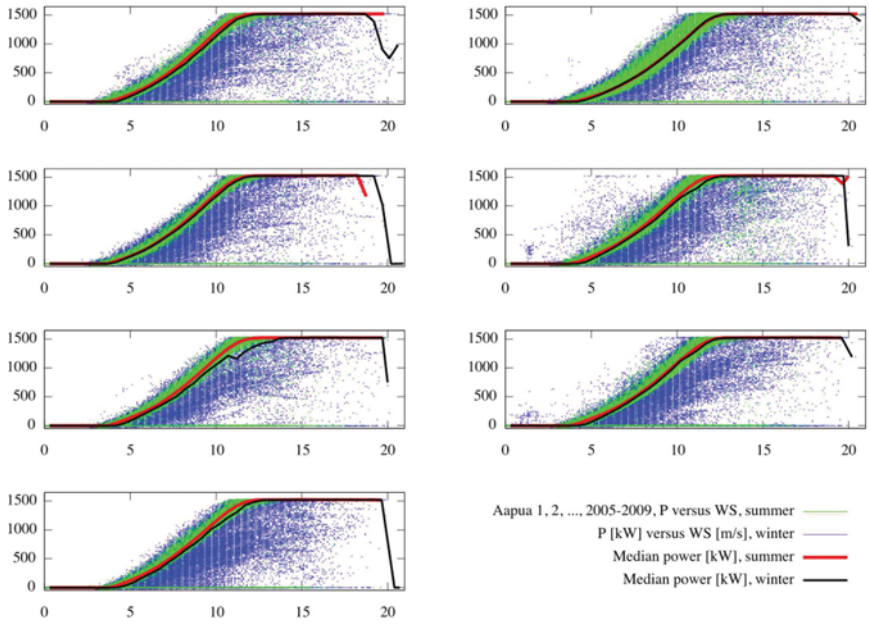

Figure 3.14: 10-min data plotted for three summers and four winters from October 1, 2005 - March 31, 2009. As data for the winters were plotted first, data for the summers (green dots) are placed on top of the winter data (blue dots). Aapua 1 is top left, Aapua 2 is top right etc.

3.5.3 Discussion

Estimation of energy losses due to iced-up blades and instruments was performed for three sites and the average for the sites are summarized in Table 3.4. It can be seen that Nygårdsfjell wind park has the lowest energy losses and Aapua has the highest. The order of power losses corresponds inversely to the size of the turbines at each site, with Nygårdsfjell having the largest turbines (2.3 MW), Sveg the intermediate (2 MW) and Aapua the smallest (1.5 MW).

These differences in energy losses give some idea of the spread of potential losses due to icing, and can indicate that power losses are less for larger turbines, but these results are incomplete in several ways. First, the data processing and filtering was not performed exactly the same at all sites due to a lack of time during the data comparison process. Secondly, no independent measurements of icing intensity or frequency to compare between the sites exist. This reduces the value of these results, but also helps to indicate what should be included in future work along these lines.

Table 3.4: Average energy losses from the three sites compared.

	Nygårdsfjell	Sveg	Aapua
Summer losses (%)	0.3	-	6.6
Winter losses (%)	0.5	5	28
Total losses (%)	0.5	5	17
Data period (months)	24	5	42
Number of turbines	3	1	7

Though the 85% filtering is a simple way to get an idea of potential icing losses, several points may be considered. First, examination of the power production data from the summer periods shows a normal power spread that is not dependent on a percentage. Therefore a future study could attempt to quantify how using a variable percentage or another method to identify low production periods could improve selection of icing periods. For example, during periods of high wind, a more correct limit could be 99.5%, since the power control scheme of the turbine normally maintains rated power within a very narrow band. On the other hand, at low wind speeds the spread is normally much larger than 15%, particularly near the nonlinear start and stop wind speeds. Second, the spread of data may vary for different sites, depending on the complexity of terrain and other site parameters.

While the energy losses due to icing were examined here, with regards to fatigue and turbine lifetime the duration and amount of ice on the wind turbine are important parameters and methods of measuring them should be documented.

3.5.4 Section summary

Estimation of energy losses due to iced-up blades and instruments was performed for three sites. It can be clearly seen that instruments which function properly during icing are absolutely critical for evaluating the performance of a wind turbine. An error condition caused by icing called overproduction was defined and the analysis showed that in the event of problems with anemometers this will affect energy loss estimates and should also be calculated. The generation of a normal power curve based on the median power production during each wind speed bin gives a simple method to relatively easily analyze energy losses due to icing. Nygårdsfjell wind park, with the largest turbines of the three sites, appears to have significantly less energy losses due to icing than the other two sites and Aapua, with the smallest turbines, has significantly more energy losses.

3.6 Summary

In this chapter the monitoring of icing and the resulting effects on power production of wind turbines was discussed.

The first section discussed why icing monitoring is important during different phases of a wind power project and was followed by a brief description of the Nygårdsfjell wind park.

In the third section it is described how, monitoring of icing of the wind turbines at Nygårdsfjell with the HoloOptics T23 icing sensor was expected to show a clear correlation with loss of production, similar to the production losses due to icing reported elsewhere. But, analysis from the first year did not show a clear correlation between indication of icing and loss of production in spite of a number of icing indications and a few incidents which show loss of production. Minor differences between the effect curves for the icing and cold periods could be seen, and several periods of reduced production, likely due to icing, were identified during each of the years. During some of these periods large jumps in production levels were seen with almost no change in wind speed. This was theorized to be the result of ice shedding from the blades and thereby restoring their aerodynamic performance. It was theorized that the low production losses in spite of icing often being indicated may indicate that larger multi-megawatt wind turbines are less susceptible to icing than smaller wind turbines. This could be due to lower collection efficiencies for the dimensionally larger blades. Alternatively, the icing periods were of too low intensity to affect production, though the icing sensor could detect them.

In the fourth section expanded icing monitoring campaign was described utilizing cameras as well. It was confirmed that monitoring icing and its effects on wind turbines is not a trivial task. The experiences from Nygårdsfjell described in this section showed that the low light and low visibility during times of typical icing make it difficult to use cameras for visual confirmation of icing. The icing indications from the icing sensor used were only weakly correlated to periods when the wind turbine operation could be seen to be outside of the normal operational envelope. At least some of the lack of correlation can be understood by the anemometers not always operating correctly during icing conditions, and the differences in ice accretion on the different geometries.

In the fifth section estimation of energy losses due to iced-up blades and instruments was performed for three sites. It was shown that instruments which function properly during icing are absolutely critical for evaluating the performance of a wind turbine. An error condition caused by icing called overproduction was defined and the analysis showed that in the event of problems with anemometers this will affect energy loss estimates and should also be calculated. The use of a method to generate an expected power curve based on the median power production during each wind speed bin was demonstrated as a simple method to relatively easily analyze energy losses due to icing. Nygårdsfjell wind park, with the largest turbines of the three sites, appears to have significantly less energy losses due to icing than the other two sites and Aapua, with the smallest turbines, has significantly more energy losses, though it can not be sure that the differences in turbine size contribute to the differences in energy losses.

Chapter 4

Icing parameter sensitivity

As mention in section 3.3.3, analysis of power losses at Nygårdsfjell indicated that power losses due to icing could be partially dependent on turbine size. In this chapter the dependence of atmospheric icing on turbine size is explored. In addition the sensitivity of icing to droplet size and ambient temperature is also examined.

The first section describes work on the size, mass and shape of rime ice accretions on four different sized stall regulated turbines at one temperature. The second section describes work on the size, mass and shape of both rime and glaze ice on five different turbines, including one pitch regulated turbine, at four different temperatures. The third section describes numerical modeling to explore icing along the length of a 5 MW turbine blade as well as changes in temperature and accretion time.

4.1 Turbine size sensitivity of rime icing

The accretion of rime ice on a wind turbine blade is a nonlinear process in which the intensity of an icing event is determined by a combination of liquid water content, droplet size, air temperature and wind speed. In addition the physics of the wind turbine also affect the ice accretion process. The collection efficiency of the blade profile depends on the relative air velocity, angle of attack and droplet size. The relative air velocity depends on the turbine design and on the wind speed as does the angle of attack. This makes analytical determination of the results of an icing event very difficult and modeling is necessary to determine parameter sensitivity.

Modeling is the only practical way of achieving this kind of parameter sensitivity comparison since it would be prohibitively expensive to erect wind turbines of different types at the same location for the express purpose of determining how icing varied between the designs. Also, even if the turbines are erected at the same location, they will not be subject to exactly the same conditions, due to micro-siting differences. Finally, it is also both difficult and expensive to measure liquid water content and droplet size which are also necessary to draw general conclusions from any experiments.

Ice accretion on the wind turbine blades is caused by the impingement of super cooled water droplets. The location of ice accretion and intensity of water impinge-

ment can be numerically determined by solving the air-water multiphase flow in proximity to the blade. The shape of the accreted ice depends upon many variables such as point of operation, the geometry of wind turbine blade, relative wind velocity, temperature, droplet diameter and the liquid water content.

It has previously been shown that icing loads on one geometry can not be directly transferred to a different geometry since the combination of droplet size and liquid water content that gives a large icing on one geometry may give a much smaller icing on a different sized geometry [64]. It has also been shown by Gent et al. [67] that airfoils with longer chords are less efficient droplet collectors. A longer chord airfoil has a larger leading edge radius, and therefore a larger percentage of the incoming droplets will be able to follow the streamlines around the blade. For the same reason a thick airfoil is a less efficient ice collector than a thin airfoil [62] and, therefore, large blades should accrete relatively less ice during a similar icing encounter than thin blades. Less efficient collection of droplets for larger turbines was also proposed in Chapter 3 as a possible reason for relatively little production losses at Nygårdsfjell wind park despite icing conditions.

Though it is known that airfoils with larger chords have a lower droplet collection efficiency and that larger wind turbines typically also have blades with a longer chord, no analysis of icing intensity relative to wind turbine and chord size was found in the literature. Since a specific wind turbine design involves an optimization of many parameters, it is difficult to predict intuitively how icing on a larger turbine will be relative to icing on a smaller turbine. The question of how much the size of the wind turbines affects icing is studied in this section with the use of a numerical icing model for the case of several, fixed speed, stall controlled wind turbines. The resulting aerodynamic effects of the changed profiles due to icing were not investigated.

To examine how ice accretion on wind turbine blades changes with wind turbine size, numerical modeling of icing for a blade section from different sized turbines was performed. Only conditions of dry rime accretion were modeled to eliminate complicating effects of differing types of ice accretion. Temperature and liquid water content (LWC) were constant for all the simulations but a range of droplet sizes (MVD) were used.

The rate of ice accretion on an object was shown in equation 2.15. In the case of rime icing, as studied here, both the sticking and accretion efficiencies are equal to 1.0, [56], and equation 2.15 simplifies to

$$\frac{dM}{dt} = k \cdot \alpha_1 \cdot v \cdot A\,, \quad \left[\frac{\text{kg}}{\text{s}}\right]. \tag{4.1}$$

Since v and A are values input to the simulation and dM/dt is the simulation output, the simulation results can be used to calculate how α_1 changes.

4.1.1 Numerical setup

The previous theory shows that icing is dependent on many parameters, including some that vary with turbine size. One in particular is the blade size, which increases with turbine size and may contribute to a reduction in icing for larger wind turbines. To examine how ice accretion on wind turbine blades changes with wind turbine

size, icing simulations for a blade section were performed. Blade and operating data from four different wind turbines, 450 kW, 600 kW, 1 MW and 2 MW, were used. The 450 kW and 600 kW were passive stall regulated, while the 1 MW and 2 MW were active stall regulated.

The TURBICE icing program was used for the modeling. TURBICE is a comprehensive numerical ice accretion program that calculates ice accretion on a two-dimensional airfoil in a potential flow field perpendicular to the surface of the airfoil. TURBICE uses the "panel" method for calculation of the potential flow, and calculates droplet trajectories by integration of the steady-state equation of motion beginning 10 chord lengths upstream of the airfoil section. The TURBICE model results have been verified through comparison with both icing wind tunnel experiments of aircraft wing sections and natural wind turbine icing, with good results for both rime and glaze conditions [32]. Additional areas of uncertainty compared with actual turbine blades are three dimensional effects due to rotating blades, which primarily are important near the blade root, and varying environmental conditions which the blade passes through during its rotation. Constant conditions were used for this work described in this section.

Turbice performs heat transfer calculations based on energy and mass balance calculations for finite areas along the surface of the blade profile. The mass and energy balances of each area are used to obtain the freezing fraction and surface temperature. The energy balance includes convection, evaporation, latent heat of freezing, droplet heating, radiation, friction caused by the airflow and heat contained in the water flowing on the blade, and is detailed in Makkonen et al. [32]. Runback water is assumed to flow in a liquid film on the surface when the freezing fraction is less than one. The local heat transfer coefficient is calculated according to the heat transfer model by Makkonen [68]. Calculation of the heat transfer coefficient in based on integral equations of the boundary layer. Local airflow velocities above the surface of the blade and ice are obtained from the potential flow solution. Surface roughness of ice significantly affects the heat transfer coefficient, and calculation of the heat transfer coefficient therefore utilizes a time dependent roughness calculation which converges to the roughness values from Shin [69] as the ice layers build up.

TURBICE does not assume a homogenous cloud, but uses a size distribution which is represented by the MVD. Using MVD for calculation of collision efficiency has been shown to be a good approximation for a droplet spectrum [70].

Since TURBICE is a two dimensional model, a section of the blades at about 85% of full radius was modeled. Since it is known that ice formation varies along the length of a wind turbine blade [71], the region of the blade around the 85% radius was chosen for this work because that area of the blade contributes the most to the turbines power production as shown in Figure 4.1.

The chord and other details for the modeled sections are shown in Table 4.1. The relative speed, v, is the air velocity relative to a point on the rotating blade at 85% radius.

It was decided to first only model conditions of dry rime accretion, to eliminate the complicating effects of different types of ice accretion. The atmospheric conditions that were chosen for the modeled icing period are shown in Table 4.2. Smaller droplet sizes were also considered, but the numerical integration time in

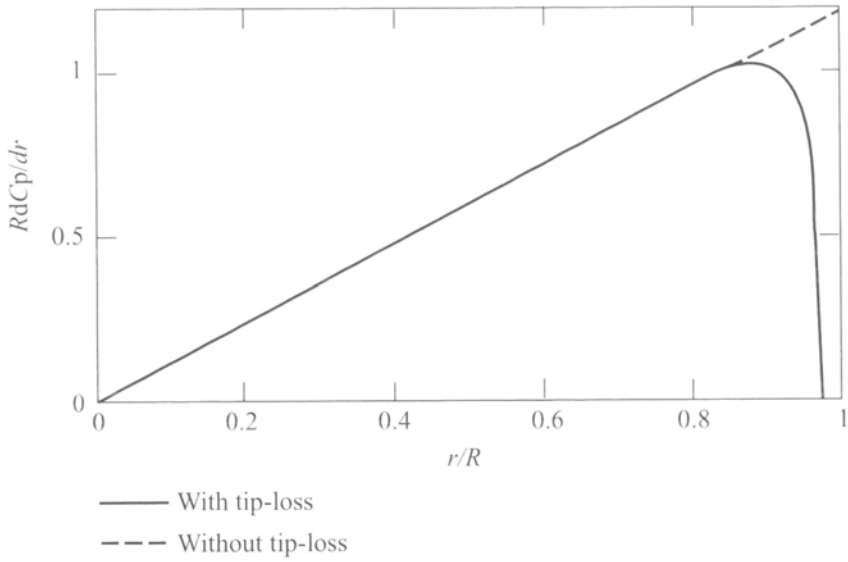

Figure 4.1: Span-wise variation of power extraction in the presence of tip-loss, illustrating that the peak of power extraction occurs at around the 85% radius [72, p.81].

Table 4.1: Wind turbine details.

Type	Passive stall		Active stall	
Power	450 kW	600 kW	1 MW	2 MW
Rotor radius [m]	18.5	22	27	35
Airfoil name NACA	63215	63417	63417	63416
Rotation speed [rpm]	30	27	22	18
Chord length [m]	0.747	0.844	0.99	1.435
Relative speed, v, [m/s]	49.66	53.20	53.87	57.37
Cross sectional area, A, [m]	0.145	0.172	0.197	0.270
Simulation radius [m]	15.5	18.5	23	30

TURBICE, for the same accuracy, increases prohibitively for smaller droplets, and since the results showed no dramatic changes with different droplet sizes it was decided to only use down to 12 µm MVD.

Table 4.2: Modeled icing conditions.

Wind speed [m/s]	10.0
Droplet size, MVD [µm]	12, 15, 17, 20, 30
Liquid water content, LWC [g/m^3]	0.20
Air temperature [°C]	-10
Simulation time [min]	120

4.1.2 Results and discussion

The results for the accreted ice mass and maximum ice thickness for the modeled test cases are shown in Table 4.3.

Table 4.3: Modeling results.

Droplet Size MVD	12µm	15µm	17µm	20µm	30µm
Turbine size	Ice mass [kg/m]				
	Maximum ice thickness [m]				
450 kW	0.666	1.23	1.309	1.452	2.002
	0.049	0.058	0.054	0.058	0.055
600 kW	1.031	1.207	1.411	1.705	2.353
	0.049	0.054	0.057	0.055	0.055
1 MW	1.047	1.247	1.579	1.718	2.481
	0.050	0.051	0.053	0.052	0.055
2 MW	1.159	1.305	1.449	1.937	2.798
	0.045	0.046	0.045	0.052	0.053

The results for all of the blades and droplet sizes give similar ice shapes, though with some variations in accretion limits and absolute accretion size for different droplet sizes. Therefore, the resulting profiles are not shown for all of the modeled cases, but only the case with 15 µm droplets is shown for all four wind turbines in Figure 4.2.

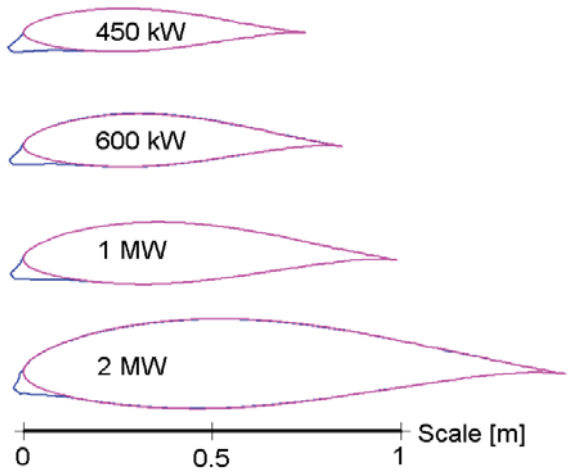

Figure 4.2: Ice shapes at 85% blade radius from the TURBICE modeling of 15 µm droplets for the blade profiles.

The maximum ice thickness is plotted in Figure 4.3, where it can be seen that the absolute ice thickness is slightly decreasing for larger wind turbines.

The mass of ice accreted at the 85% blade radius location for the various turbines was also examined, and the results are shown in Figure 4.4, where it can be seen that the accreted ice mass is highly dependent on the droplet size, more so than on the turbine size. This can explain why two apparently similar ice storms can give

very different amounts of ice accretion and highlights the importance of droplet size measurements for wind park planning at ice prone sites. It can also be seen that the local ice mass was increasing with turbine size. Importantly, the local ice mass relative to turbine power, radius and chord decreases for all of the droplet sizes.

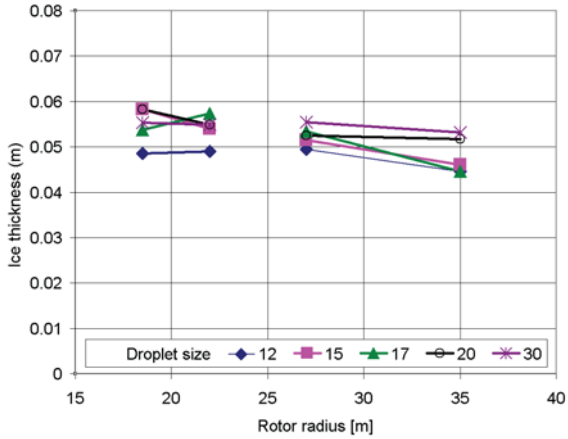

Figure 4.3: Ice thickness at the 85% blade radius for different droplet and turbine sizes.

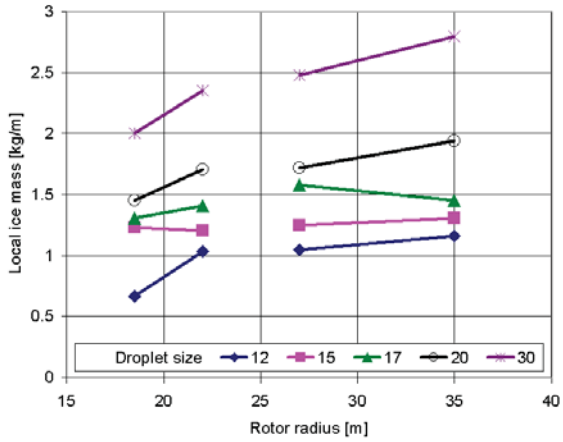

Figure 4.4: Local ice mass at the 85% blade radius.

The NEW ICETOOLS project [73] showed that the aerodynamic effect of icing causes more significant unbalanced loads than uneven mass distribution, and that these can be easily modeled by the use of a pitch angle offset for one blade. Therefore the aerodynamic effect of icing on energy production and loading was also considered. But, since the drag and lift coefficients for the iced blades were not available, the ice thickness relative to the chord seemed to be the best indica-

tor for how much the icing will affect energy production. In other words, a 2 cm thick ice accretion on the leading edge of a blade will reduce the performance of a 50 cm chord blade more than that of a 100 cm chord blade with the same 2 cm ice accretion, assuming the ice shapes are similar, as is the case here. Therefore, the ice thickness was plotted as a percentage of chord, as shown in Figure 4.5. It can be seen that the ice thickness relative to chord decreases with increasing wind turbine size for all of the droplet sizes examined.

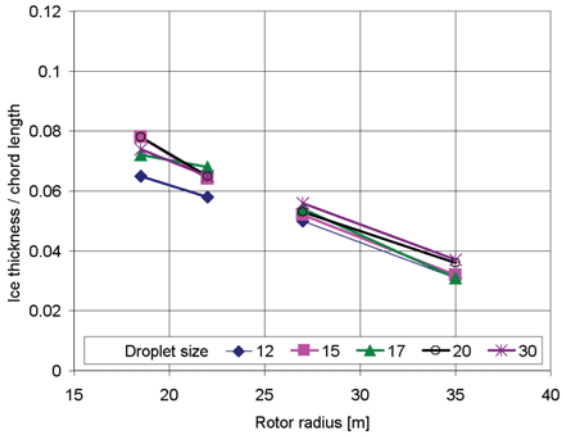

Figure 4.5: Relative ice thickness is less for larger wind turbines.

The modeled results indicate that for the turbine designs examined here, dry rime icing is less severe for larger wind turbines, both in terms of relative mass accretion and in terms of relative ice thickness.

It must be emphasized that these model results did not give specific information about the changes in the aerodynamic performance of the iced blades. Since aerodynamic loads may be more significant than the ice mass loads, conclusions about the load changes caused by icing can not be complete without understanding the aerodynamic changes, and these changes are studied in Chapter 5.

Since the icing rate depends on the relative velocity of the droplets, see equation 2.15, it was interesting to check the relative velocity of the modeled test sections to see if changes in the relative velocity were increasing or decreasing the icing. As can be seen in Table 4.1, the relative velocity was actually higher for the larger wind turbines studied here. The higher relative wind speed of the larger turbines is one reason for the increase in local ice mass. This means that the reduction in relative icing on the larger turbines was in spite of the increase in velocity.

The fact that ice mass was only slightly increasing while both speed and cross sectional area of the blade are increasing means that the collection efficiency of the large blades is decreasing. This is plotted in Figure 4.6. It seems that this reduction in collection efficiency is the main reason that icing is becoming relatively less significant for larger turbines. These relative reductions in ice mass and ice thickness are a positive sign for wind turbines in areas susceptible to the types of dry rime icing simulated here.

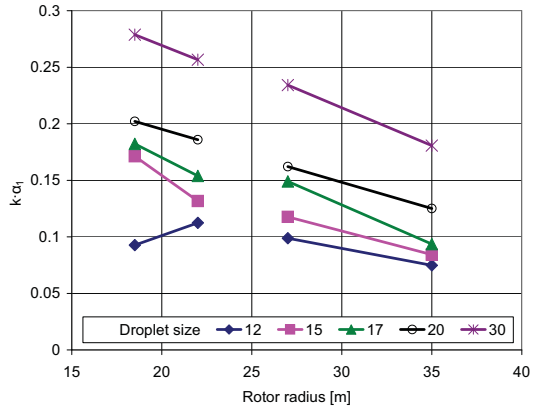

Figure 4.6: $k \cdot \alpha_1$ (collection efficiency) at 85% blade radius.

Based on the results of these simulations, a trend of reduced relative ice thickness for larger wind turbines was identified, as shown in Figure 4.5. This reduction in relative rime icing is not a direct result of the rotor radius, but rather can be viewed as a result of the larger chord and thereby dimensionally thicker blades used on larger wind turbines.

There may also be many conditions where the trend identified here will not apply. One example could be at a location where a larger wind turbine, with its greater height, comes in contact with low clouds more often than a smaller wind turbine would at the same location. Another example could be with freezing rain, where the large droplets are not significantly affected by the airflow around the blades. Future work may reveal other conditions where this trend also does not apply. But, in the case of situations where wind turbines will operate in similar icing conditions this trend may be of use to give a general idea of how rime icing may affect different size wind turbines.

Finally, it should be clarified that in spite of icing being relatively less significant for larger wind turbines, icing will still be able to cause all of the problems mentioned in Chapter 1 when the proper conditions exist and therefor de- and anti-icing systems will still be needed at some sites.

4.1.3 Section summary

Icing on a section of blade for four different wind turbine sizes were modeled using TURBICE. The results indicate that dry rime icing is less severe for larger wind turbines both in terms of local ice mass and in terms of relative ice thickness. The results indicate that a major reason seems to be the lower collection efficiency of the larger chord, and thereby dimensionally thicker, blades.

These results give rise to a number of new questions about icing on wind turbines. Modeling of other conditions, including different wind speeds, glaze icing and

the transition from rime to glaze should be performed. In addition, wind tunnel experiments to verify the results would be useful. The effects on power production should be investigated by calculation or wind tunnel experiments to determine the change in drag and lift coefficients. Additionally, modeling of larger pitch regulated wind turbine profiles would also be interesting to see if the same trend applies to them. Comparison of full-scale measurements on wind turbines of different sizes at the same location would be useful to determine if the results also occur in actual conditions, but the results would still be limited to the turbines tested, and may be prohibitively expensive.

4.2 Turbine size sensitivity of rime and glaze ice

The previous section showed that for dry rime icing the icing becomes less significant for larger turbines, in terms of local ice mass and in terms of relative ice thickness. In this section the different types of icing shapes that result from atmospheric icing are described, and their effects on aerodynamic properties of airfoils. Thereafter modeling work to determine how atmospheric ice accretion changes for different sized turbines under a wider range of atmospheric parameters than that used in the previous section are described together with their results.

4.2.1 Ice shapes

Atmospheric icing of an airfoil gives a range of ice shapes resulting from different temperature/heat balance situations. Gent et al. [67] describes transition between three main types; rime, glaze and beak, as the accretion temperature goes from low to high. Shin et al. [30] showed the transition between different ice shapes with only changing air temperature and showed some additional intermediate shapes not shown by Gent et al. [67]. The same general shapes were duplicated with the TURBICE icing model [32], and are shown in Figure 4.7.

A short description of the shapes and transitions between them follows. Rime icing forms at the lowest temperatures when all droplets freeze upon impact and can be described as an extended nose, as shown in Figure 4.7a. At some higher temperature, the stagnation line (center of the nose) reaches 0 °C and the ice there forms with a higher density. This causes the nose to become flattened on the front, as shown in Figure 4.7b.

For even higher temperatures, not all of the impinging water at the stagnation line freezes at impact, some begins to drain away from the stagnation line and as the center of the nose becomes shorter, a double horn shape forms, with the horns pointing more forward, as seen in Figure 4.7c. For even higher temperatures the horns begin to rotate away from the stagnation line.

For still higher temperatures the lower horn flattens and the upper horn points forward and upward, combined they form somewhat of a boot shape, as seen in Figure 4.7d. The lower horn then goes over to runback icing while the upper horn flattens as seen in Figure 4.7e. Finally, there is runback icing forming on both surfaces of the blade, Figure 4.7f, before the leading edge melts away and beak icing occurs.

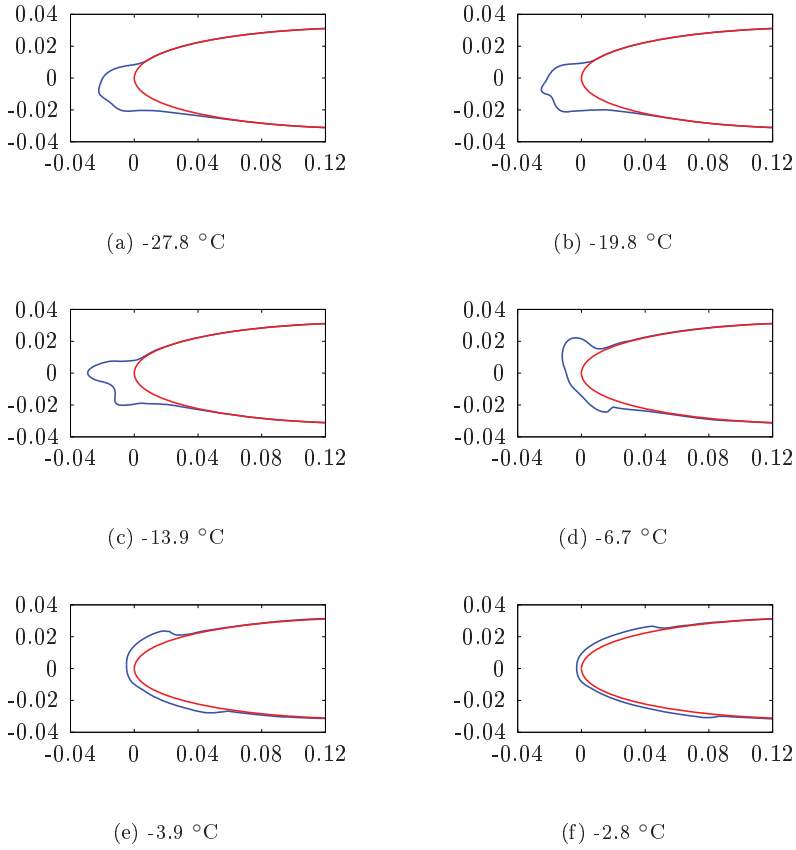

(a) -27.8 °C (b) -19.8 °C

(c) -13.9 °C (d) -6.7 °C

(e) -3.9 °C (f) -2.8 °C

Figure 4.7: Typical airfoil ice shapes showing effect of air temperature on ice shapes. Profile in NACA 0012, chord length 0.53 m, $V_\infty = 58$ m/s, angle of attack 4°. Calculated by TURBICE and previously shown in Makkonen et al. [32]

The examples in Figure 4.7 illustrate the general transitions between ice shapes. Many variations which may be difficult to quantify as exactly one of these shapes have been seen both in windtunnel experiments and in the field. This is due to, amongst other things, changing conditions during the icing encounter.

4.2.2 Aerodynamic effects of ice shapes

Shin et al. [30] investigated the effect of icing on the drag coefficient of an airfoil. It was shown, as can be seen in Figure 4.8, that the drag coefficient had a temperature dependence that is relatively constant through the rime ice region, increases with increasing temperature (due to the transition to formation of horns and upward facing horns) and then drops sharply as higher temperatures melt the horns and finally all ice. The higher drag coefficient at intermediate temperatures corresponds

to the horn shaped icing causing a larger aerodynamic disturbance than the more streamlined dry rime.

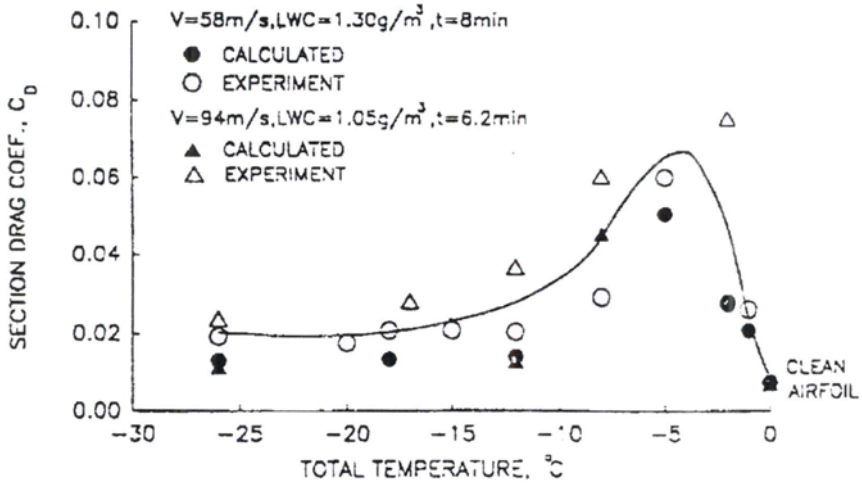

Figure 4.8: Variation of drag coefficient with total temperature. Differences in drag are due to different ice shapes forming with different temperatures. The highest drag shapes result from glaze ice with upward facing horns [30, p.20].

The work in the previous section showed that dry rime icing was less significant for larger wind turbines than for smaller, in terms of local ice mass and in terms of relative ice thickness. The objective of the work described in this section was to determine if that trend holds also at higher temperatures, or if the transition to glaze icing changes the previously observed trend.

4.2.3 Numerical setup

The TURBICE icing program, [32], was used for the modeling, as described in section 4.1.1.

Since it was possible to model only a few types of conditions in a reasonable amount of time, the conditions used in the previous section were repeated for higher temperatures, and a 5 MW pitch controlled turbine was added. This gave a total of 100 different modeled events.

The conditions chosen are shown in Table 4.4. The relative speed is the wind speed relative to the modeled section of the blade for the turbine operating with a free stream wind speed of 10 m/s. Of the five wind turbines modeled, two were passive stall controlled, two active stall control and one pitch controlled.

Details of the wind turbines and blade profiles at the modeled radius are shown in Table 4.5.

Table 4.4: Modeled icing conditions.

Wind speed [m/s]	10
Droplet size, MVD [µm]	12, 15, 17, 20, 30
Liquid water content, LWC, w, [g/m^3]	0.2
Air temperature, T, [°C]	-10, -7.5, -5, -2.5
Simulation time [min]	120

Table 4.5: Wind turbine details.

Type	Passive stall		Active stall		Pitch controll
Power	450 kW	600 kW	1 MW	2 MW	5 MW
Rotor radius [m]	18.5	22	27	35	63.5
Airfoil name NACA	63215	63417	63417	63416	634618
Rotation speed [rpm]	30	27	22	18	12
Chord length [m]	0.747	0.844	0.99	1.435	1.846
Relative speed, v, [m/s]	49.66	53.20	53.87	57.37	67.3
Angle of attack, [deg]	8.4	8.2	7.8	7.0	6.0
Radius of simulation [m]	15.5	18.5	23	30	53

4.2.4 Results and discussion

In spite of the limitations placed on the number of parameter variations there were considerable combinations of parameters and effects that could be examined with these simulations. The effect of the following parameters are discussed in more detail; ice mass, ice thickness, ice shapes, stagnation line temperatures and the heat balance at the stagnation line.

Ice mass

While local ice mass increases slightly with increasing turbine size, the mass relative to the total blade mass decreases. Simple scaling would give an increase in blade mass as the cube of the radius, but for production blades a lower exponent ($R^{2.3}$) was found by Veers et al. [74]. Since the simulation results give the amount of icing per meter, Figure 4.9 shows the blade mass trend from Veers et al. [74] divided by rotor radius, in other words, ($kR^{2.3}/R = kR^{1.3}$), where k here was set to $1/30$ so that the ice and blade mass trends can be compared in the same figure. From this figure it is clear that the ice mass relative to the blade mass is becoming less significant for the larger turbines in all of the conditions.

Since there were variations in both droplet size and turbine size for each temperature, a two dimensional plot did not illustrate the ice mass changes well. Therefore the ice masses were plotted as a three dimensional surface at each of the four temperatures, as shown in Figure 4.10. It can be seen that the absolute ice mass tends to increase slightly with turbine size for all but the smallest, 12 µm, droplets. It can also be seen that the dependence of ice mass on droplet size increases with turbine size, making knowledge of droplet size more important for estimating ice loads on larger turbines. The ice mass is relatively unaffected by the air temperature. This

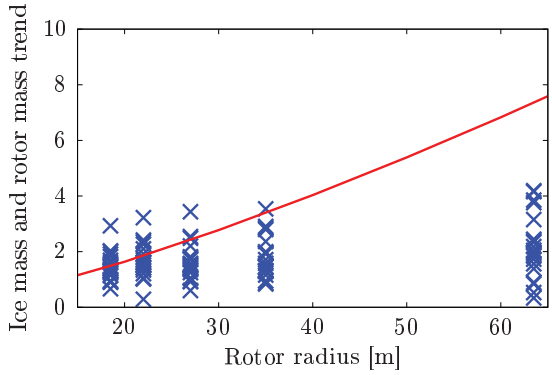

Figure 4.9: Ice mass per meter for all modeled cases (X) compared to the trend of rotor mass per meter (line) found by Veers et al. [74].

must mean that all or nearly all of the collected water droplets are freezing on the surface in all of the cases.

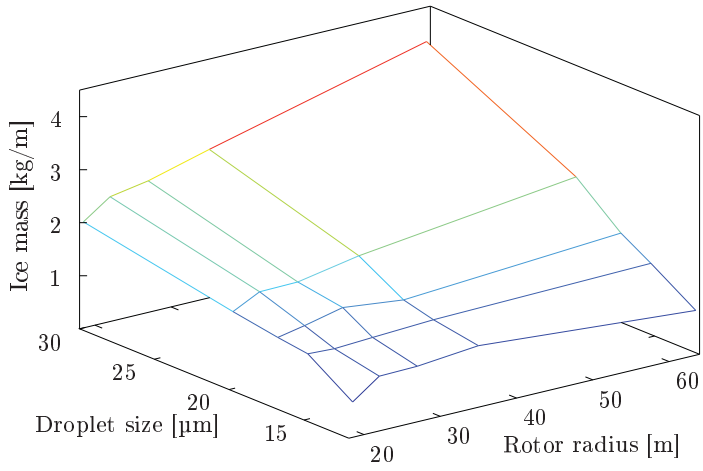

(a) -10 °C

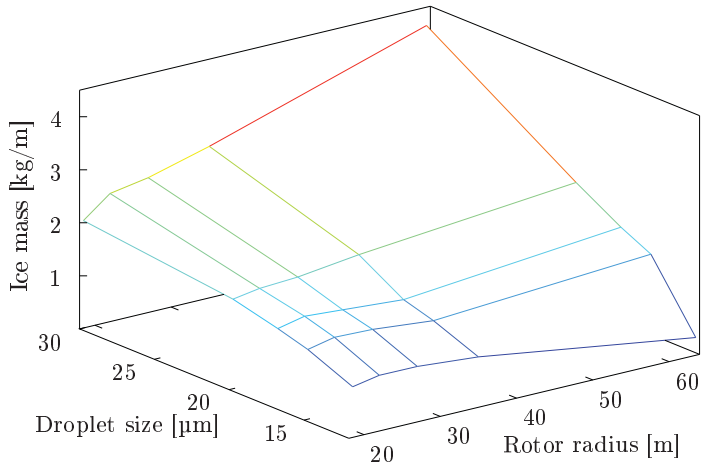

(b) -7.5 °C

Figure 4.10: Modeled ice mass increases more with rotor radius for larger droplets than for small. Temperature does not have a large effect on the ice mass.

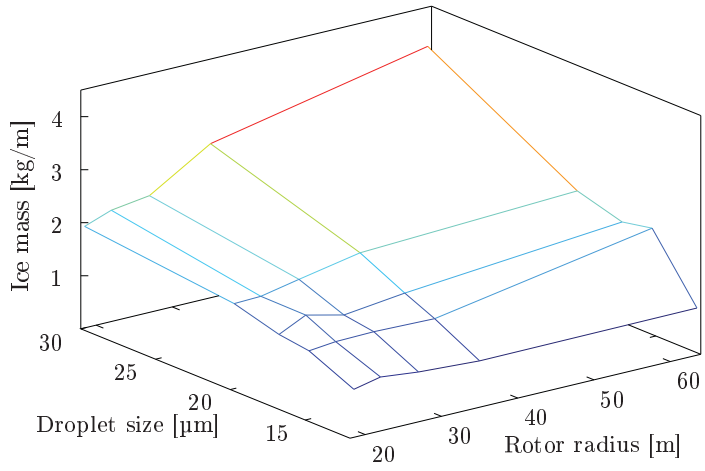

(c) -5 °C

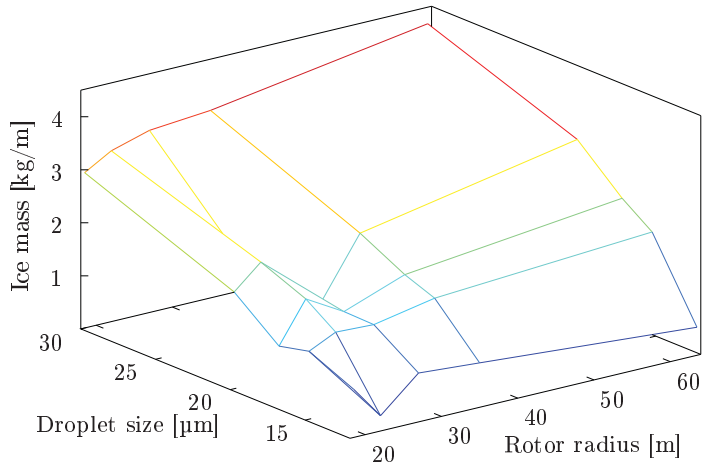

(d) -2.5 °C

Figure 4.10: Modeled ice mass increases more with rotor radius for larger droplets than for small. Temperature does not have a large effect on the ice mass.

Ice thickness

TURBICE also gives as output the maximum ice thickness for each simulation, so that for similar shapes the ice thickness can be compared directly. The ice thickness is measured perpendicular to the airfoil surface, and is the distance from the airfoil surface to the ice surface. For the set of conditions modeled here the ice shapes were not all similar so that the maximum ice thickness is perhaps less relevant, but the thickness is examined in any case. The maximum ice thickness for each condition is shown in Figure 4.11. The ice thickness is nearly constant for the dry rime conditions at -10 °C and -7.5 °C. For -5 °C the maximum thickness increases slightly with turbine size and for -2.5 °C it seems to be decreasing slightly with turbine size, but the variation also increases. The reasons for this change in the relationship to turbine size are explored further in the discussion of the heat balance analysis.

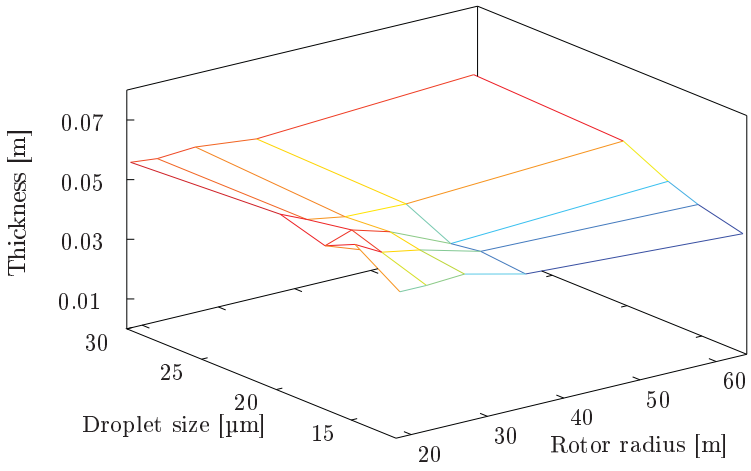

(a) -10 °C

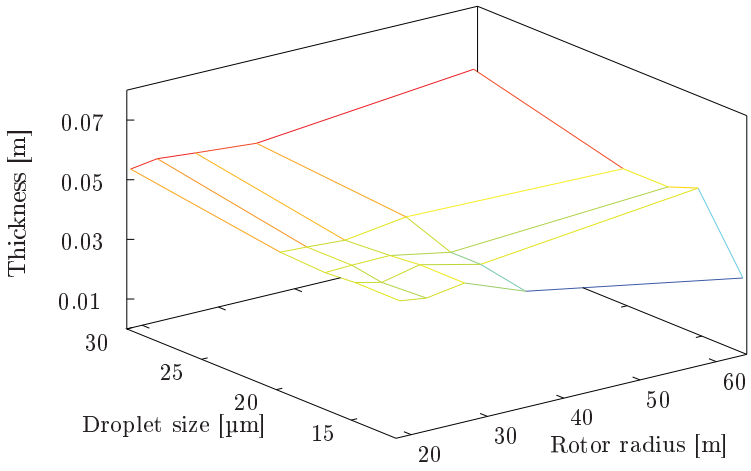

(b) -7.5 °C

Figure 4.11: The relationship from droplet size and rotor radius to ice thickness changes slightly with temperature.

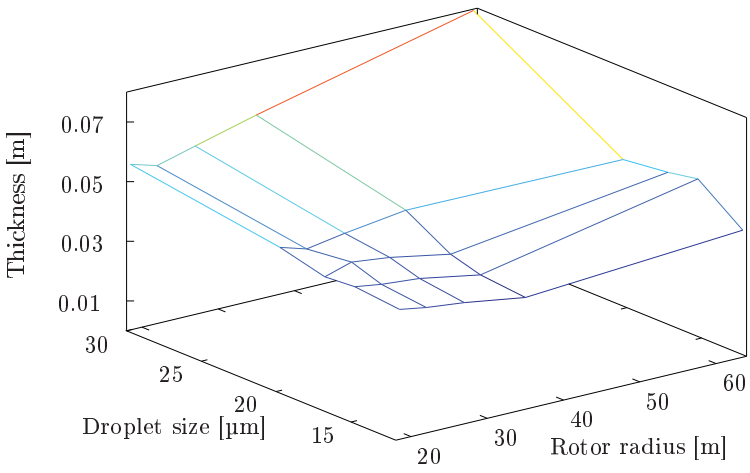

(c) -5 °C

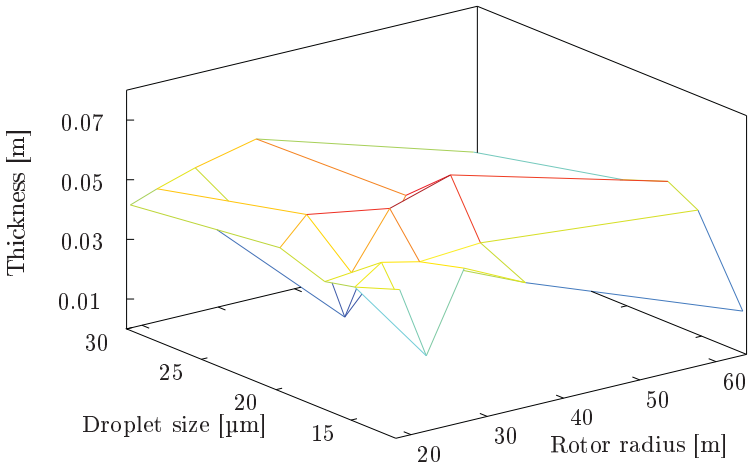

(d) -2.5 °C

Figure 4.11: The relationship from droplet size and rotor radius to ice thickness changes slightly with temperature.

Ice shapes

For the ice shapes, it is not practical to show all 100 shapes, and these 100 are only examples, but Figure 4.12 shows a set of the model results for all turbine sizes, four temperatures and with 30 µm droplets, to illustrate the general trends.

Figure 4.12a shows that at -10 °C the ice shapes on the different size turbines are nearly the same and have similar thickness, thereby becoming less significant in terms of relative ice thickness for larger turbines, as shown in the previous section. The same is also true at -7.5 °C, as seen in Figure 4.12b. For similar ice shapes, the ice thickness relative to chord seems to be the best indicator of the relative performance penalty incurred by the ice accretion, since the drag and lift data is not available. On this basis the icing at these temperatures (-7.5 °C and -10 °C) is also becoming less significant in terms of the aerodynamic penalty for the larger turbines.

Comparing the subfigures in Figures 4.10 and 4.11 shows that the maximum ice thickness and mass trends are relatively insensitive to temperature. Figure 4.12c shows, however, that the ice shapes are not similar. Here it can be seen that while the 450 kW turbine is still accumulating an extended nose type of ice, the 2 and 5 MW turbines are accumulating horn ice, with the largest horns on the 5 MW turbine. Aerodynamically these horns are a worse problem than an extended nose, as they typically cause separation of flow and large changes in lift and drag [30, 67, 9]. These conditions seem, therefore, to be more severe aerodynamically for larger turbines, though CFD simulations are necessary to confirm this.

Finally, at the highest simulated temperature of -2.5 °C, the situation seems to be better for the larger turbines with the horns being more pronounced for the smaller turbines.

Figure 4.13 shows the range of ice shapes on the 5 MW turbine at -2.5 °C and illustrates that with increasing droplet size, the icing becomes wetter, with the horn being more melted and rotated rearward for the larger droplets.

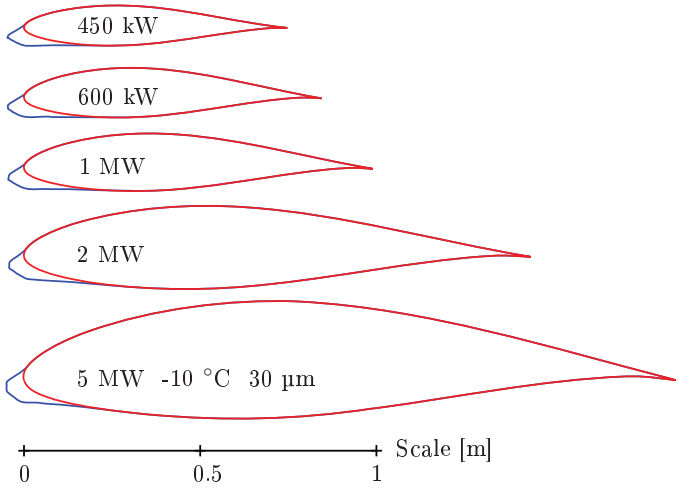

(a) -10.0 C

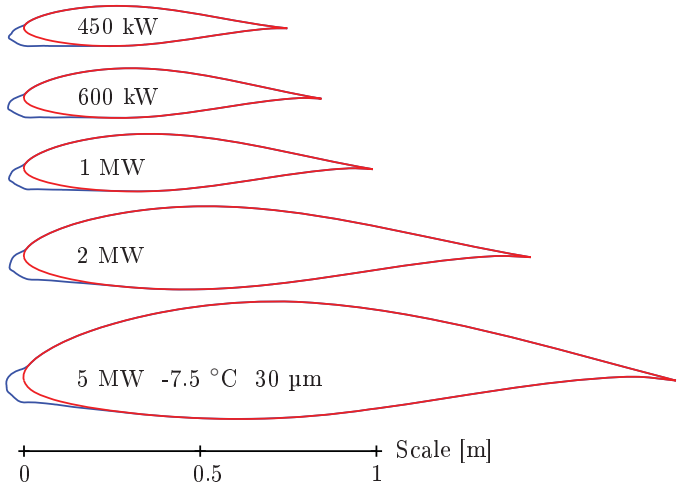

(b) -7.5 C

Figure 4.12: Ice shapes change with temperature.

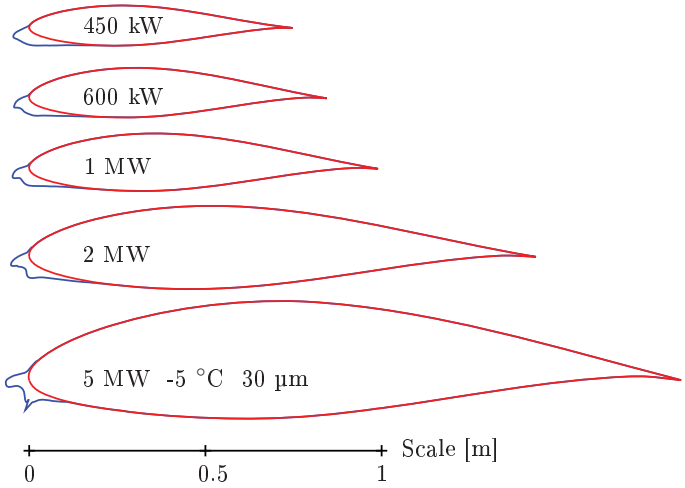

(c) -5.0 C

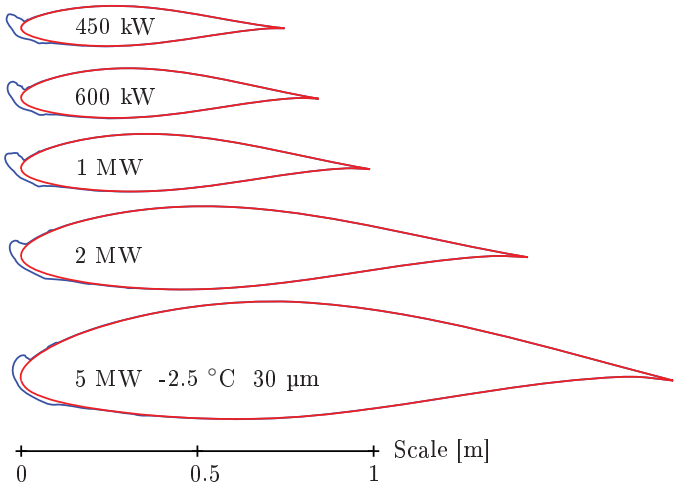

(d) -2.5 C

Figure 4.12: Ice shapes change with temperature.

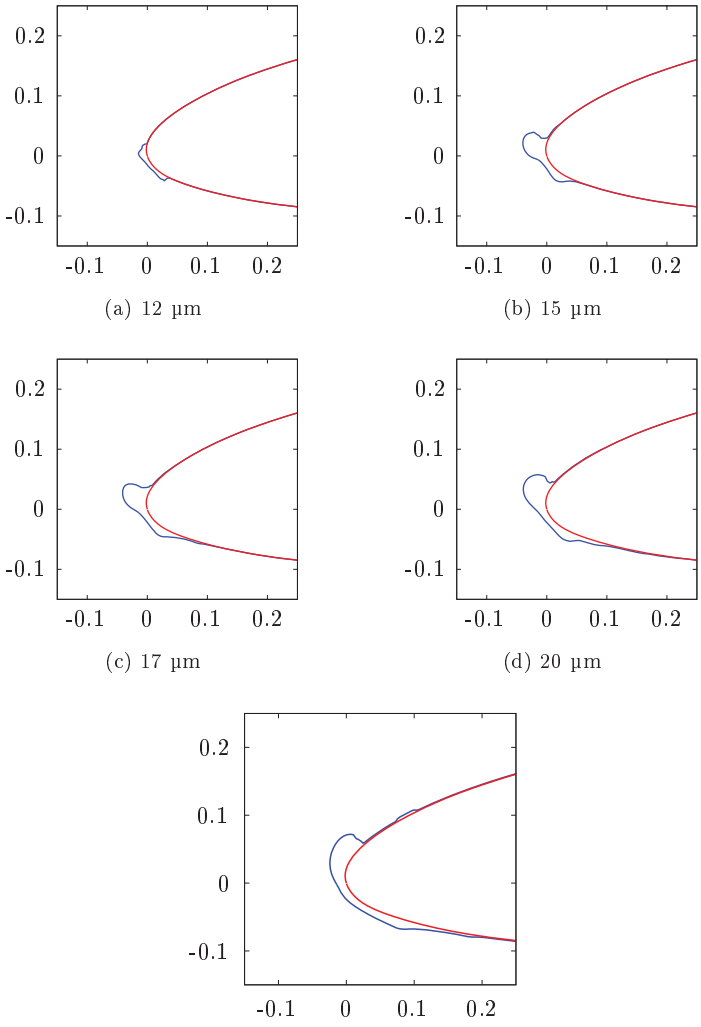

(a) 12 µm (b) 15 µm

(c) 17 µm (d) 20 µm

(e) 30 µm

Figure 4.13: Ice shapes on 5 MW turbine at -2.5 °C. The horn is rotated more rearward for the largest droplets.

Stagnation line temperature

It was noted that the stagnation line temperature is always higher than the ambient temperature and that the temperature difference between ambient and the stagnation line varies with turbine and droplet size. Figure 4.14 illustrates these temperature variations for each of the temperatures modeled. This variation in temperature means that the transitions between icing types will occur at different temperatures depending on the turbine and droplet sizes, and probably also with wind speed and liquid water content, though the impact of changing the last two was not investigated in this work.

Since this dependence of the stagnation line temperature on turbine size is important for which types of ice shapes the different size turbines will collect for the same temperature, the change in the stagnation line temperature was further investigated. This was done by examining the local heat transfer coefficient and collection efficiency at the stagnation line for the case of 100% rime icing so that complications due to water runback could be avoided. In this case the results at -10 °C were chosen. Figure 4.15 shows that the heat transfer coefficient and collection efficiency are both decreasing for larger turbines. To evaluate the change in blade heating caused by the change in collection efficiency, the latent heat released during freezing, q_f, was calculated.

$$q_f = \alpha_1 \cdot \alpha_2 \cdot \alpha_3 \cdot w \cdot v \cdot L_f \,, \quad \left[\frac{\mathrm{W}}{\mathrm{m}^2}\right] \tag{4.2}$$

where $L_f = 333$ [J/g] is the heat of fusion for water, w [g/m^3] is the mass concentration of the particles, v [m/s] is the relative velocity of the particles and the α_1, α_2 and α_3 terms are the correction factors introduced in equation 2.15. The sticking efficiency, α_2, and accretion efficiency, α_3, are both set equal to 1.0 for rime icing, as in this case. The result is shown in Figure 4.16 and illustrates that while the collection efficiency is decreasing for the larger turbines, the increased relative velocity at which larger turbines operate results in heating from droplet freezing that is nearly constant at the stagnation line.

This combination of decreasing heat transfer coefficient and constant heating due to droplet freezing is the main cause of the higher stagnation line temperatures observed for the larger turbines. This is significant because it shows that icing of wind turbines cannot be classified by the air temperature and droplet size alone, but the resulting icing type also depends on the size of the turbine.

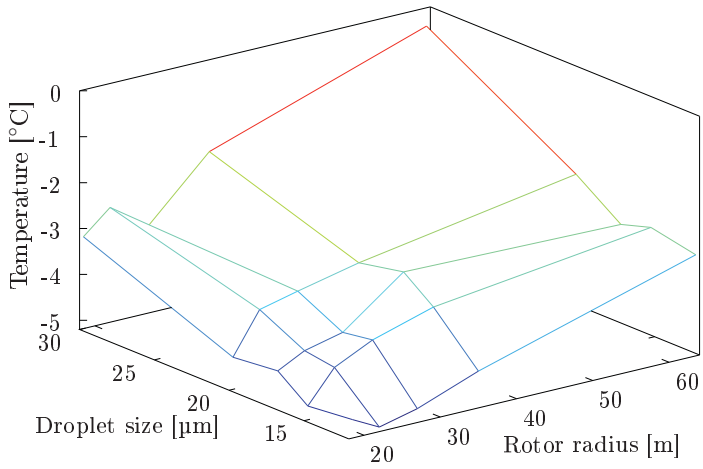

(a) -10 °C

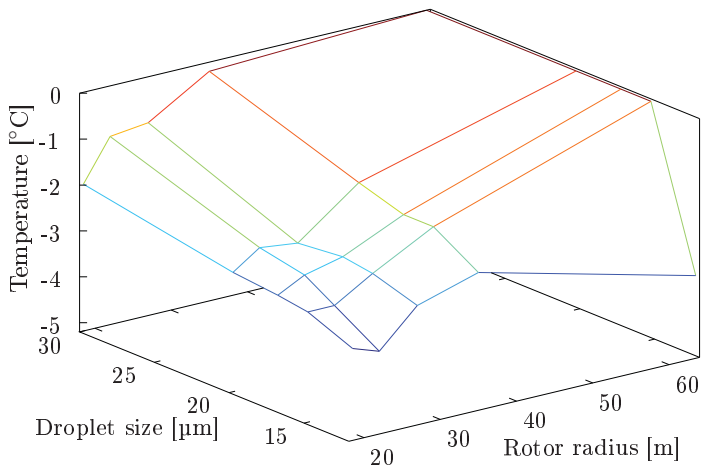

(b) -7.5 °C

Figure 4.14: Stagnation line temperatures

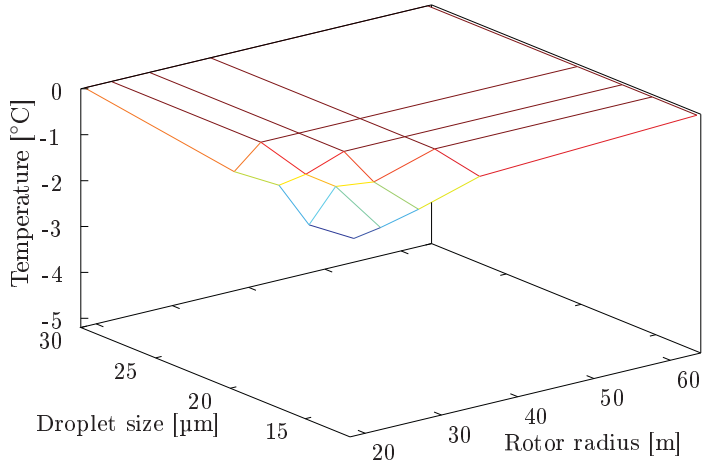

(c) -5 °C

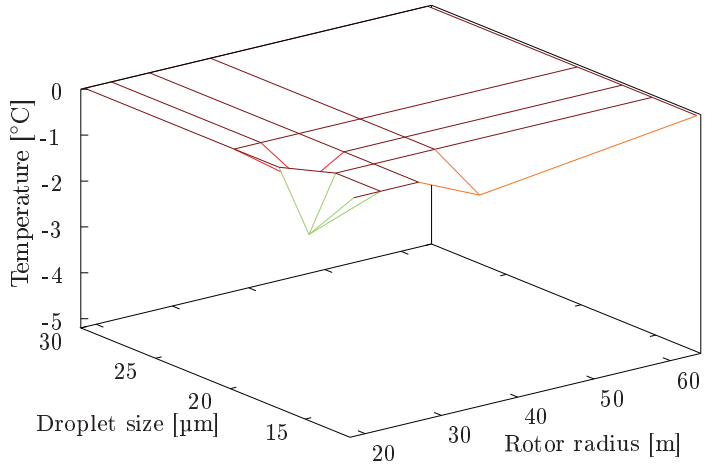

(d) -2.5 °C

Figure 4.14: Stagnation line temperatures

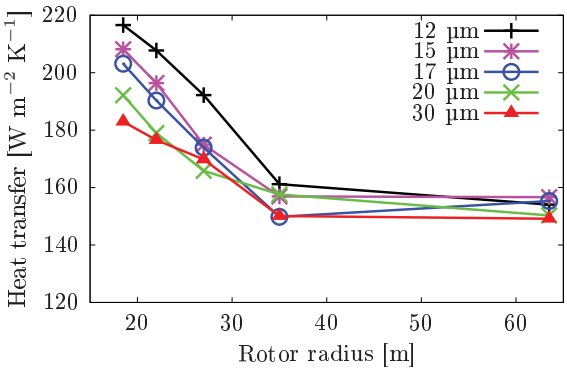

(a)

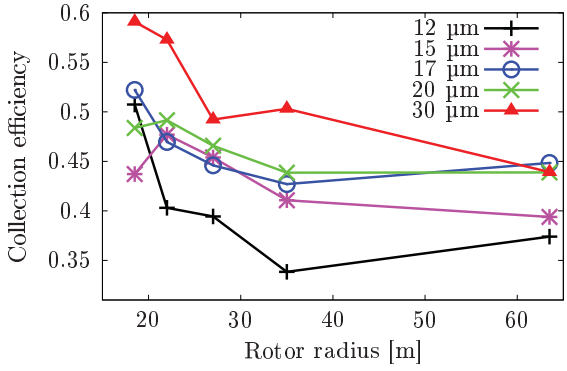

(b)

Figure 4.15: Local heat transfer coefficient (a) and collection efficiency (b) calculated by Turbice for the stagnation line after 120 min. modeled icing.

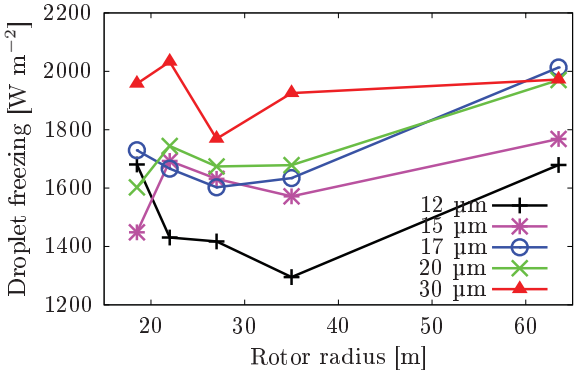

Figure 4.16: Local heating from droplet freezing at the stagnation line.

Heat balance analysis

To better understand the changes in temperature occurring at the stagnation line, the terms of the heat balance equation

$$q_{freeze} + q_{aero} + q_{kin} - q_{conv} - q_{sub} - q_{warm} - q_{rad} = 0\,, \qquad \left[\frac{\mathrm{W}}{\mathrm{m}^2}\right] \tag{4.3}$$

were examined. Each of the terms was calculated for the case of 17 µm droplets at -10 °C and the values calculated for the 2 MW turbine are shown in Table 4.6, in order of their significance for the 2 MW case. The increase in the values from the 450 kW to the 5 MW turbine is also shown. It can be seen that the dominant term is the heat of freezing q_{freeze} at over 1600 W/m^2, with convective cooling and sublimation as the main cooling terms at 1054 and 599 W/m^2 respectively.

Table 4.6: Heat balance terms for MVD = 17 µm and T= -10 °C.

	Value for 2 MW [W/m^2]	Difference 5 MW - 450 kW [W/m^2]	Percentage change Difference / 2 MW * 100 [%]
q_{freeze}	1638	284	17
q_{conv}	1056	147	14
q_{sub}	599	160	27
q_{aero}	208	85	41
q_{warm}	176	62	35
q_{rad}	15	6	38
q_{kin}	8	7	90

The aerodynamic heating, as the fourth largest term, is clearly having a noticeable impact on the result, especially for the larger turbines, as the increase in relative velocity, v, outweighs the decrease in the heat transfer coefficient, h. The increase in relative velocity results in a higher stagnation temperature. The difference between the air stagnation temperature (total temperature),

$$T_0 = T + \frac{v^2}{2C_p}\,, \qquad [^\circ\mathrm{C}] \tag{4.4}$$

and the free stream temperature (T) increases from 1.2 K for 49.66 m/s to 2.3 K for 67.3 m/s.

The droplet kinetic energy, q_{kin}, while not included in the current TURBICE heat balance calculation, increases sharply with relative velocity but is still more than a factor of 100 less than q_{freeze}.

Discussion

In the work described in this section it was found that the ice surface temperature varies both with the turbine size and the cloud droplet size. This means that for equal conditions, different sized turbines may collect different ice shapes, which cannot be intuitively compared.

While the aerodynamic effects of similar ice shapes may be evaluated based on their size relative to the chord, ice shapes which are dissimilar can not be evaluated

in this way, as different ice shapes can have very different effects on drag and lift. For the coldest case studied, the ice shape did not vary with turbine size when the conditions were constant. On the other hand, at warmer temperatures, the ice shapes show a dependency on turbine size and become dissimilar. For these warmer temperatures it can not be assumed that a given icing event will be less significant for a larger turbine, since the ice shape may be quite different for a larger turbine. This different ice shape can have either a higher or lower aerodynamic penalty compared to the ice shape accreted on a smaller turbine, even though the relative ice mass and thickness can be less.

Therefore, it can be concluded from this study that the trend of less significant rime ice accretions for larger turbines identified in the previous section cannot automatically be extended to warmer conditions because glaze ice shapes depend on turbine size. It will be necessary to perform CFD and/or wind tunnel testing of the calculated ice shapes to determine their effect on aerodynamic performance.

This dependence of ice shape on turbine size results from the changing heat balance with turbine size, and is affected by the changes in chord length, blade profile and relative wind speed. All of these parameters are results of an optimization process during the design of a wind turbine. Hence, by considering icing in the design process, it may be possible to influence the resulting heat balance and improve the performance of a wind turbine subject to icing.

Some ice shapes are aerodynamically worse than others and the work of Shin et al. [30] showed the highest drag ice shapes occurred with a total temperature of around -4 °C (air temperature -6.7 °C), shown in Figure 4.8. However, it can be seen from the transition between extended nose and horn ice shapes in that work that the stagnation line reached 0 °C at even lower air temperatures. This can be explained by the higher liquid water content (1.3 g/m^3) used in those experiments compared to this work. The key point is that the shape of the ice formed depends on the heat balance during ice accretion.

Based on the work performed here it can be seen that the heat balance is getting warmer for larger turbines, which corresponds to shifting the curve of Figure 4.8 to the left. It was also seen here that the size of the ice shapes as percentage of chord is reduced for larger wind turbines. In the work of Kim and Bragg [75] it can be seen that smaller ice shapes (as percentage of chord) resulted in less of a detrimental impact on the drag coefficient. Since the larger turbines are seen to accrete relatively smaller ice shapes, this corresponds to shifting the curve of Figure 4.8 downward. The combination of these two effects is shown in Figure 4.17, a theorized version of how airfoil drag versus temperature curves for different sized turbines might compare. While there are yet many uncertainties in this theory, including the effects of changing Reynolds number for different sized turbines, it seems that icing will have less of a detrimental impact on the energy production of larger wind turbines.

The simulations of this study also show that atmospheric icing is a complex physical process and that even under identical conditions different wind turbines are likely to accrete ice differently. This suggests that maps of the number of icing days per year at various sites may not adequately show how a certain wind turbine will perform at that site. Rather it becomes necessary to know the temperature and droplet size during the specific icing event to be able to predict the effect on a

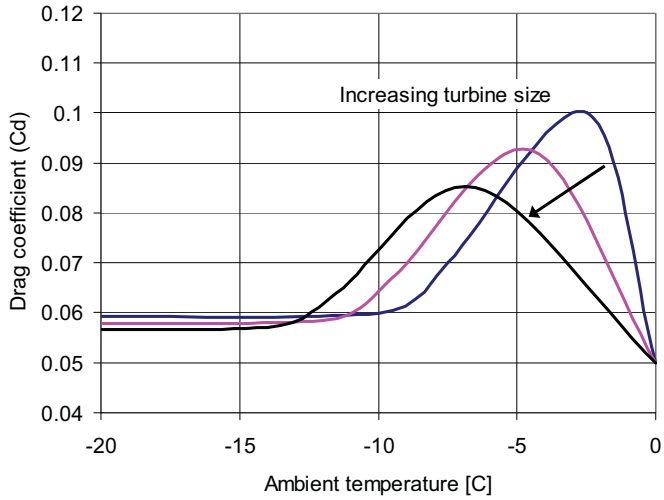

Figure 4.17: Theorized set of iced airfoil drag curves from different icing temperatures for different sized turbines.

specific wind turbine.

4.2.5 Section summary

Two dimensional modeling of atmospheric icing on blade sections at 85% radius of five different wind turbines was performed by varying droplet size and air temperature. The results show that the stagnation line temperature during rime ice accretion is warmer on larger turbines than smaller turbines when the other parameters are kept constant. This occurs because, with increasing turbine size, the decrease in the heat transfer coefficient is more significant than the decrease in the droplet collection efficiency. The higher speed of the larger turbine blades also acts to increase their surface temperature.

The higher stagnation line temperature means that the ambient temperature at which the ice shapes with highest drag coefficients (horn ice) form is lower for larger turbines. Therefore, while atmospheric icing is generally becoming less significant in terms of relative ice mass and thickness for larger turbines, the temperatures at which the transition shapes between glaze and rime form is generally lower for larger turbines.

The results showed that the dependence of ice mass on droplet size increases with turbine size. This indicates that knowledge of droplet size is important for estimation of ice loads on larger turbines.

Future work should include testing how the different ice accretions affect the drag and lift coefficients of the blades as well as icing wind tunnel verification of these results. Further analysis to examine the effects of varying other parameters

would also be interesting, as changes in wind speed and liquid water contents can be expected to produce relevant, although more predictable, changes.

4.3 Ice Accretion on Large Wind Turbine Blades

In this section computational fluid dynamics based numerical analyses were carried out to study the rate and shape of ice growth on a large wind turbine blade. The NREL 5MW wind turbine blade [1] was selected as the test case for this study, mainly because of its large radius and geometric features, and because the geometry data is openly available. Analyses were carried out at different atmospheric icing temperatures and time intervals. The objective of this study was to analyze the rate and shape of ice growth at different locations along a large wind turbine blade. Effects of blade geometric and atmospheric parameters variation are also included in this study.

Atmospheric icing on the wind turbine blades has been numerically modeled for a variety of cases in the past [6, 13, 14, 15], where major parts of these numerical analyses were of 2D. It should be noted that, while important information can be learned from two-dimensional modeling, certain physical phenomenon must be obtained from three-dimensional numerical modeling, because angular movement of the wind turbine blade can produce significant span wise radial flow and also the turbine blades in use are both tapered and twisted in the radial direction, which can significantly alter the aerodynamic characteristics of the blade.

Since all of the parameters are changing along the length of a wind turbine blade, it is necessary to model the changes to understand how the combined variations of these parameters affect the resulting ice accretion.

4.3.1 Numerical Setup

The NREL 5 MW wind turbine's blade radius used for this study is 63 m long and it was not possible to numerically model the icing on the whole blade due to limited computational resources. Therefore five sections were selected along the blade radius, where each section was 0.5 m long. The selection of the tested sections was weighted towards the outer portion of the blade, as previous work has shown more ice on the outer half of the wind turbine blade [71, 76]. The numerical analyses were carried out at different atmospheric temperatures and time intervals to study the rate and shape of ice growth for each section. These numerical analyses were carried out using an ice accretion solver FENSAP-ICE from NTI [77]. Each selected section along the blade has different geometric characteristics (chord length, twist angle, thickness to chord ratio). Figure 4.18 shows the blade profiles along the blade. Table 4.7 shows the geometric characteristics of the complete blade, where the highlighted sections were used for these analyses.

These numerical analyses were performed at five different radial positions (13.25, 33.75, 41.95, 54.25 and 63.13 m). Each numerical simulation included two major parameters, the relative wind speed (v) and the angle of attack (α). These parameters depend upon the free stream wind speed (V_∞), the axial and tangential induction factors (a and a'), the modeled section's radius (r), the local speed ratio

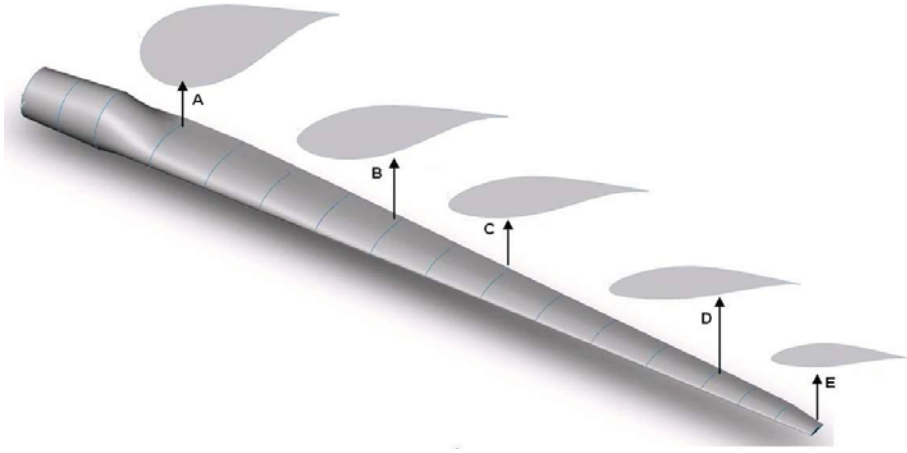

Figure 4.18: 3D CAD of the NREL 5 MW wind turbine blade, showing the selected sections.

Table 4.7: Distributed NREL 5 MW wind turbine's blade geometric properties [12]. The highlighted sections were used for these analyses.

Node	Blade radial location [m]	Chord length [m]	Aerodynamic twist [deg]	Airfoil table
1	4.3667	3.542	13.308	Cylinder
2	7.1	3.854	13.308	Cylinder
3	9.833	4.167	13.308	Cylinder
4	13.25	4.557	13.308	DU 40
5	17.35	4.652	11.480	DU 35
6	21.45	4.458	10.162	DU 35
7	25.55	4.249	9.011	DU 30
8	29.65	4.007	7.795	DU 25
9	33.75	3.748	6.544	DU 25
10	37.85	3.502	5.361	DU 21
11	41.95	3.256	4.188	DU 21
12	46.05	3.010	3.125	NACA 64618
13	40.15	2.764	2.319	NACA 64618
14	54.25	2.518	1.526	NACA 64618
15	57.66	2.313	0.863	NACA 64618
16	60.4	2.086	0.370	NACA 64618
17	63.13	1.419	0.106	NACA 64618

(λ_r) and the blade twist angle (ϕ) at that section. The relative wind speed and angle of attack at each section is calculated by ;

$$v = \sqrt{(V_\infty(1-a))^2 + (V_\infty \lambda_r)^2}, \qquad [\mathrm{m/s}]. \tag{4.5}$$

$$\beta = \tan^{-1}\left(\frac{\lambda_r(1+a')}{1-a}\right) \tag{4.6}$$

And the local speed ratio was calculated by;

$$\lambda_r = \frac{\lambda r}{R} \tag{4.7}$$

where R is the rotor radius. The axial and tangential induction factors were iteratively calculated using the blade element momentum theory without tip loss corrections and assuming $C_d = 0$, with the following equations [16], where σ_r is the local solidity and $\beta = 90 - \alpha - \phi$ is the angle of the relative wind.

$$a = \frac{1}{1 + \frac{4\cos^2\beta}{\sigma C_l \sin\beta}} \tag{4.8}$$

$$a' = \frac{1}{\frac{4\sin\beta}{\sigma C_l} - 1} \tag{4.9}$$

Blade element momentum theory (BEM) is commonly used in analysis of wind turbine rotors and is based on the principal that the forces exerted on the rotor must be reflected in a change in momentum of the air passing through the rotor. The aerodynamic lift coefficients used for the BEM method were obtained from the tables published by NREL [1].

All the analyses were carried out at a free stream velocity, V_∞, of 10 m/s, and blade tip speed ratio, λ, of 7.55. Table 4.8 shows the values of axial induction factors, relative wind speeds and the angle of attacks at each selected section along the blade used for this study.

Table 4.8: Test sections operating conditions.

Blade section	Blade radius [m]	Relative wind velocity [m/sec]	Angle of attack [degree]	Axial induction factor (a)
A	13.25	17.36	9.0	0.2969
B	33.75	41.07	3.5	0.2766
C	41.95	50.7	3.3	0.3317
D	54.25	65.33	4.3	0.3303
E	63.13	75.88	5.8	0.2134

A structured type numerical grid was used for each section, where as to accurately determine the boundary layer characteristics (shear stresses and heat fluxes), a y+ value less than 1 was used near the wall. The blade profiles roughness height was calculated according to Shin et al. [30]. The air flow around the wind turbine is typically turbulent at high Reynolds numbers. The one equation Spalart Allmaras turbulence model was used as a compromise between acceptable computational cost and the required accuracy in modeling the turbulent flow. The two phase flow was solved using Eulerian-Eulerian approach in FENSAP-ICE. The main advantage of using Eulerian-Eulerian approach is that, the same mesh can be used for multiphase flow calculations and ice geometry. All the numerical modeling was carried out at the operating conditions specified in Table 4.9.

Table 4.9: Modeled icing conditions.

Free stream wind velocity, V_∞, [m/s]	10
Droplet size, MVD [µm]	20
Liquid water content, LWC [g/m^3]	0.22
Air temperature [°C]	-2.5, -5, -10, -15
Simulation time [min]	60, 180

4.3.2 Results and discussion

Flow Behaviour and Droplet Distribution

Numerical analyses of the air flow behaviour show a change in the velocity and pressure distribution along each selected section of the wind turbine blade. Change of geometric characteristics at each section from blade tip to root leads to changes in the relative velocity and angle of attack (Table 4.8) that effectively changes the flow behaviour along each section. Such change in the blade geometric characteristics is generally to avoid the stall of the blade root section. High flow separation is observed at root section (Section A) as compared to the blade center section (Section C) and tip section (Section E). Analyses show a shift in the position of the stagnation point at each section while moving from tip to root sections. This shift in the stagnation point changes the flow behaviour over the blade profiles and also effects the liquid water droplets distribution around the blade section and the rate of droplet impingement on the blade. Figure 4.19 shows the velocity distribution at three different sections (root, center and tip) of the wind turbine blade.

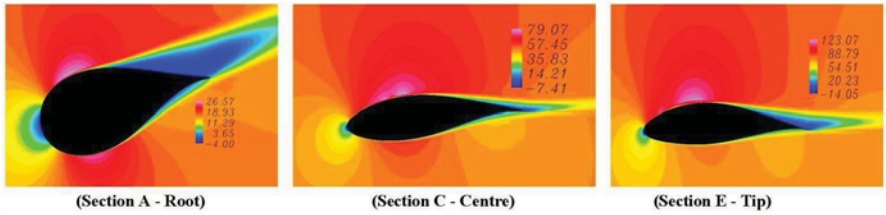

Figure 4.19: Velocity distribution at different sections of the NREL 5 MW wind turbine blade [m/s].

A liquid water droplet moving in the air stream is generally influenced by its drag and inertia, when neglecting the gravity and buoyancy [78]. If drag dominates the inertia the droplet follows the stream line whereas for the case where inertia dominates the particle hits the object. The ratio of inertia to drag depends upon the droplet size, velocity of air stream and dimensions of the object in question. Therefore with an increase in blade size (chord length) more droplets and especially the small droplets, move along the streamlines around the blade. As the blade sections near the root have larger chord length and thickness, results show low droplet

collision efficiency near the root section of the blade, while a high value of droplet collision efficiency is observed near the tip section. This trend is strengthened by changes in relative velocity. Lower relative velocity nearer the blade root reduces the influence of the inertial component of droplet motion and also allows more droplets to follow the streamlines around the blade. Figure 4.20 shows the droplet collision efficiency at three different sections of the wind turbine blade.

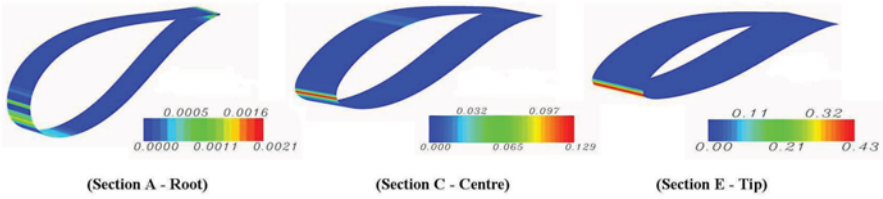

Figure 4.20: Droplet collision efficiency at different sections of the NREL 5 MW wind turbine blade.

Rate and Shapes of Ice Accretion

To study the rate and shape of ice accretion at different sections along the wind turbine blade, the numerical analyses were carried out for t = 60 and 180 min. The initial study was carried out for t = 60 min, to understand the ice growth mechanism at each selected section of the blade and later analyses were carried out for t = 180 min, to understand the effect of increase in icing time on rate and shape of ice growth. Results show that with the increase of blade profile chord length and thickness and reduced air velocity, the relative size of the accreted ice reduces. Such decrease in the size of accreted ice is mainly due to the decrease in collision efficiency of the droplets with the blade and the reduction in velocity, as can be seen in equation 2.15. Section E, which is at the blade tip, has a smaller chord and blade thickness ratio, as well as a higher velocity, therefore more ice accretion was found at this section, whereas results show a gradual decrease in rate and shape of ice accretion, when moving towards the root section of the blade. Figure 4.21 shows the ice growth and distribution at different sections of the blade at constant atmospheric temperature of -2.5 °C for t = 60 min.

A significant difference in ice growth can be seen between section E (blade tip) and section C (blade center). Although the area covered by the ice on section C is larger, the ice layer at section C is very thin, while at section E the accreted ice is considerably thicker as compared to section C. As mentioned above, with the increase of blade profile size, more of the super cooled water droplets follow the stream line and their collision efficiency reduces which leads to decrease in rate of ice growth at these sections. As section C has a larger chord and blade thickness therefore more water droplets follow the streamline at this section and do not hit the blade section. Meanwhile at section E, due to smaller profile size, the collision efficiency of the droplet is high and more ice accretion is observed at this section.

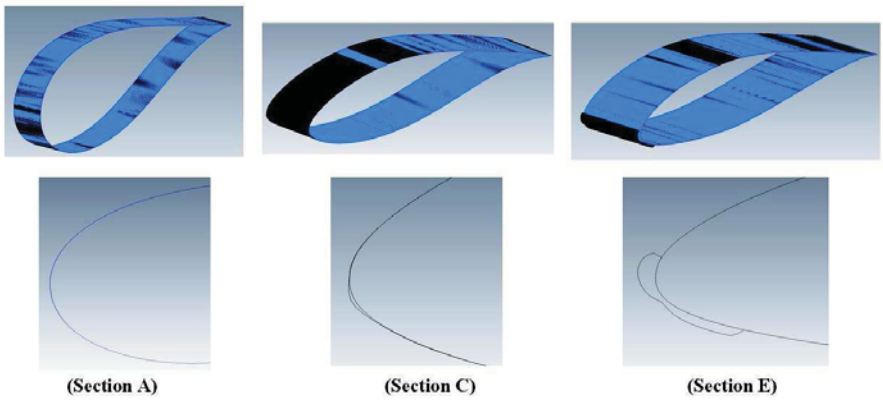

Figure 4.21: Rate and shape of ice accretion at different sections of the NREL 5 MW wind turbine blade at T=-2.5 °C for t = 60 min. (Black shaded area in the figure is the area covered by ice.)

To study the effect of atmospheric temperature variations on the rate and shape of ice accretion, analysis was carried out at four different temperatures (-2.5 °C, -5 °C, -10 °C and -15 °C), assuming a constant MVD of 20 µm, for t = 60 min. The purpose of this study was to understand the effect of atmospheric temperature variation on ice growth at different locations along the blade. Figure 4.22 shows the accreted ice shapes obtained from FENSAP-ICE at three different temperatures, on different sections of the blade.

To study the change in rate and shape of ice growth with icing time interval, numerical analysis were carried out at two different time intervals, 60 min and 180 min. Analysis show a significant change in the ice growth with the increase of icing time. The change was more significant near the blade tip section, whereas near the blade center section and root section, the change in ice growth was not significant. Results showed an increase in accreted ice thickness at blade tip section (Section A), whereas at center part of the blade (Section B), this change was not prominent. Although the area covered by the ice at blade center section (Section B) was greater, the thickness of ice at this section was almost negligible. Figure 4.23 shows the change in rate and shape of ice growth with respect to time at two different sections of the blade.

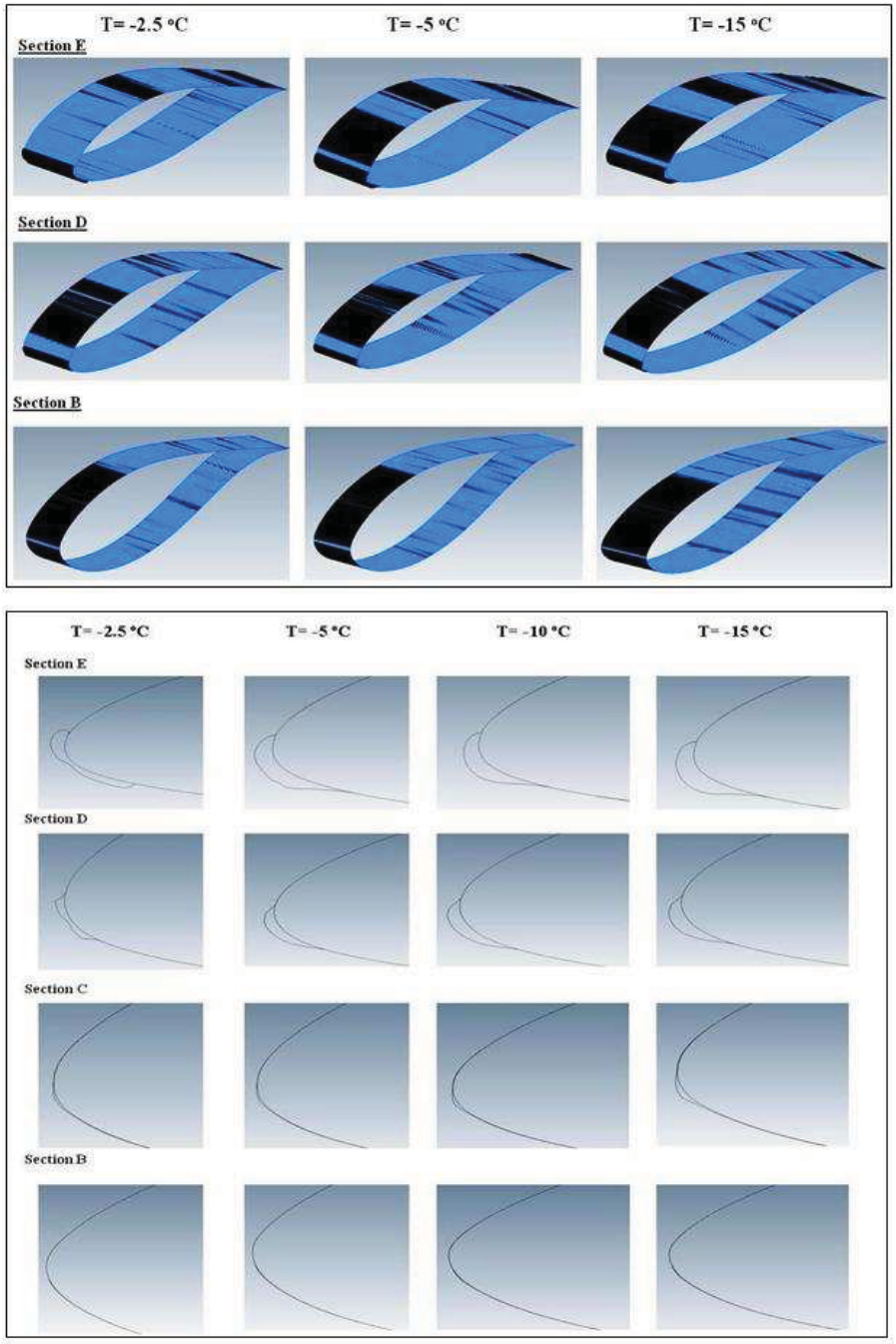

Figure 4.22: Effect of atmospheric temperature variation on rate and shape of ice accretion at different sections of the NREL 5 MW wind turbine blade for t = 60 min. (Black shaded area in the figure is the area covered by ice.)

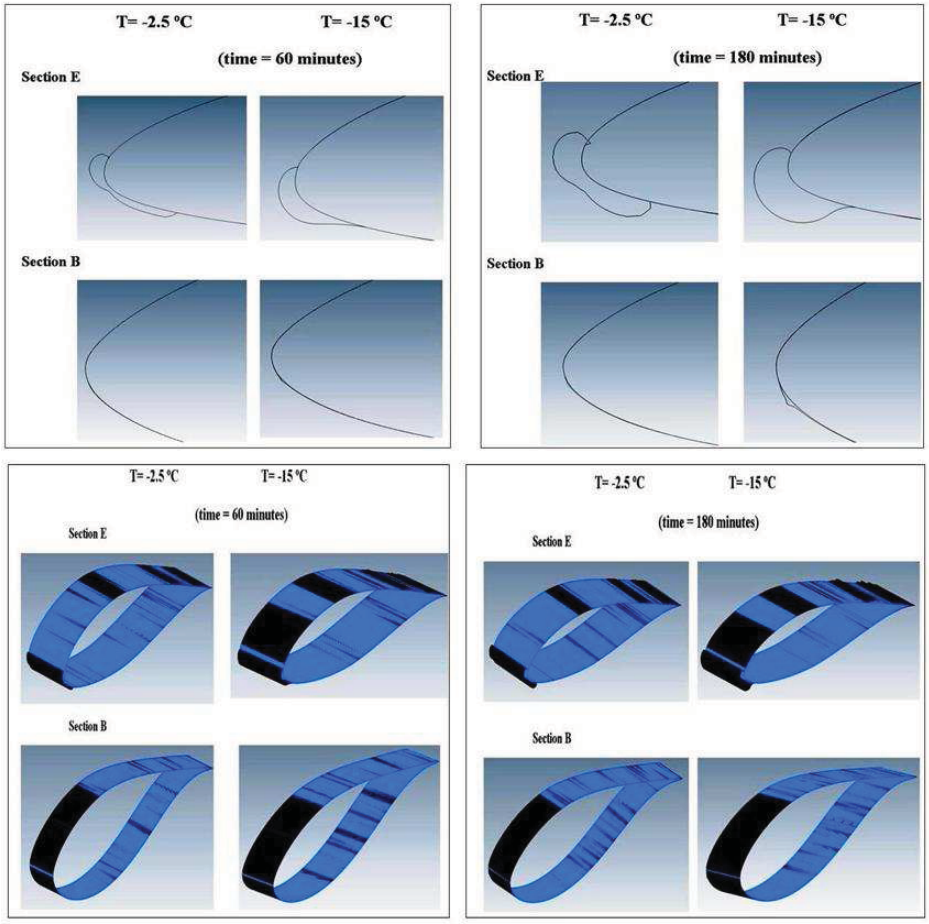

Figure 4.23: Change in rate and shape of ice accretion with time at blade tip and center sections for t = 60 and 180 min.

Discussion

Results in the previous section showed that variation in atmospheric temperature and icing duration not only affect the shape of ice growth, but also affect the blade ice covered area. For T = -2.5 °C, at blade tip section (Section E) the area covered by the ice is less than the iced area at T = -15 °C. The effects of temperature variation are considerable near the blade tip area, whereas near the root section the ice growth is almost similar for all the temperatures. At T = -2.5 °C, the ice shape at the leading edge near the tip section E is more abrupt as compared to the ice shape at T = -15 °C.

The accreted ice mass and ice thickness along the blade profile were also analyzed. Figure 4.24 shows the accreted ice mass and ice thickness variation at different atmospheric temperatures along the complete blade. Figure 4.24 shows that the value of ice thickness and the accreted ice mass is highest at the blade tip section and reduces continuously towards the root section. The most effected area of the blade by ice is from tip to the center of the blade (from 30 m to 63 m), while rest of the area from blade center to the blade root is not having considerable effects of icing. Similar trends were observed, when the analysis were carried out at t = 180 min. Figure 4.25 shows the change in accreted ice mass and thickness with the change in icing time interval from t = 60 min to t = 180 min.

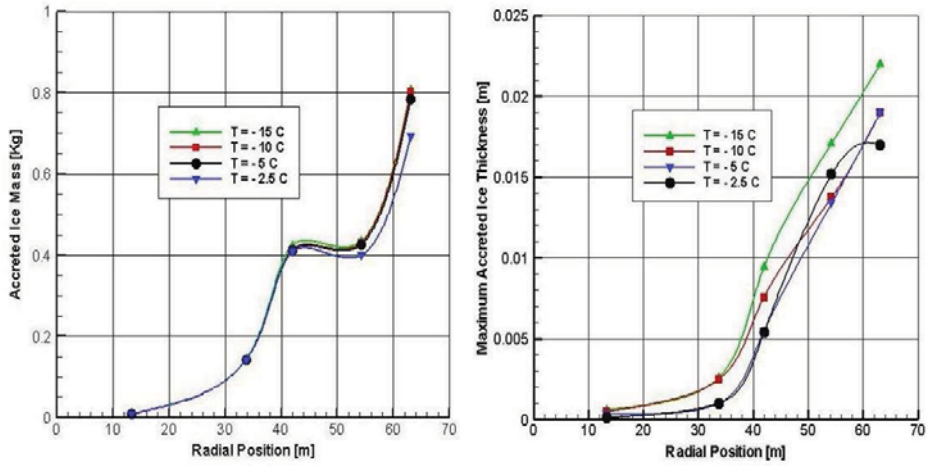

Figure 4.24: Effect of atmospheric temperature variation on accreted ice mass and thickness along the blade for t = 60 min.

Analysis of Figure 4.25 shows that with increasing duration of the icing event both the accreted ice mass and thickness increases along the blade. The change in the accreted ice mass and thickness with the time interval is more significant on the outer portion of the blade than on the inner portion. The trends shown in these two graphs generally agree with previous observations of more ice near the blade tips [76] and modeling with other icing codes which also show more ice near the tips [71].

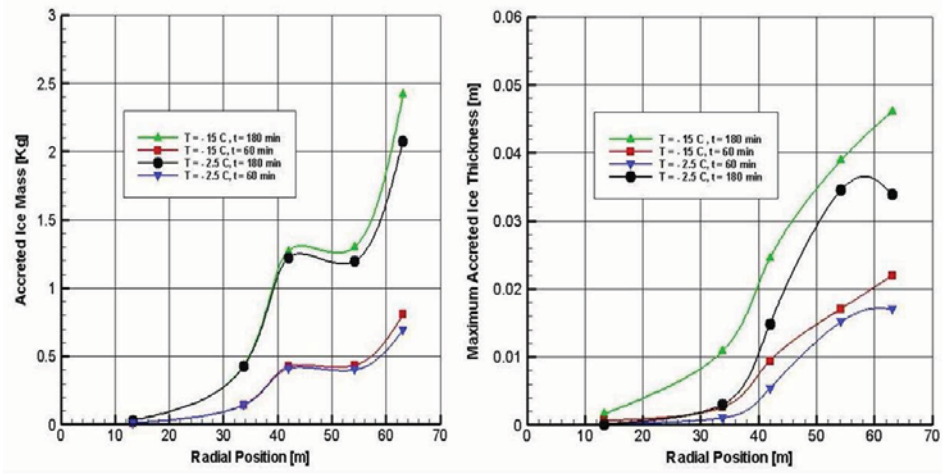

Figure 4.25: Effect of icing time interval variation on accreted ice mass and thickness along the blade for t = 60 and 180 min.

4.3.3 Section summary

The rate and shape of ice accretion on a NREL 5 MW wind turbine blade was modeled using three dimensional numerical techniques. Analysis was carried out at five different sections of the blade and the results were interpolated to have a broader picture. The results indicate that the combined changes in blade profile size and relative velocity at each section considerably influences the rate and shape of ice growth. At blade sections near the tip, where the blade chord length and thickness is less, and relative velocity is higher, more ice accretion was found as compared to the blade sections near the root. Overall the results indicate that the icing is less severe for the blade sections where the blade profiles are larger and thicker and relative velocity lower, both in terms of local ice mass and in terms of ice thickness. Study shows that the effect of temperature variation is more significant for the outer portions of the blade. Similarly study on the effect of icing time variation shows that change in rate and shape of ice growth with icing duration for large wind turbine blades is more significant for the outer portion of the blade, and that for the inner section of the blade (center to root), the effect of icing duration on the rate and shape of ice growth is not significant.

From the results it was found that there is a considerable change in the rate and shape of ice growth with the changes in geometric parameters such as chord length, blade thickness and the twist angle. It may mean that by optimizing the blade geometric parameters the ice accretion on the wind turbine blades can be minimized. This could reduce the need for de- and anti-icing systems on the wind turbine blades installed in the cold regions. Future work must include a detailed optimization study of the blade geometric parameters to minimize the ice accretion effects on the wind turbine performance.

4.4 Summary

In this chapter the dependence of atmospheric icing on turbine size was explored together with the sensitivity of icing to droplet size and ambient temperature.

The first section described modeling icing on a section of blade for four different wind turbine sizes were using TURBICE. The results indicate that dry rime icing is less severe for larger wind turbines both in terms of local ice mass and in terms of relative ice thickness. The results indicate that a major reason seems to be the lower collection efficiency of the larger chord, and thereby dimensionally thicker, blades.

The second section described two dimensional modeling of atmospheric icing on blade sections at 85% radius of five different wind turbines with varying droplet size and air temperature. The results show that the stagnation line temperature during rime ice accretion is warmer on larger turbines than smaller turbines when the other parameters are kept constant. The higher stagnation line temperature means that the ambient temperature at which the ice shapes with highest drag coefficients (horn ice) form is lower for larger turbines. Therefore, while atmospheric icing is generally becoming less significant in terms of relative ice mass and thickness for larger turbines, the temperatures at which the transition shapes between glaze and rime form is generally lower for larger turbines. An implication of the indicated fact that dependence of ice mass on droplet size increases with turbine size is that knowledge of droplet size will be more important for estimation of ice loads on larger turbines.

The third section described how the rate and shape of ice accretion on a NREL 5 MW wind turbine blade was modeled using three dimensional numerical techniques. The results indicate that the combined changes in blade profile size and relative velocity at each section considerably influences the rate and shape of ice growth. At blade sections near the tip, where the blade chord length and thickness is less, and relative velocity is higher, more ice accretion was found as compared to the blade sections near the root. Overall the results indicate that the icing is less severe for the blade sections where the blade profiles are larger and thicker and relative velocity lower, both in terms of local ice mass and in terms of ice thickness. Study shows that the effect of temperature variation is more significant for the outer portions of the blade. Similarly study on the effect of icing time variation shows that change in rate and shape of ice growth with icing duration for large wind turbine blades is more significant for the outer portion of the blade, and that for the inner section of the blade (center to root), the effect of icing duration on the rate and shape of ice growth is not significant.

Chapter 5

Icing - effects on aerodynamics and power production

To determine the effect of icing on power production it is necessary to do more than just model the ice shapes formed on the blades. The aerodynamic parameters of the iced airfoils must be determined and the resulting performance reduction calculated. Work related to that is presented in this chapter.

The first section describes results of work regarding the effect of rime ice accretions on the aerodynamic characteristics of four different sized wind turbines, ranging in size from 450 kW to 2 MW. The second section describes the results of modeling to determine the effect of changes in temperature and droplet size on the aerodynamic characteristics of the resulting iced profiles for a 5 MW turbine. The third section describes results of a modeled icing event on the power performance of the 5 MW NREL reference turbine and discusses a possibility of partially mitigating the performance degradation.

5.1 Effect of rime ice accretion on aerodynamic characteristics of wind turbine blade profiles

This section describes a numerical study of rime ice accretion and resultant flow field characteristics of blade profiles for four different sized, fixed speed, stall controlled wind turbines. Analyses were carried out at Reynolds numbers ranging from of $2.5 \cdot 10^6$ to $5.5 \cdot 10^6$), corresponding to the operational wind speeds and angles of attack ranging from -10 degrees to +20 degrees. A significant change in the flow behavior and aerodynamic characteristics is observed, when a comparison is made between plain and iced blade profiles. Results show an increase in both lift and drag coefficients of wind turbine blade profiles with the leading edge ice.

5.1.1 Introduction

Most investigations of this subject have been performed using either ordinary wind tunnel testing with artificial ice templates attached to the blade profile or icing wind tunnel testing, but for the last decade or so the CFD and panel method

based numerical techniques have begun to play a significant role in modeling and determining the performance of wind turbines under icing conditions. Icing on the wind turbines and its resulting effect on power production have been modeled for a variety of cases [6, 13, 14, 15]. Bak et al. [79] and Ferrer and Munduate [80] utilized custom made 3D CFD models to investigate the rotor aerodynamics for the wind turbines. Chi et al. [81] studied several turbulence models to analyse the flow behaviour around leading edge ice accreted airfoils. Kwon and Sankar [82] and Mirzaei et al. [83] compared the experimental and CFD based numerical results about performance analyses of the leading edge ice accreted airfoils. Zhu et al. [84] used CFD based numerical approach for determining the drag of the iced airfoils.

It has been previously reported by Gent et al. [67] that airfoils with larger chords are less efficient droplet collectors. In Chapter 3 this was also proposed as a possible reason for the low production losses at Nygårdsfjell wind park, despite icing conditions. In Chapter 4 it was shown that larger turbines, with their longer chord airfoils were modeled to collect relatively less dry rime ice than smaller turbines. The effect of ice accretion on aerodynamic characteristics is studied here for rime icing conditions for four different wind turbine blade profiles.

The rate of ice accretion on an object has been described in Section 2.7 and the effect of icing on aerodynamics in Section 1.3.1. This is mainly because of changes in the flow behavior due to ice accretion. From equation 1.1, a torque coefficient,

$$C_y = (C_l \sin\phi - C_d \cos\phi) \ , \tag{5.1}$$

was defined for analysis. The changes in the torque coefficient are quite important, when analyzing the effect of icing on the power producing capability of a wind turbine.

5.1.2 Numerical Setup

Numerical modeling of the rate of ice accretion and its resulting effect on the aerodynamic characteristics of the wind turbine blade profiles was carried out using a combination of panel method and computational fluid dynamics based numerical techniques. These numerical models were focused on studying the effect of change of blade profile size, particularly the chord length, and the relative velocity on the rate and size of accreted ice at leading edge and resultant aerodynamic characteristics of the blade profiles.

Three blade profiles of four different wind turbines, 450 kW, 600 kW, 1 MW and 2 MW were numerically analyzed for two cases; normal and leading edge ice accretion conditions. These blade profiles are taken from approximately 85% of the blade radius, as described in Chapter 4. Results obtained from the ice accreted case are compared with the plain profiles to determine the effect of ice on the aerodynamic performance.

The ice shapes used for this study were generated as described in Section 4.1. To study the effect of icing on the flow behavior and aerodynamic characteristics of the wind turbine blade profiles, two dimensional steady state numerical analysis was carried out using FLUENT. The numerical analysis was carried out at Reynolds numbers ranging from $2.5 \cdot 10^6$ to $5.5 \cdot 10^6$, corresponding to the relative velocity

of the blade sections during the operational conditions used, and angles of attack ranging from -10 degrees to +20 degrees. Thereafter a computational fluid dynamics based Navier-Stokes equation solver FLUENT [85] was used to numerically analyze the flow behavior and the resulting aerodynamic characteristics of the blade profiles for normal and leading edge ice. The Navier-Stokes equation was discretized using the finite volume method to numerically model the complex flow behavior around the blade profiles. The flow is considered as incompressible and the k-ϵ (realizable) turbulence model is used. A structured type numerical grid is used, as shown in Figure 5.1, as the grid around the airfoil shape, whereas to determine the boundary layer, a y+ value less than 10 is used near the wall. All the numerical modeling is carried out at relative wind speeds specified in Table 4.1, assuming dry rime ice accretion resulting from 15um droplets at the atmospheric conditions shown in Table 4.2.

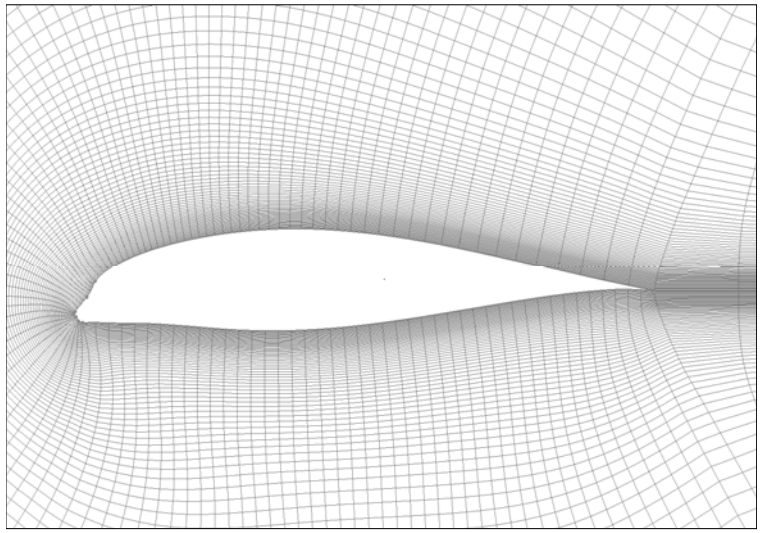

Figure 5.1: Iced airfoil grid distribution around a NACA 63215 profile. The shadows and patterns visible near the airfoil result from optical effects related to printing the very fine grid in this region.

5.1.3 Results and Discussion

Rate and Size of Rime Ice Accretion

The ice shapes generated by TURBICE are shown in Figure 4.2. Similar shapes of accreted ice have also been reported by the Finish Meteorological Institute [17]. Rime iced profile shapes obtained from the TURBICE for this particular case of study were not too irregular. Particularly along the lower surface the ice shape is almost smooth which increases the effective chord length and camber of the blade profile, while along the upper surface there is some irregularity.

The analysis in section 4.1 showed that with increasing blade profile size (chord length), the relative size of the accreted ice reduces. Such a decrease in the size of accreted ice is mainly due to the decrease in collision efficiency of the droplets with the blade, and it was shown that this resulted in the blades on larger wind turbines having less severe rime icing in terms of mass accretion and ice thickness than the blades on smaller turbines.

Velocity and Pressure Distribution

Numerical analysis of the flow behavior shows a significant change in the velocity and pressure distribution along blade profiles in the case of icing. A shift in the position of the stagnation point is observed in case of iced profiles that effects the velocity and pressure distribution. Results show that for positive angles of attack a high velocity zone exists on the upper surface of the blade profiles near the leading edge, where as a flow recirculation zone is found near the trailing edge along the upper surface of the iced profiles. Analysis shows that for the positive angles of attack the flow recirculation zone exists along upper surface, where as for the negative angles of attack this shifts to the lower surface. This can be seen in the plots of velocity distribution shown in Figure 5.2. The strength of such recirculation zone is high for the negative angles of attack for this particular case study, due to the smooth ice surface along lower side of the blade profile.

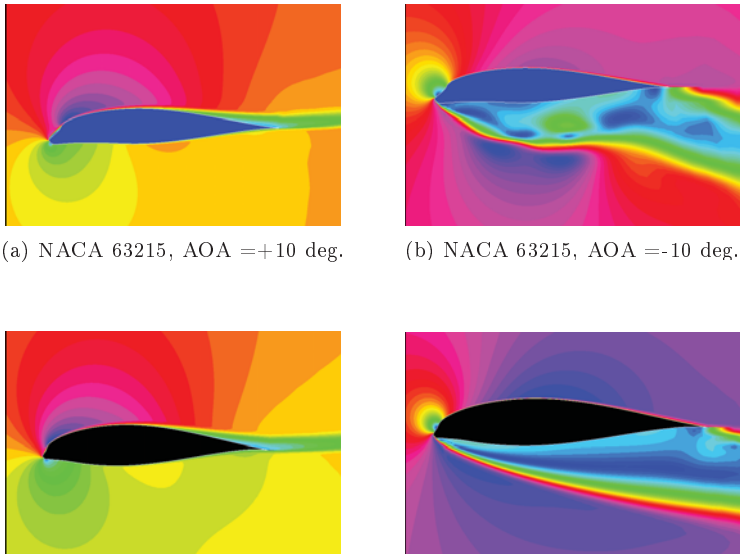

(a) NACA 63215, AOA =+10 deg. (b) NACA 63215, AOA =-10 deg.

(c) NACA 63416, AOA =+10 deg. (d) NACA 63416, AOA =-10 deg.

Figure 5.2: Relative velocity distribution for iced NACA 63215 and 63416 profiles at AOA =+10, -10 degree. The velocity color codes are relative for each subfigure.

Analysis shows that due to less relative ice accretion at the leading edge of the

NACA 63416 (2 MW)the velocity distribution is slightly smoother than the NACA 63215 (450 kW), but for negative angles of attack a strong flow separation zone exists along the lower side of both blade profiles. Plots of streamlines showing the flow recirculation can be seen in Figure 5.3. It can also be seen that in the case of the NACA 63215, the strength of the flow recirculation zone at negative angles of attack is greater than for the NACA 63416.

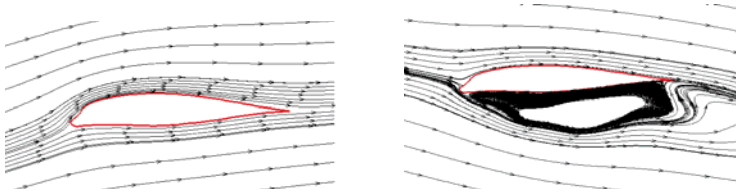

(a) NACA 63215, AOA =+10 deg. (b) NACA 63215, AOA =-10 deg.

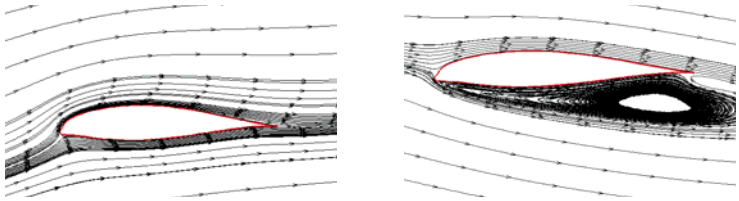

(c) NACA 63416, AOA =+10 deg. (d) NACA 63416, AOA =-10 deg.

Figure 5.3: Streamlines for iced NACA 63215 and 63416 profiles.

Turbulence Intensity

Turbulence intensity defines the turbulence level. Results show high turbulence intensity near the leading edge of all iced blade profiles due to the irregular shape because of accreted ice. Due to the relatively larger size of the accreted ice for the NACA 63215 (450 kW) the level of turbulence intensity is higher as compared to the NACA 63416 (2 MW) and 63417 (1 MW). The turbulence intensity for two of the profiles can be seen in Figure 5.4. Such behavior of the turbulence intensity affects the aerodynamic characteristics of the iced blade profiles.

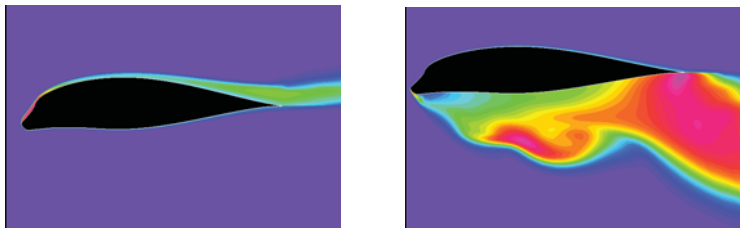

(a) NACA 63215, AOA =+10 deg. (b) NACA 63215, AOA =-10 deg.

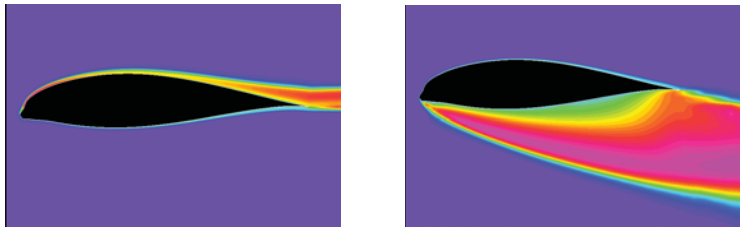

(c) NACA 63416, AOA =+10 deg. (d) NACA 63416, AOA =-10 deg.

Figure 5.4: Turbulence intensity variation for iced NACA 63215 and 63416 profiles.

Lift and Drag Coefficients

Numerical analysis showed a higher value of lift coefficient for iced profiles when compared to the plain profiles at positive angles of attack. The main reason for this is the accreted rime ice shape from TURBICE. The smooth surface area along the lower surface of the iced profiles increases the effective chord length and camber of the blade profile which improves the lift coefficient and stall range at positive angles of attack for this particular case of study. At negative angles of attack, flow hits the irregular shape on the upper surface of the iced profile which leads to an increase in the flow separation. Figure 5.5 shows the lift coefficients for NACA 63215 (450 kW) and NACA 63416 (2 MW) for normal and iced conditions.

Figure 5.5 shows that in the case of positive angles of attack the iced NACA 63416 blade profile stalls around +12 degree AOA, while the iced NACA 63215 blade profile stalls at +14 degrees. In the case of negative angles of attack the iced NACA 63215 stalls at -7 degrees, while the iced NACA 63416 stalls at about -5 degrees. Figure 5.6 shows a comparison of lift and drag coefficients for all four blade profiles under icing conditions.

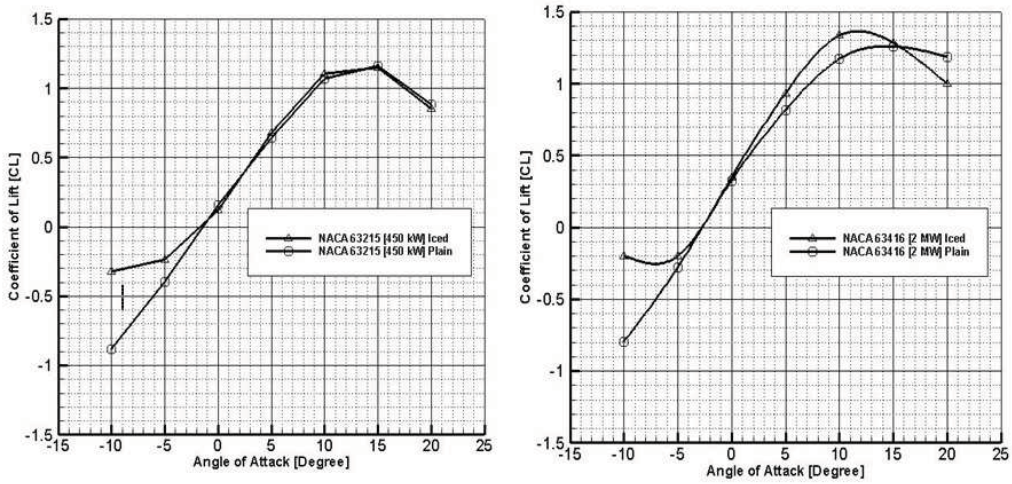

Figure 5.5: Comparison of lift coefficient for plain and iced NACA 63215 and 63416.

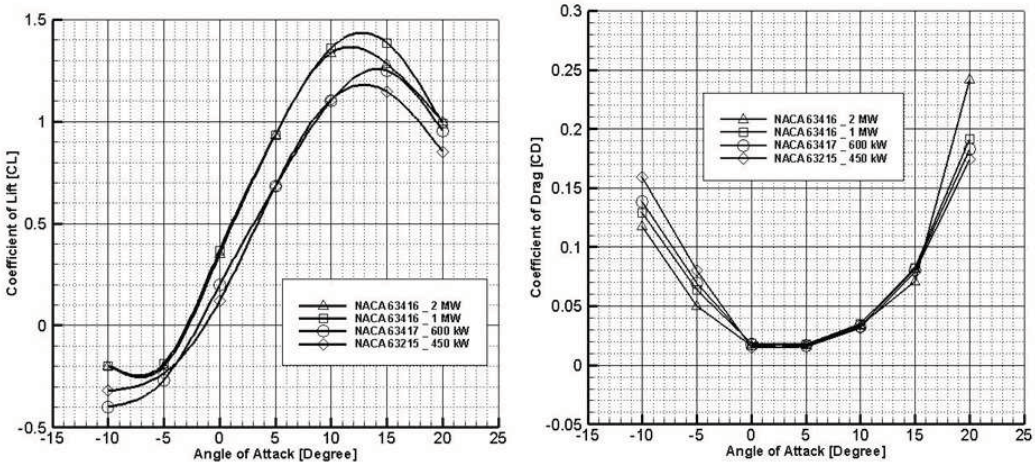

Figure 5.6: Lift and drag coefficient for iced NACA 63215, 63416 and 63417 blade profiles.

Torque Coefficient

For these numerical calculations the drag calculation with FLUENT did not account for the change in surface roughness from an initially smooth profile surface to a rough iced surface. To account for the changes in surface roughness the calculated iced profile drag was increased by a factor of 2.5. This was the average increase in the drag for a 1.5 mm equivalent sand grain roughness found by Dahlqvist [8].

To evaluate the affect of the modeled icing on the wind turbine performance the lift and drag coefficients were converted to the in-plane rotating force coefficient (torque coefficient) C_y, by using equation 5.1. The calculated C_y curves both with and without icing are shown in Figure 5.7. It can be seen that the calculated C_y curves show a lower torque with icing for all cases and that the decrease in C_y is greater for the smaller wind turbines. Energy losses caused by icing are not calculated here because this numerical study is carried out on single profile section of the wind turbine blade, where as for the calculation of the energy production losses of a wind turbine blade due to icing, numerical analyses of the full blade is needed. Typically a lower torque causes lower energy production.

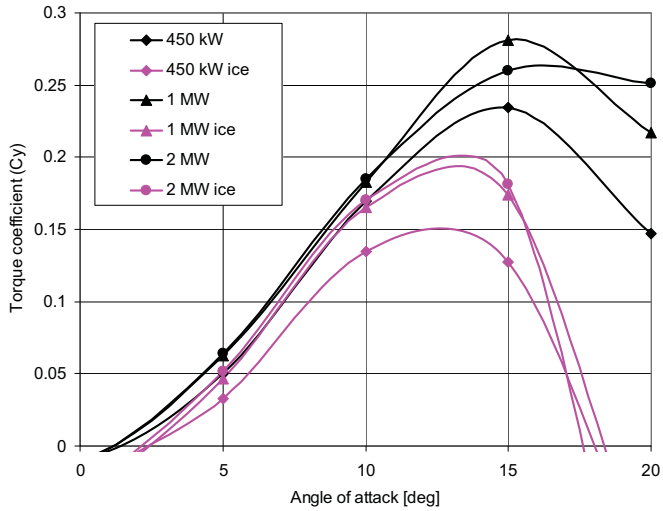

Figure 5.7: Calculated torque coefficients with the drag coefficient increased by a factor of 2.5.

5.1.4 Section summary

Icing on the blade profiles for four different size wind turbines was modeled using numerical techniques. Previous work has indicated that dry rime icing is less severe for larger wind turbines both in terms of local ice mass and in terms of ice thickness, and a significant change in the flow behavior and aerodynamic characteristics is observed here. It was found that the decrease in the torque coefficient was greater for the smaller wind turbines, which supports the hypothesis that dry rime icing affects larger wind turbines less than smaller wind turbines.

In addition to these results some questions remain. For more detailed results other icing conditions, including different wind speeds and operating conditions should also be modeled. Further studies of the change in surface roughness should be included in the future work.

5.2 Effect of rime and glaze ice accretion on aerodynamic characteristics of wind turbine blade profiles.

To explore how the growth of atmospheric ice on wind turbine blades changes with variations in the temperature and the droplet size, numerical tools were used and ice shapes formed on a 5 MW turbine blade with different conditions were analyzed for their effect on aerodynamic performance.

5.2.1 Numerical setup

Numerical modeling was carried out for a 5 MW, pitch controlled wind turbine blade profile section (NACA 64618) to analyze the effect of variations in atmospheric temperature and water droplet size on the rate and shape of ice growth. The blade profile was taken from approximately 85% of the blade radius, with 100% being the tip, as described previously. The numerical modeling was performed using a combination of the panel method and computational fluid dynamics based techniques in two steps. In the first step TURBICE generated the iced profiles, and in the second step CFD modeling with FLUENT was performed for the iced and non-iced profiles to compare the aerodynamic characteristics. The models are not coupled, rather the ice profiles generated by TURBICE are used as the input shape to FLUENT. This compares with what could be expected for the turbine at the end of an icing event.

The air flow around the wind turbines is typically turbulent at high Reynolds numbers. Therefore k-ϵ turbulence model is used in FLUENT as a compromise between acceptable computational cost and the required accuracy in modeling the turbulent flow. To properly deal with the turbulence effects in the thin boundary layer, the Log-law function is used for this study near the wall. This differentiates between the turbulence scale in the flow domain and near the wall. At high Reynolds numbers the viscous sub layer of the boundary layer is so thin that it is difficult to use a sufficient number of grid points to resolve it, therefore the log-law function method of Launder and Spalding is used here to estimate the thin boundary layer. The main advantage of the log-law function is that the first element near the wall can have a high value of y+ (up to 100), quite large compared to other turbulence models. This reduced the total number of grid points. Although turbulence models such as large eddy simulations are increasingly applied to wind engineering problems, the k-ϵ still remains in common use for the wind engineering applications [86]. A structured type numerical grid was used, where as to determine the boundary layer, a y+ value less than 10 was used near the wall.

While TURBICE computes the surface roughness of the iced profiles for calculation of the heat transfer coefficient, this data was not easily used as an input to the CFD modeling. Therefore the same surface roughness equation used by TURBICE, from Shin [69] was used to calculate an equivalent sand grain roughness which was then input to FLUENT for the second stage of processing.

The ice profiles from TURBICE resulted from the modeled conditions shown in Table 5.1. The CFD modeling to determine the aerodynamic characteristics of the resulting iced profiles did not include droplets, but were modeled at the relative air speed shown in Table 5.2.

Table 5.1: Modeled icing conditions.

Wind speed [m/s]	10.0
Droplet size, MVD [µm]	12, 17, 30
Liquid water content, LWC [g/m^3]	0.20
Air temperature [°C]	-7.5, -5, -2.5
Modeled time [min]	120

Table 5.2: Wind turbine details.

Type	Pitch controll
Power	5 MW
Rotor radius [m]	63.5
Airfoil name NACA	634618
Rotation speed [rpm]	12
Chord length [m]	1.846
Relative speed, v, [m/s]	67.3
Angle of attack, α, [deg]	6.0
Modeled radius [m]	53

5.2.2 Results and Discussion

Effect of Atmospheric Temperature Variations

To study the effect of atmospheric temperature variations on the rate and shape of ice accretion, numerical analysis were carried out at three different atmospheric temperatures (-2.5 °C, -5 °C and -7.5 °C), and with a constant MVD of 17 µm. Figure 5.8 shows the accreted ice shapes obtained from TURBICE for all three cases. Results show that the accreted ice shape changes with the temperature. At -5 °C and -7.5 °C the shape of accreted ice is more streamlined, while for -2.5 °C, a horny shape is found. Such changes in the accreted ice shapes significantly disturb the flow behavior and the resultant aerodynamic characteristics of the blade profiles.

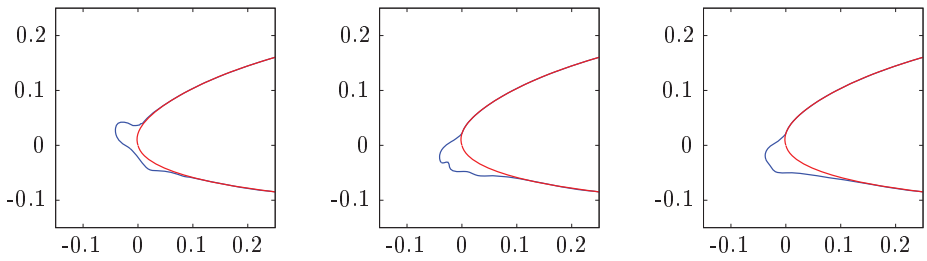

(a) -2.5 °C (b) -5 °C (c) -7.5 °C

Figure 5.8: Effect of temperature variation on rate and shape of ice accretion with MVD = 17 µm after t = 120 min.

To analyze the effect of the accreted ice shapes on the aerodynamic character-

istics, numerical analyses were carried out using FLUENT. Profiles obtained from TURBICE were used as the input to FLUENT to analyze the flow behavior and the resulting aerodynamic characteristics at different angles of attack ranging from -10 degrees to +20 degrees. Figure 5.9 shows the velocity streamlines calculated by FLUENT for the plain profile and iced profiles, at all modeled temperatures, at two different angles of attack, +5 and +15 degrees.

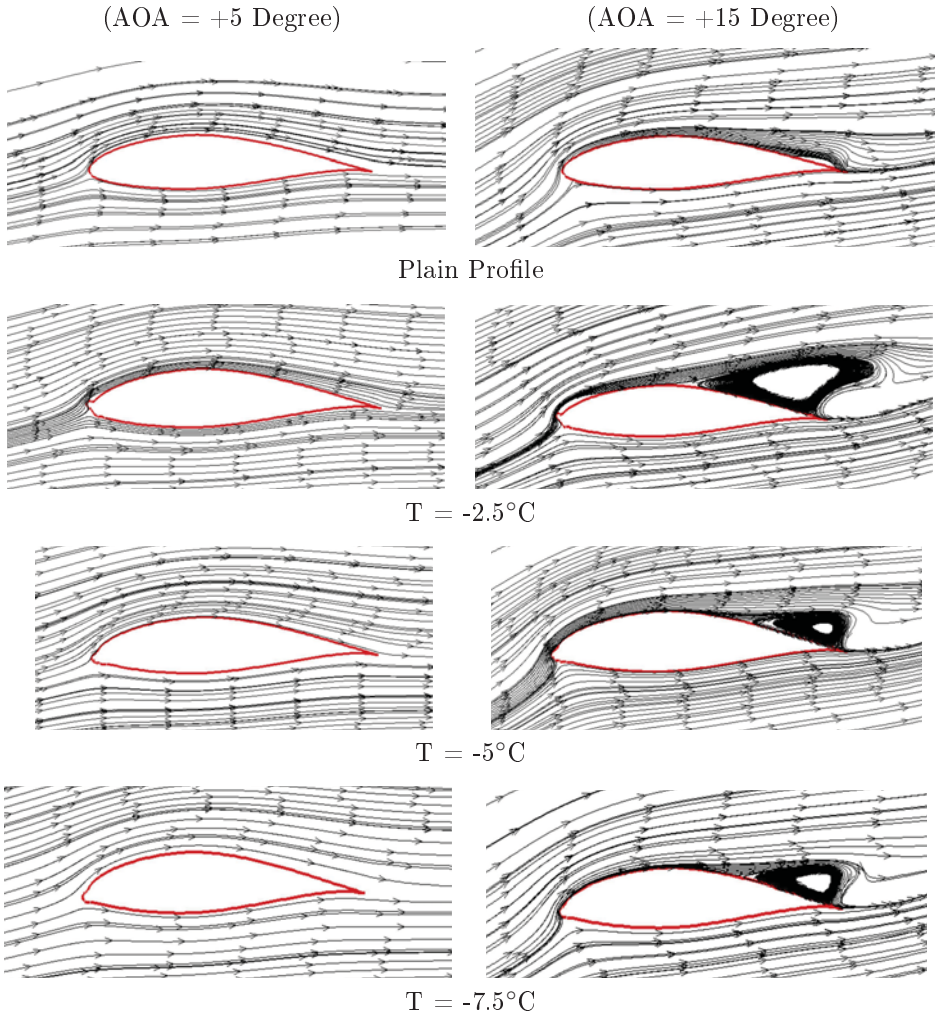

Figure 5.9: Streamlines around plain and iced NACA 64618 profiles. The iced profiles were formed at different temperatures with MVD = 17 µm.

The results show no visible flow separation at a +5 degree angle of attack, but at a higher +15 degree angle of attack, it can be seen that all of the profiles have a flow separation, though it is only barely separating on the plain profile and with markedly greater separation on the iced profiles. In addition, the accreted ice shape

formed at -2.5 °C caused a greater separation than the icing at -5 °C and -7.5 °C. This difference in the flow separation leads to a shift in the aerodynamic characteristics of the profile. This difference can be seen in the lift and drag coefficients calculated by FLUENT, as shown in Figure 5.10, where the iced profiled at -2.5 °C has the lowest lift and highest drag in the range of angle attack on the operating wind turbine.

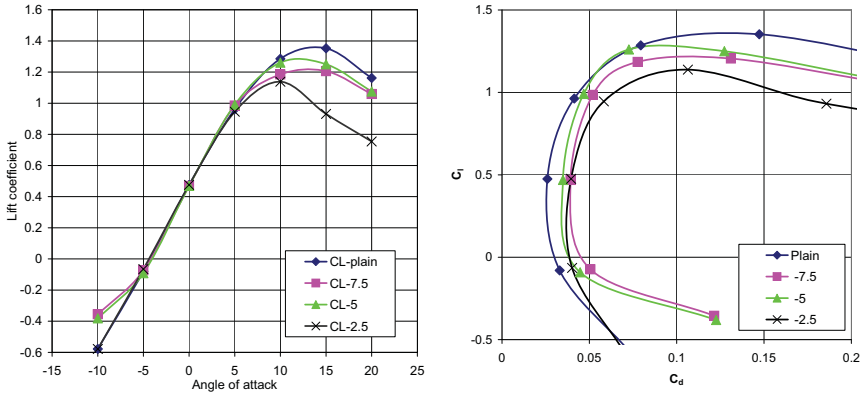

Figure 5.10: Lift coefficients (left) and lift/drag performance (right) curves for iced and plain NACA 64618 blade profiles at different atmospheric temperatures.

Effect of Droplet Size Variation

To study the effect of droplet size variation on the rate and shape of ice accretion, the numerical analyses were carried out for three different droplet sizes, with MVD of 12 µm , 17 µm and 30 µm, and a constant atmospheric air temperature T = -2.5 °C. Figure 5.11 shows the accreted ice shapes obtained from TURBICE for three different droplet sizes. Results show that change in the droplet size affects both the rate and shape of ice accretion. Increasing droplet size increases the area covered by the accreted ice as well as the ice shape. The main reason for this can be explained by the fact that larger diameter droplets have larger inertia compared to smaller droplets. Therefore the movements of larger droplets are less affected by the airflow and more of the droplets strike the airfoil surface.

Change in the rate and shape of ice accretion with the droplet size also affects the aerodynamic characteristics of the blade profile. Figure 5.12 shows the velocity streamlines for the plain and iced profiles for three different sized droplets with temperature -2.5 °C. Results show that at a +5 degree angle of attack there is no noticeable flow separation, while a +15 degree angle of attack shows obvious recirculation zones.

Analysis shows that the 12 µm droplet size has the smallest recirculation zone, while the icing from 17 µm and 30 µm droplet sizes show larger recirculation zones. As described in section 4.2, an increase in the droplet size increases the collision

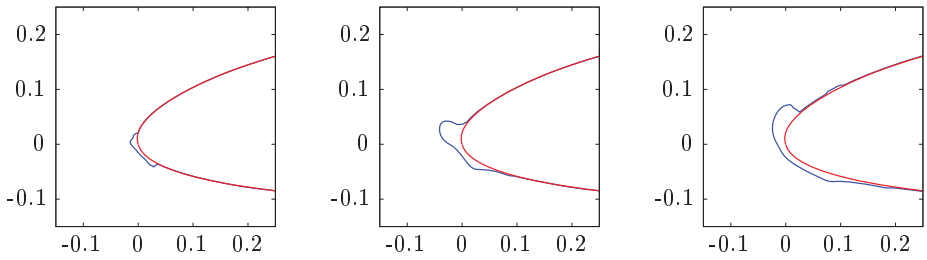

(a) 12 µm (b) 17 µm (c) 30 µm

Figure 5.11: Effect of droplet size variation on rate and shape of ice accretion, at T = -2.5 °C after t = 120 min.

efficiency of the droplets which leads to increased ice accretion. Figure 5.13 shows the effect of change of ice growth on the aerodynamic characteristics (lift and drag coefficients) of the blade profile.

Torque Coefficients

To evaluate the effect of the modeled ice growth on the wind turbine blade profile performance, the lift and drag coefficients were converted to the in-plane rotating force coefficient (torque coefficient), by using equation 5.1 and using a fixed twist angle of 0.537 degrees, which is the twist angle of the modeled blade at the 85% radius. The calculated torque coefficient curves for different droplet sizes and atmospheric temperatures are shown in Figure 5.14. It can be seen that starting from a baseline ice shape formed with 17 µm droplets at -2.5 °C, either smaller droplet size or lower temperatures result in icing that is much less significant for the wind turbine torque. These results support previous work which classified glaze icing as more significant in terms of its effects on power production, since it is the horn shapes associated with the transition to a "warmer" type of icing that cause the largest flow separations in these numerical models, and lead to significantly lower lift and higher drag and thereby lower torque coefficients.

Energy losses caused by each icing case are again not calculated here because this numerical study was carried out on a single profile section of the wind turbine blade.

5.2.3 Section summary

Two dimensional numerical modeling of atmospheric icing on a blade profile section (NACA 64618) at approximately 85% radius of a 5 MW wind turbine was performed with varying droplet sizes and temperatures. The results show that while icing causes the lift coefficients to be reduced in all cases, the amount of reduction varied and the least change in lift was observed for the cases that seemed to produce rime type of streamlined ice shapes. The icing which causes horn type of glazed icing shapes had larger reductions in lift. These results show that to be able to accurately

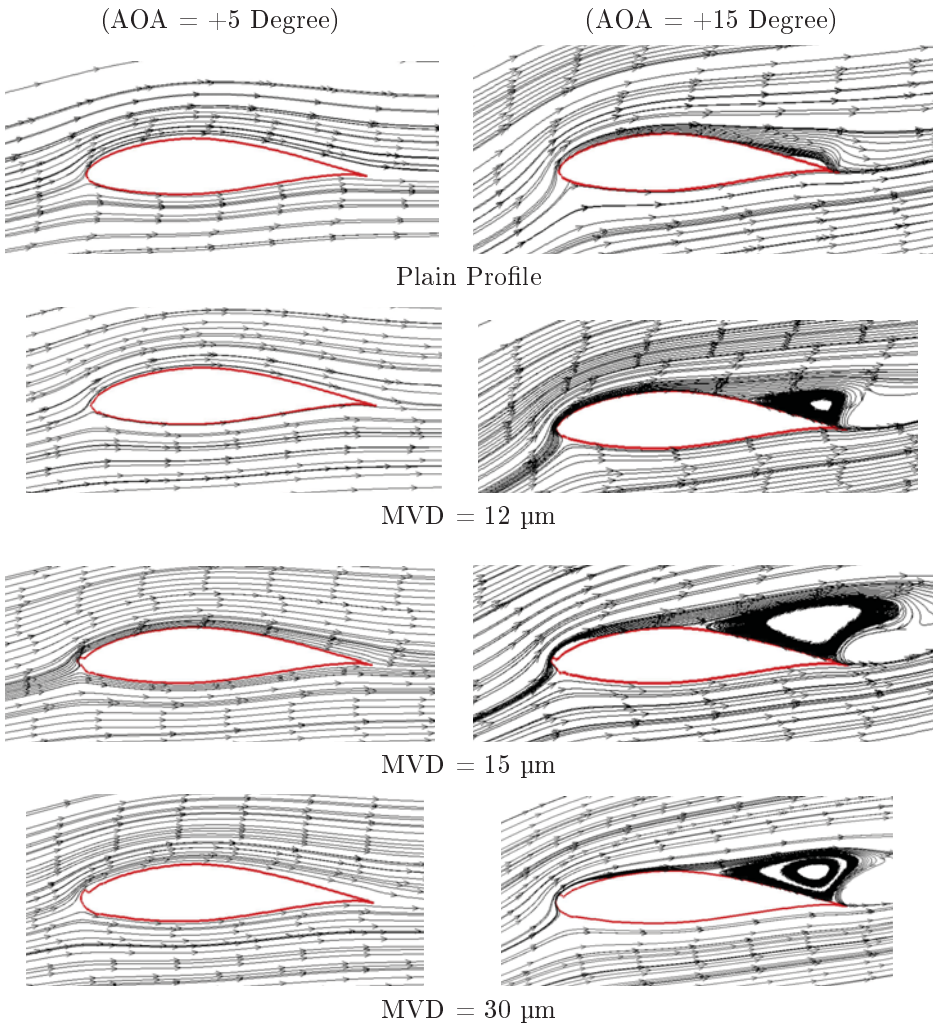

Figure 5.12: Streamlines around plain and iced NACA 64618 profiles. The iced profiles were formed at different droplet sizes with temperature of -2.5 °C.

estimate energy production losses based on atmospheric icing, it will be necessary to have measurements of the atmospheric conditions during the icing such that the shape and type of icing can be found. It was also shown that air temperature alone can not be used to differentiate between rime and glaze ice, but that droplet size can also change the effect of an icing event.

Future work should include more detailed turbulence analysis and investigating the different turbulence models to better understand and numerically model the thin boundary layer characteristics near the wall and overall turbulence behavior across the wind turbine under different icing conditions. Moreover full scale three dimensional numerical analysis should be carried out to better understand the effect

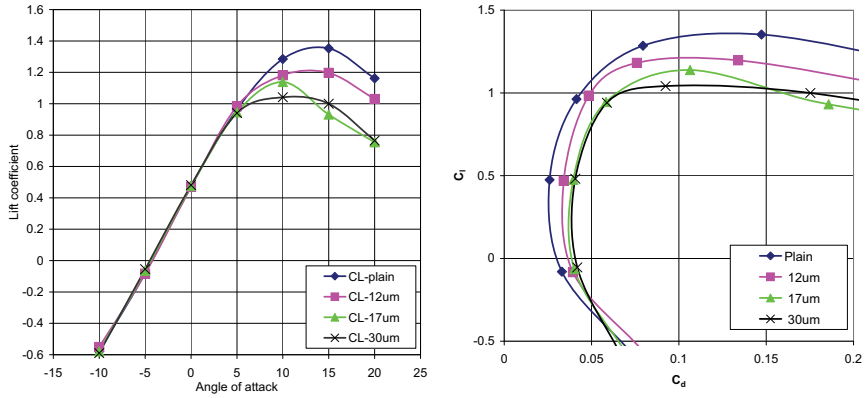

Figure 5.13: Lift coefficients (left) and lift/drag performance (right) curves for iced and plain NACA 64618 blade profiles at different atmospheric temperatures.

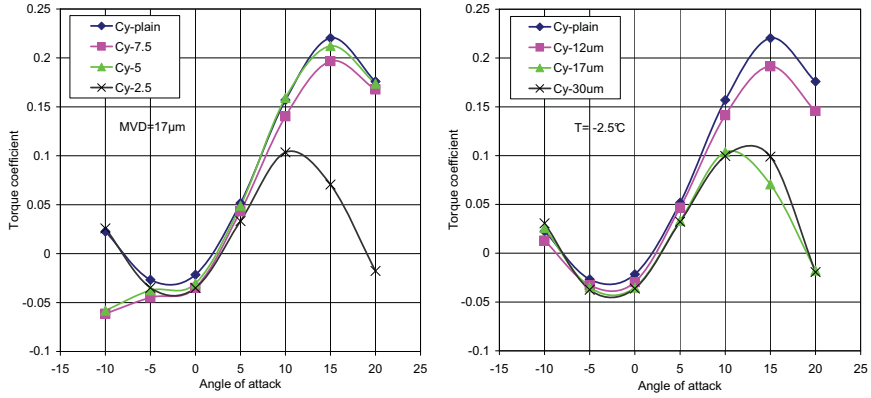

Figure 5.14: Torque coefficients for NACA 64618 at different temperatures (left) and droplet sizes (right).

of change in aerodynamic characteristics on overall performance of the wind turbine blade in icing conditions. A method for annual energy production estimation (AEP) including icing effects on production should be developed. This kind of method or tool would be valuable for developers of wind energy projects in icing climates.

5.3 Power performance losses due to ice accretion for a 5 MW wind turbine

The work presented in the two previous sections indicated that for dry rime icing the icing becomes less significant in terms of reduction in aerodynamic performance

for larger turbines, but the effect on energy production was not investigated. The objective of the work in this section was to use models to explore how atmospheric ice accretion along the length of a blade affects the energy production capabilities of a large standard wind turbine.

5.3.1 Numerical setup

For this work the NREL 5 MW wind turbine described in section 4.3 was used with the same five radial positions analyzed. The model setup was as described in section 4.3, where FENSAP-ICE was used to calculate ice shapes for the operating conditions specified in Table 5.3. The roughness height for the iced blade profiles was calculated according to Shin et al. [30]. Since the ice accretion code showed slight ice accretion over most of the blade surface, the roughness height was applied to the entire blade surface. Following the calculation of the ice shapes, the aerodynamic properties of the iced sections were found by calculating the lift and drag forces for varying angles of attack around the test sections' normal operating angles. FENSAP-ICE outputs the resultant force acting on the blade profile surface, which is decomposed to the lift, L, and drag, D, forces. Thereafter the lift and drag coefficients were calculated to be,

$$C_l = \frac{2L}{\rho V^2 A}\,, \tag{5.2}$$

and

$$C_d = \frac{2D}{\rho V^2 A}\,. \tag{5.3}$$

Table 5.3: Modeled icing conditions.

Free stream wind velocity, V_∞, [m/s]	10
Droplet size, MVD [µm]	20
Droplet size distribution	mono-disperse
Liquid water content, LWC [g/m^3]	0.22
Air temperature [°C]	-10
Modeled time [min]	60

The blade element momentum (BEM) theory is commonly used to evaluate the aerodynamic performance of a wind turbine design. A rotor analysis code to perform the BEM analysis and to calculate the operating points of the wind turbine, was developed using the Octave language. The solution of the BEM equations is an iterative process, described in Manwell et al. [87] where for a given tip speed ratio (λ), initial values of the axial (a) and angular (a') induction factors are chosen and used to calculate the inflow angle of the wind to the rotor plane,

$$\beta = \tan^{-1}\left(\frac{\lambda_r(1+a')}{1-a}\right) \tag{5.4}$$

The local speed ratio is calculated as,

$$\lambda_r = \frac{\lambda r}{R} \tag{5.5}$$

With r as the local radius and R as the rotor radius. Thereafter C_l and C_d are found from the blade profile data using the angle of attack, $\alpha = 90 - \beta - \theta_r$, where θ_r is the local blade twist angle. The thrust coefficient is

$$C_T = \frac{\sigma(1-a)^2(C_l \sin\beta + C_d \cos\beta)}{\cos^2\beta} \tag{5.6}$$

With the local solidity, $\sigma = (Bc_r)/(2\pi r)$, the number of blades, B, and the chord length, c_r. It is then determined if the section is lightly ($C_t < 0.96$) or heavily ($C_t > 0.96$) loaded. For lightly loaded conditions, the new axial induction factor is,

$$a = \frac{1}{1 + \frac{4\cos^2\beta}{\sigma C_l \sin\beta}} \tag{5.7}$$

while for heavily loaded conditions the new axial induction factor is the empirical fit.

$$a = 0.143 + \sqrt{0.0203 - 0.6427(0.889 - C_T)} \tag{5.8}$$

A relaxation factor for the axial induction factor may be required to ensure convergence in all situations, and in this work a value of 0.5 was used. The next value of the tangential induction factor is also calculated.

$$a' = \frac{1}{\frac{4\sin\beta}{\sigma C_l} - 1} \tag{5.9}$$

These new values of a and a' are then used as inputs and a new iteration is performed until the values converged. The relative air velocity at each sector can then be calculated.

$$v = \sqrt{(V_\infty(1-a))^2 + (V_\infty \lambda_r)^2}\,, \qquad [\mathrm{m/s}]. \tag{5.10}$$

To evaluate the turbine performance with and without icing it was also necessary to calculate the torque, power and power coefficient (C_p) of the rotor. The total torque of the rotor was found by integrating the torque of one blade,

$$\tau = F_y r\,, \qquad [\mathrm{Nm/m}] \tag{5.11}$$

over the length of the blade and multiplying by the number of blades. The power of the rotor was found by multiplying the torque with the rotational speed and the power coefficient was calculated by dividing the power of the rotor by the kinetic energy of the air mass moving through the rotor area.

The conditions for each section used for the calculation of the ice shapes are shown in Table 5.4.

Table 5.4: Test sections operating conditions at 10 m/s.

Section	A	B	C	D	E
Section radius, r, [m]	13.25	33.75	41.95	54.25	63
Airfoil name	DU40-A17	DU25-A17	DU21-A17	NACA64-A17	NACA64-A17
Chord length, c_r, [m]	4.557	3.478	3.256	2.518	1.419
Relative air velocity, v, [m/s]	17.36	41.07	50.70	64.14	75.88
Twist angle, θ_r, [deg]	13.308	6.544	4.188	1.526	0.106
Angle of attack, α, [deg]	9.044	3.478	3.320	4.430	5.824

5.3.2 Results and discussion

Shape and location of ice growth

To study the shape and location of ice accretion at different sections along the wind turbine blade, the numerical analyses were carried out for t = 60 min. Results show that with increasing blade profile chord length and thickness, and reduced air velocity, the relative size of the accreted ice reduces. This decrease in the size of accreted ice is mainly due to the decrease in collision efficiency of the droplets with the blade and the reduction in velocity, as discussed previously. Section E, which is at the blade tip, has a smaller chord and blade thickness ratio, as well as a higher velocity, therefore more ice accretion was found at this section, whereas results show a gradual decrease in rate and shape of ice accretion, when moving towards the root section of the blade. This is reflected in the peak values of local collection efficiency for the different sections, section E has a peak value of 0.43, while at section C the peak value is only 0.13.

Figure 5.15 shows the ice growth and distribution at different sections of the blade at constant atmospheric temperature of -10 °C after 60 min. The black shaded areas indicate areas where ice was calculated to accrete. Most of the shaded areas only have slight traces of ice accretion. While ice has not normally been reported on the areas back from the leading edge, neither are observations so detailed in terms of ice traces. The ice thickness for section E is 1.4 % of the chord length, while for section A it is 0.01%.

A significant difference in ice growth can be seen between section E (blade tip) and section C (blade centre). Although the area covered by the ice on section C is larger, the ice layer at section C is very thin, while at section E the accreted ice is considerably thicker. The changes in ice accretion size and shape found here are similar to what has been previously reported [88, 67]. At the inner sections the larger chord gives a lower collection efficiency [67], and the lower relative velocity contributes in the same direction. The result is thinner ice relative to chord length. The ice mass accreted by the different profiles was not studied here.

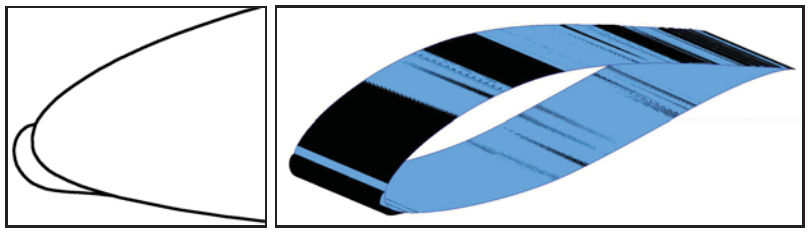

(a) Section E

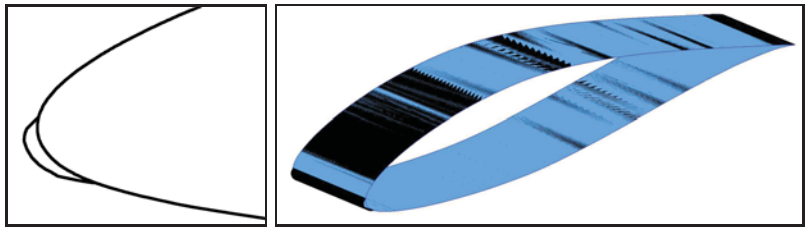

(b) Section D

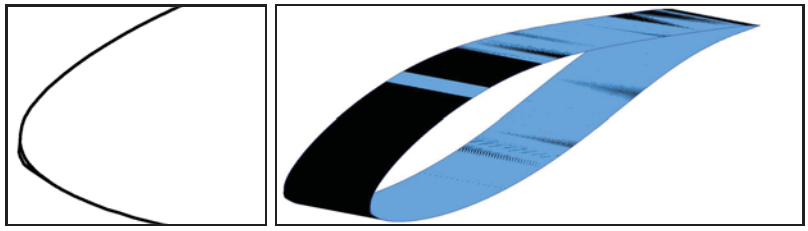

(c) Section C

Figure 5.15: Shape and location of ice accretion at three sections along NREL 5 MW wind turbine blade at T = -10 °C. The left hand figures show the thickness and shape of the leading edge ice. The black shaded areas in the right hand figures indicate the areas where FENSAP has calculated some ice accretion

Aerodynamic coefficients

The aerodynamic coefficients of the clean and iced blade profiles were calculated using the Reynolds-Averaged-Navier-Stokes (RANS) solver in FENSAP. The results obtained were compared with the data in the NREL report [1], which is for a clean blade, and a reasonable agreement was found in the range of normal operation. The NREL data was 2D measured coefficients corrected for rotational stall delay. The original coefficients are from Appendix A of DOWEC document 10046_009.pdf [89] and the NACA coefficients from Abbott and von Doenhoff [90].

Figures 5.16 and 5.17 show the lift and drag coefficients values for three sections (A,C and E) along the NREL 5 MW wind turbine blade at different angles of attack. For the lift and drag analyses carried out in FENSAP, a simplification was done in that rotational effects on aerodynamic performance were not included. This causes an underestimation of the lift coefficient at the inner most section (section A), but

the influence of rotation depends on the span wise location along the blade [91] so this does not significantly affect the mid and outer sections. The inboard section is least significant in terms of power production so this simplification was deemed acceptable. Particularly as the difference due to the ice was the subject of study here and the same simplification was done for both the clean and iced profiles.

The higher peak lift of the modeled results compared to NREL, is perhaps due to the modeling being performed at a higher Reynolds number than the NREL data, though it may also be related to known shortcomings of the RANS methods for separated flow conditions at stall. And, as mentioned previously, the lift curves are in good agreement in the range of normal operation. While there is some discrepancy between the NREL and modeled clean drag data, this is considered less important since it occurs primarily at high angles of attack, outside the operating ranges considered in this study.

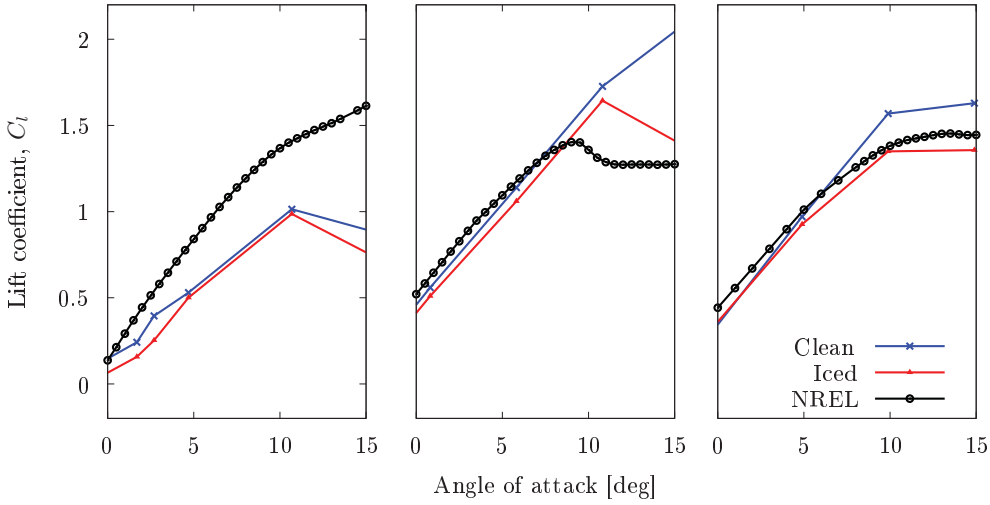

(a) Section A (b) Section C (c) Section E

Figure 5.16: Comparison of lift coefficients for clean and iced blade profiles of three blade sections (A, C and E) along NREL 5 MW wind turbine blade. The NREL data for comparison was obtained from Jonkman et al. [1].

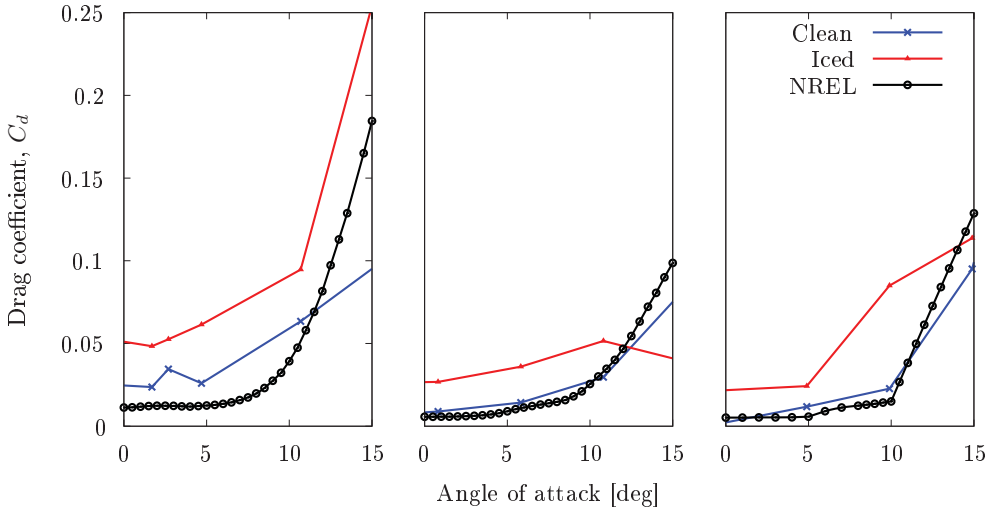

(a) Section A (b) Section C (c) Section E

Figure 5.17: Comparison of drag coefficients for clean and iced blade profiles of three blade sections (A, C and E) along NREL 5 MW wind turbine blade. The NREL data for comparison was obtained from Jonkman et al. [1].

Blade element momentum calculations

The blade element momentum calculation was initially performed for the five clean sections to establish the baseline performance. Thereafter BEM calculations were performed for the iced blade profile sections using the C_l and C_d values calculated from computational fluid dynamics based numerical analyses, and using the C_l and C_d values in the NREL report [1]. The BEM calculations were performed to determine the coefficient of performance (C_p) for the blade, and the results of these calculations are shown in Figure 5.18. It can be seen that the plain C_p curve matches well with the NREL curve in spite of the relatively coarse BEM calculation performed and differences in the calculated lift and drag curves. To illustrate why this is the case, the lift and drag data along the blade for the design tip speed ratio are shown in Figures 5.19 and 5.20. Here it can be seen that the good agreement in the C_p curve is due to good agreement in lift and drag for the outermost sections of the blade at the angles of attack for normal operation. While there is a significant discrepancy at the innermost section, at least partly resulting from not including the spanwise flow, the contribution of this section to the total rotor performance is small, as can be seen in Figure 5.22 which shows the torque contribution along the blade. Finally, in regards to the C_p curve, it can be seen that the iced performance is at a significant penalty and that the performance degradation due to ice increases with higher tip speed ratios.

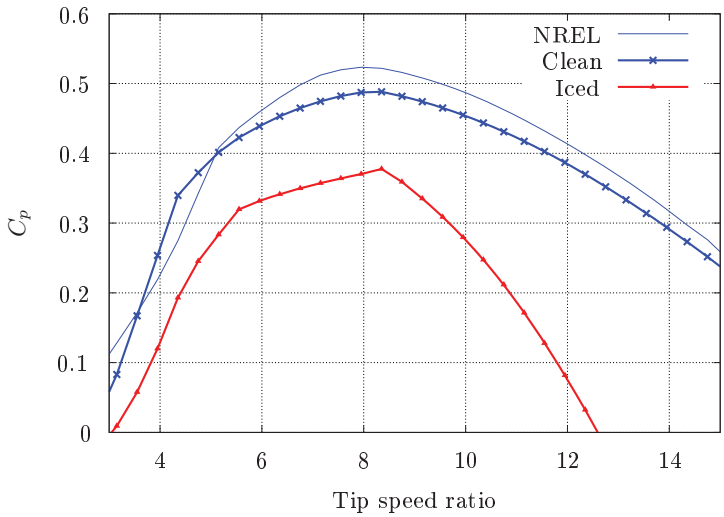

Figure 5.18: Power coefficient vs. tip speed ratio from BEM analysis using blade aerodynamic data from NREL report, clean case and iced case.

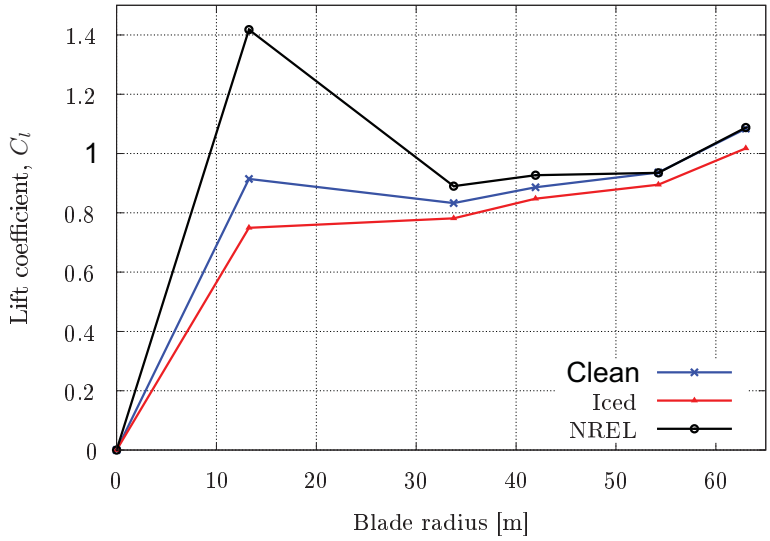

Figure 5.19: Lift coefficients along the blade radius for the clean, iced and NREL cases with $\lambda = 7.55$.

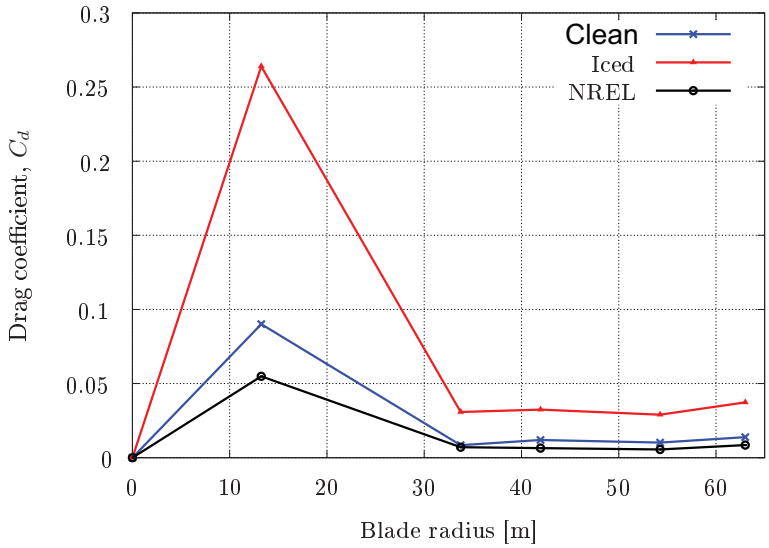

Figure 5.20: Drag coefficients along the blade radius for the clean, iced and NREL cases with $\lambda = 7.55$.

Turbine controller and operating point

The NREL turbine controller is designed with five control regions, 1 (below cut-in wind speed, no power capture), $1\frac{1}{2}$ (linear transition between regions 1 and 2), 2 (optimized power capture), $2\frac{1}{2}$ (linear transition between regions 2 and 3) and 3 (constant power is maintained) [1]. Regions $1\frac{1}{2}$ and 2 were studied here as the pitch controller should still limit the power in region 3 regardless of ice accretions. The turbine generator-torque controller is designed to follow a tabulated torque-speed curve, which was provided by NREL [92]. This curve has a high tip speed ratio at startup ($\lambda = 14$), which decreases through region $1\frac{1}{2}$ and is then optimized for maximum power capture in region 2 by following the torque-speed curve corresponding to a tip speed ratio of 7.55 (the tip speed ratio for maximum C_p for the NREL design). This torque-speed operating curve from the NREL turbine was then used together with the torque-speed curves for the clean and iced rotors to determine the operating point of the rotor at each wind speed and corresponding power output. The operating point of the turbine is defined by the intersection of the torque-speed curves for the turbine and controller.

To illustrate visually what is occurring, Figure 5.21 shows the torque-speed curve for the generator-torque controller together with the torque-speed curves for the clean (ice-free) and iced rotors at a wind speed of 10 m/s. The crossing point of the controller curve and the clean rotor torque-speed curve determines the operating point for the clean rotor at this wind speed, while the crossing point of the controller curve and iced curve determines the operating point for the iced rotor at this wind speed. For the clean curve the intersection point at rotor speed of 1.2 rad/s corresponds to a tip speed ratio of 7.55, as the turbine is designed for, while for the iced rotor the intersection at 1.08 rad/s corresponds to a tip speed of 6.8. In Figure 5.18 it can be seen that this results in the iced rotor operating at a lower C_p than optimal.

The total power of the rotor was found by integrating the linearly interpolated torque curve for the blade for each wind speed. The plots of torque along the length of the blade for the clean and iced cases are shown in Figure 5.22 for a wind speed of 10 m/s.

The torque-speed curves for the iced case at each wind speed were then used to determine the operating points of the wind turbine. Finally, the iced blade data was used to determine if an improvement could be gained by changing the turbine controller to adapt to the iced profiles. It has been shown that an adaptive controller can increase power capture in the event of aerodynamic uncertainty [93]. In this work it was assumed that the controller used a measure of wind velocity to maintain the design tip speed ratio, rather than maintaining operation along the torque-speed curve for the clean blade. This modified controller situation is called the improved iced case.

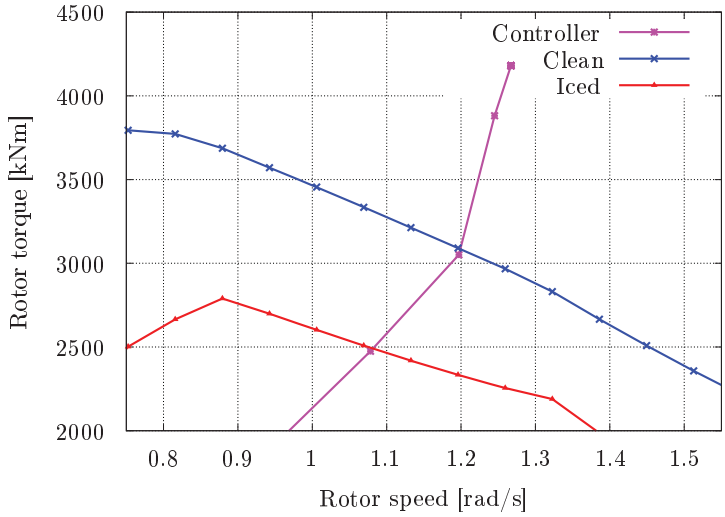

Figure 5.21: Torque-speed curves for the generator-torque controller, the clean rotor and the iced rotor for $V_\infty = 10$ m/s. The intersections of the curves correspond to the operating points of the turbine at this wind speed.

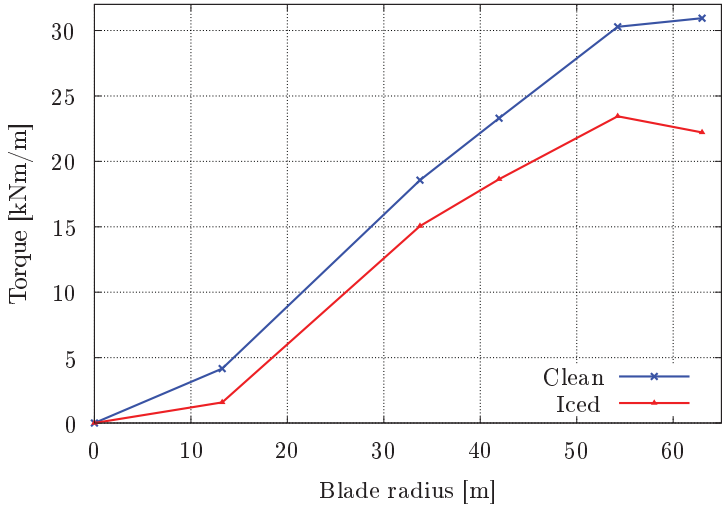

Figure 5.22: Torque along the blade radius for the clean and iced cases with $V_\infty = 10$ m/s.

Power coefficient

The power coefficient versus tip speed ratio calculated using the NREL lift and drag data, and the FENSAP lift and drag data for the clean and iced blade cases are shown in Figure 5.18. The shapes are as expected for a modern three bladed wind turbine, with the peaks being around a tip speed ratio of 8. It can be seen that the maximum performance drops clearly with the ice shapes, from a peak of 0.49 for the clean case to a peak of 0.38 for the iced case. While the entire C_p curve for the iced case is lower than for the clean case, it can also be seen that the decrease is greatest at higher tip speed ratios, where the higher drag caused by the rough ice surface has more significance.

Power curves

The power curves for the clean case and for the iced case are shown in Figure 5.23, together with the curve published by NREL, and a curve for the improved iced case. The NREL curve is nearly indistinguishable from the clean case. It can be seen that there is a significant power loss of about 27% in control region 2 due to the icing. Since the iced blade has different aerodynamic properties than the clean blade, the default generator-torque controller is no longer the optimal in the iced case. Therefore the improved iced case uses the iced rotor, but assumes that the generator-torque controller is modified such that it maintains the design tip speed ratio for each wind speed. The power gained for the improved ice case compared to the iced case is shown in Figure 5.24. It can be seen that for windspeeds of $7 - 13$ m/s there is a significant power gain for the improved iced case. On the other hand it can be seen that for wind speeds of $3 - 6$ m/s the improved iced case actually is slightly worse than the iced case. While the energy production gained overall outweighs this area of worse performance, the reason for the lower performance was examined. It was found that this was due to the turbine having a high tip speed ratio, 14, at the cut-in wind speed. For high tip speed ratios the slope of the C_p curve is negative, which means that it is advantageous to operate at lower tip speeds. The opposite occurs from $7 - 13$ m/s when the tip speed ratio is lower and the slope of the C_p curve is positive.

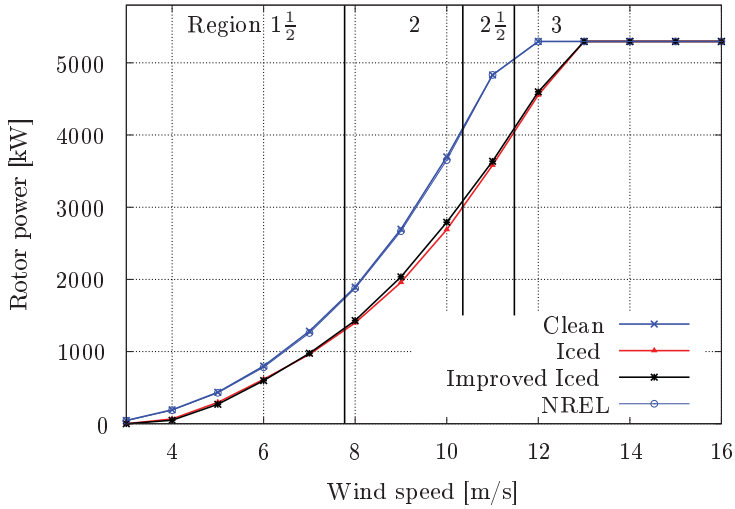

Figure 5.23: Calculated power performance curves together with the published NREL curve.

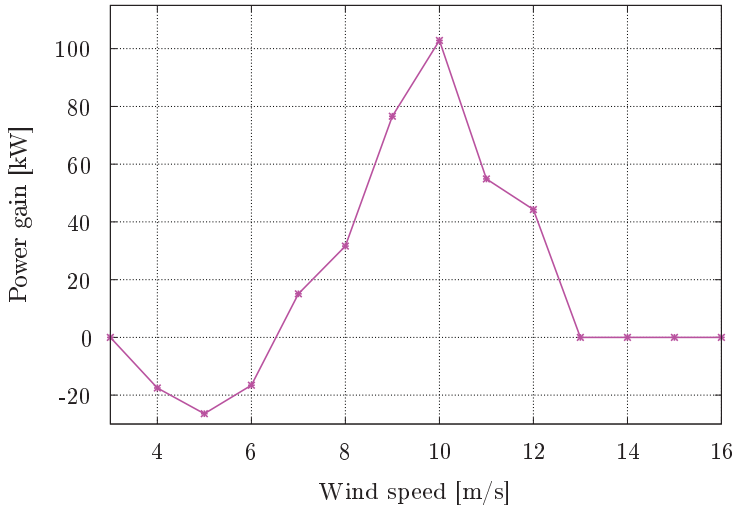

Figure 5.24: Power increase by changing the turbine controller.

Discussion

In this icing event modeled for the NREL 5 MW reference turbine it was found that the power curve was reduced by approximately 28% between cut-in and rated speed. This is similar to what has been reported for other icing studies with similar ice shapes. Barber et al. [94] found a 22% loss for a full blade ice shape, Seifert and Richert [9] $20-30\%$ for a leading edge ice accretion, Laakso and Peltola [95] described 30% losses for small ice accretions and Kimura et al. [12] showed $19-35\%$ power reduction for heavy rime. This shows that atmospheric icing will continue to be an issue at icing prone sites even for large pitch controlled turbines.

It was shown that a variable speed turbine with a generator-torque controller which operates along a fixed torque-speed curve becomes suboptimal when the blades become iced. The exact power losses for an iced rotor will be unique for each specific icing case, but for the case modeled here, the performance lost due to the icing could be reduced by up to 10% for wind speeds of $7-13$ m/s, though the scheme used here gave a penalty for wind speeds of $3-6$ m/s. For this scheme the turbine was controlled to operate at its design tip speed ratio for a given wind speed, rather than regulating it to follow a fixed torque-speed curve as is common today. Regulating a wind turbine based only on the input of a fallible wind sensor will also involve some challenges. Therefore an approach which combines the inputs may be preferable, or perhaps some type of maximum power point tracking could be implemented. In any case it is shown that changing the control scheme can increase the energy capture of an iced turbine. Since the controller is implemented in software, this means that an improved controller can be implemented relatively cheaply, without a need to change the physical construction of the wind turbines.

While a change in the controller algorithm can allow increased power production of an iced turbine, this will be possible as long as the rotor imbalance caused by the ice mass or the iced airfoil aerodynamics is not too large. In the case where an aerodynamic or mass imbalance causes the turbine to shut down due to vibrations, changing the controller will not give an improvement.

5.3.3 Section summary

Modeling of an icing event and the resulting effect on the power curve of the NREL 5 MW Baseline wind turbine was performed. The modeling show that a variable speed wind turbine that is using a generator-torque controller to operate along an optimal torque-speed curve based on an assumed clean blade, is operated in a suboptimal way when the blade becomes iced. Allowing the turbine to operate at its design tip speed ratio also when iced, reduced the power loss due to the icing from 27% to 24% for operation in region 2, though with a slight performance penalty in region $1\frac{1}{2}$. Further work in this area is recommended, both to confirm the results presented here, and in the actual redesigning of the controller to improve the iced operation of wind turbines. Prior to implementing a new controller it will also be necessary to estimate how the loads on the turbine will change due to the ice accretions. Additionally, modeling of more severe icing cases would be interesting to determine if the results presented here can be applied to severe icing cases as well.

5.4 Comparison with measured performance losses on large pitch controlled turbine

The modeling results shown in the previous section showed a a dramatic decrease in the power production curve for the iced wind turbine rotor compared to the clean case. In this section the calculated reduction in power curve from the icing is compared with measured results from Nygårdsfjell windpark.

5.4.1 Experimental setup

Ideally the modeled turbine would have been the same as the actual turbines, but the turbine geometry and control parameters from the turbines at Nygårdsfjell were not available for this work. Therefor the 5 MW NREL reference turbine was used instead. The operation prinicple is the same for both the NREL turbine and the turbines at Nygårdsfjell. Both are modern, pitch controlled, variable speed, multi-megawatt turbines. Finally, no measure of droplet size or liquid water content was performed at Nygårdsfjell, so those input parameters had to be assumed. The liquid water content and droplet size was chosen similarly to previous studies such that the results can be compared.

To calculate the power curve performance of these wind turbines some filtering and pre data analysis was necessary. The measured power curves for the wind turbines are quite different for easterly and westerly winds, probably due to complex terrain around the site. Wind primarily blows from only those two directions, as can be seen in Figure 5.25, so a separate power curve was generated for each primary direction.

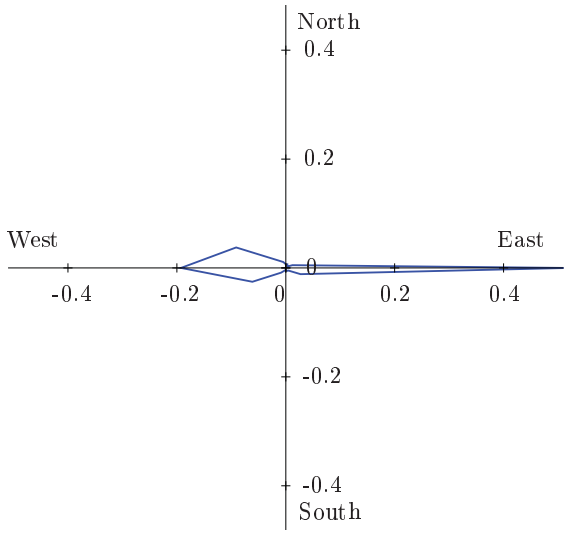

Figure 5.25: Wind frequency radar plot showing the percentage of time the wind comes from different sectors. East and west are clearly the two dominant directions.

The power curves were generated by the following process. First, all periods during which the turbine was stopped were removed. Thereafter the data was binned using the wind speed, as described in the IEC standard [57], using bins of 0.5 m/s. The wind speed was corrected for changes in density resulting from temperature changes according to the IEC standard.

The data in a bin consists of a spread of points. The spreading of the data is dependent on many factors, including: variations in wind speed, wind direction, wind shear, turbine misalignment, and uncertainty in the measurements of wind speed and output power. The spread of data points are reduced to one average wind speed and one average power production for each bin. This spread of data points can be seen as a band of data points when the measured power production from a wind turbine is plotted relative to wind speed. The filtered production data used to generate the power curve for one direction of one of the wind turbines at Nygårdsfjell is shown together with the resulting calculated power curve in Figure 5.26.

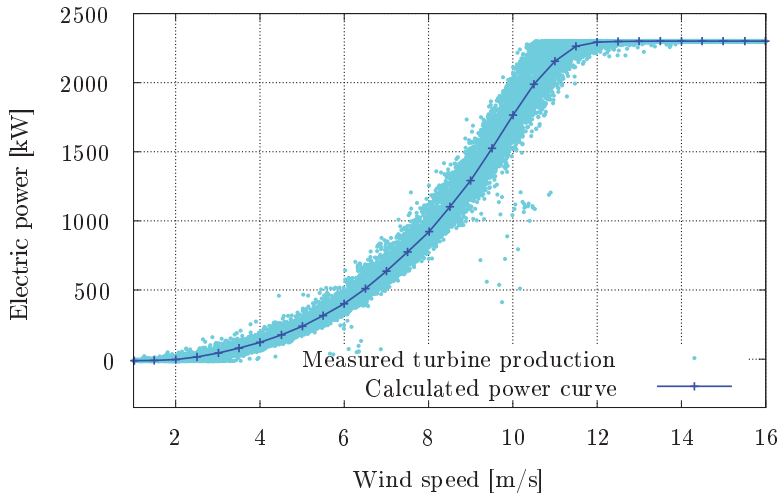

Figure 5.26: All data used to generate a power curve for one direction and the resulting power curve.

5.4.2 Icing events

Several periods of operation during icing conditions were identified during the 2008-2009 winter. Two of the periods are here described in more detail.

The first period was in the time frame December 5 - Dec. 9, 2008, with the main icing apparently occurring on December 5. During this icing period the cup anemometers were seen to slow and finally stop, while the ultrasonic anemometers were reporting nearly constant wind speed. Photographs from the fifth were not usable for identification of icing due to poor visibility, but photographs of the tail section of the nacelle from the sixth clearly show rime icing on the cup anemometer and lightning rods, as can be seen in Figure 5.27.

Figure 5.27: Rime ice visible on the sensors following the icing event Dec. 5.

In Figure 5.28 the production can be seen to decrease at 8-10 m/s wind speed to much below the normal range of operation as the icing event progresses even as the wind speed is relatively unchanged. Production then ceases as the wind speed eventually decreases. When this is compared with the calculated power loss due to icing shown in Figure 5.23 it can be seen that the power production here gradually decreases below the modeled curve for the iced case. This is as expected for a turbine operating in icing conditions. For a certain build-up of ice the turbine should operate as in the modeled ice case, and when the ice is further increased the performance should decrease further.

The second period was in the time frame January 7 - January 10, 2009, with the main icing apparently occurring in the evening of January 8. Due to the event occurring at night, no pictures were able to show clearly any ice or lack thereof. In Figure 5.29 the production can be seen to remain below the range of normal operation as the wind speed increases from near 0 up to rated wind speed. At about 20% over rated wind speed rated power is finally attained, and thereafter maintained. When this is compared with the calculated power loss due to icing shown in Figure 5.23 it can be seen that the power production here is initially much less than the modeled curve for the iced case, but then jumps up to nearly the modeled case and then varies about somewhat below the modeled case as wind speed increases. The jump in production is perhaps due to partial ice shedding from the blade, but no observations exist to corroborate this hypothesis.

One item of interest observed during this icing event was the turbine pitch angle. This is shown in Figure 5.30 and it can be seen that the pitch angle is first well below the normal range as rated wind speed is first reached. Thereafter the pitch angle remains 1-2 degrees below normal for the duration of the event. This shows that the turbine pitch control compensates for the lower aerodynamic performance of a slightly iced blade by increasing the pitch angle. This increased pitch angle

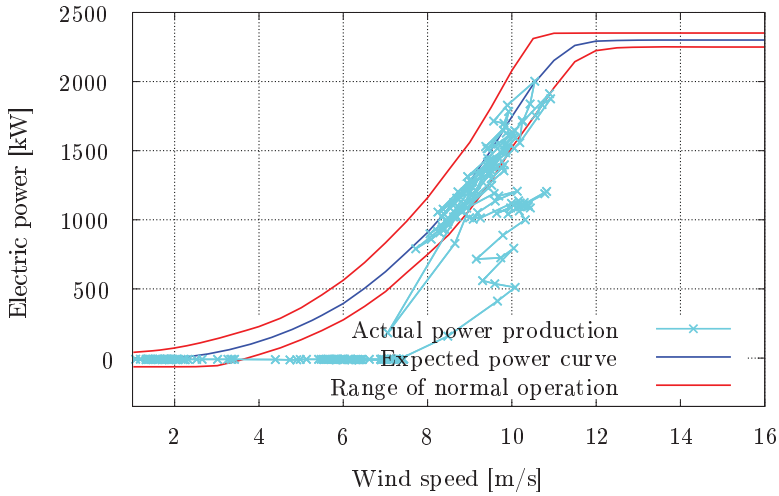

Figure 5.28: Measured power production during the icing event of Dec. 5 (consecutive points are connected) can be seen to decrease from normal operation at 8-10 m/s wind speed to much below the normal range of operation as the icing event progresses even as the wind speed is relatively unchanged. Production then ceases as the wind speed eventually decreases.

means that the turbine blade and tower are likely subjected to greater than normal bending moments, but the analysis of such forces was beyond the scope of this work.

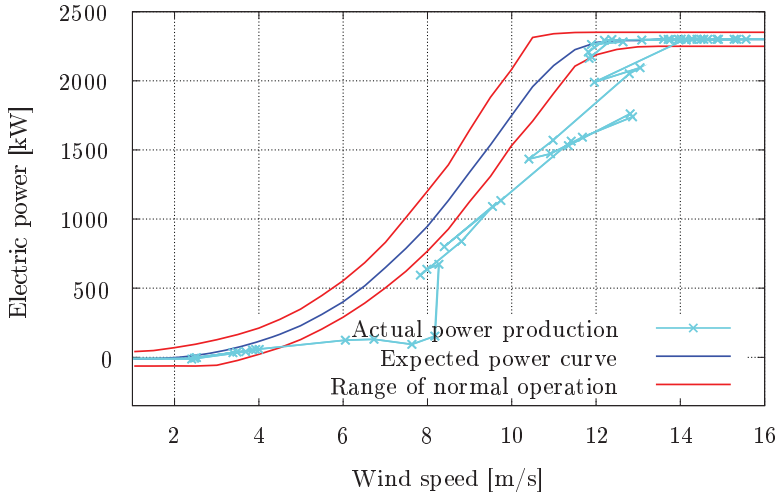

Figure 5.29: Measured power production during the icing event of Jan. 8 (consecutive points are connected) can be seen to remain below the range of normal operation as the wind speed increases from near 0 up to rated speed. At about 20% over rated speed rated power is finally attained, and thereafter maintained.

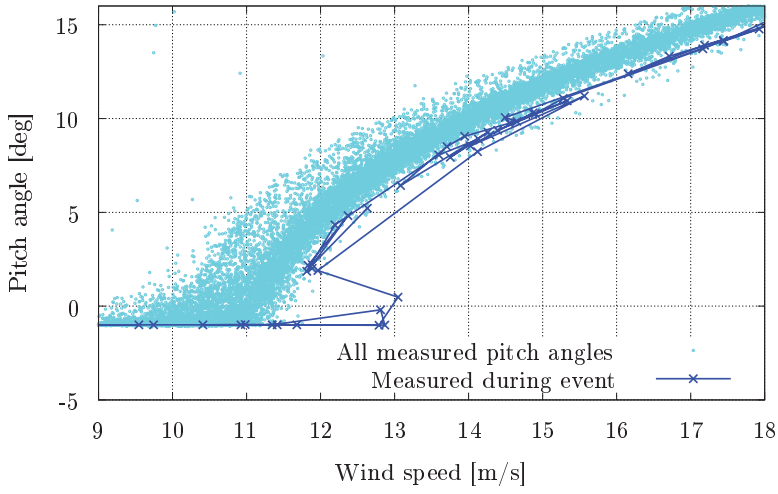

Figure 5.30: Measured pitch curve during the icing event of Jan. 8 (consecutive points are connected) can be seen to be well below the range of normal operation as the wind speed increases above rated wind speed. It thereafter approaches normal pitch angle for higher wind speeds but continues to operate with a pitch angle of about 1-2 deg less than usual.

5.4.3 Discussion

While it is far from a conclusive proof or verification of the model results, due to lack of data on the actual icing conditions during the period, and longer icing duration than that modeled, these cases show that reductions in the power performance of actual turbines can be similar to the reductions in the modeled case. These cases thereby act to support the modeled results and give greater confidence in the modeling results. The modeled case represents an idealized case where constant icing conditions are maintained for one hour.

5.4.4 Section summary

The analysis of two icing events at Nygårdsfjell wind park and comparison with the modeled icing case for the NREL wind turbine indicate that actual reductions in power production can be greater than those modeled, which is reasonable when the duration of the modeled and actual icing events are compared. The results are deemed to correspond reasonably well with the observed effects and give confidence that the modeling methods used can be useful in estimating the effects of icing and exploring methods of reducing the adverse effects of icing.

It was seen from the operational data that a pitch controlled turbine can compensate for a partly iced blade in terms of power production, though this will have some effect on the loads the turbine is then subjected too. Future work regarding the effects of icing on fatigue of wind turbines should examine the effect of operating with this kind of changed pitch angle.

5.5 Summary

Icing on the blade profiles for four different size wind turbines were modeled using numerical techniques. Previous work had indicated that dry rime icing was less severe for larger wind turbines both in terms of local ice mass and in terms of ice thickness, and a significant change in the flow behavior and aerodynamic characteristics is observed here. It was found that the decrease in the torque coefficient was greater for the smaller wind turbines, which supports the hypothesis that dry rime icing affects larger wind turbines less than smaller wind turbines. In addition to these results some questions remain. For more detailed results, modeling other icing conditions, including different wind speeds and operating conditions should also be performed. Further studies of the change in surface roughness should be included in future work.

Two dimensional numerical modeling of atmospheric icing on a blade profile section (NACA 64618) at approximately 85% radius of a 5 MW wind turbine were performed with varying droplet sizes and temperatures. The results show that while icing causes the lift coefficients to be reduced in all cases, the amount of reduction varied and the least change in lift was observed for the cases that seemed to produce rime type of streamlined ice shapes. The icing which causes horn type of glazed icing shapes had larger reductions in lift. These results show that to be able to accurately estimate energy production losses based on atmospheric icing, it will be necessary to have measurements of the atmospheric conditions during the

icing such that the shape and type of icing can be found. It was also shown that air temperature alone can not be used to differentiate between rime and glaze ice, but that droplet size can also change the effect of an icing event.

Future work in this area should include more detailed turbulence analysis and investigating the different turbulence models to better understand and numerically model the thin boundary layer characteristics near the wall and overall turbulence behavior across the wind turbine under different icing conditions. Moreover full scale three dimensional numerical analysis should be carried out to better understand the effect of change in aerodynamic characteristics on overall performance of the wind turbine blade in icing conditions.

Modeling of an icing event and the resulting effect on the power curve of the NREL 5 MW Baseline wind turbine was performed. The modeling showed that a variable speed wind turbine that is using a generator-torque controller to operate along an optimal torque-speed curve based on an assumed clean blade, is operated in a suboptimal way when the blade becomes iced. Allowing the turbine to operate at its design tip speed ratio also when iced, reduced the power loss due to the icing from 27% to 24% for operation in region 2, though with a slight performance penalty in region $1\frac{1}{2}$. Further work in this area is recommended, both to confirm the results presented here, and in the actual redesigning of the controller to improve the iced operation of wind turbines. Prior to implementing a new controller it will also be necessary to estimate how the loads on the turbine will change due to the ice accretions. Additionally, modeling more severe icing cases would be interesting to determine if the results presented here can be applied to severe icing cases as well.

The analysis of two icing events at Nygårdsfjell windpark and comparison with the modeled icing case for the NREL wind turbine indicate that actual reductions in power production can be greater than those modeled, which is reasonable when the duration of the modeled and actual icing events are compared. The results are deemed to correspond reasonably well with the observed effects and give confidence that the modeling methods used can be useful in estimating the effects of icing and exploring methods of reducing the adverse effects of icing. It was seen from the operational data that a pitch controlled turbine can compensate for a partly iced blade in terms of power production, though this will have some effect on the loads the turbine is then subjected too. Future work regarding the effects of icing on fatigue of wind turbines should examine the effect of operating with this kind of changed pitch angle.

Chapter 6

Conclusions

6.1 Discussion and summary

The work presented in this thesis extends the current knowledge of icing on wind turbines on three fronts. In this section the three areas will first be mentioned briefly and then revisited with a longer discussion of the results.

- First, the monitoring of icing and its effects on production at Nygårdsfjell wind park has been described. While there are certainly many who have monitored icing and its effects on wind turbines, relatively little has been published. Published data is important to distribute for use by other researchers and allow progress in the field, and the methods described herein may ease the data collection and analysis for future research in this field.

- Second, the sensitivity of atmospheric icing to turbine size, with all of the combinations of changes that accompany changes in size, and to several atmospheric parameters,including droplet size and temperature was explored through models using both the panel method (TURBICE), and a CFD solver (FENSAP-ICE). Knowledge of how ice accretion scales with turbine size as well as how it changes with variations in atmospheric parameters can allow a more focused analysis of which design parameters can be varied to minimize the consequences of icing.

- Third, the effect of modeled ice shapes on the aerodynamic performance of the wind turbines were examined through CFD modeling (FLUENT) and these changes in the aerodynamic performance were used to estimate the resulting effect on the power curve of a modern wind turbine. The results were then compared back to observations from Nygårdsfjell wind park. Understanding how the different ice shapes affect energy production is necessary both for determining where to install wind turbines and to decide if de- or anti-icing systems should be installed.

Overall the most important results of the work described in this thesis are considered to be:

- It has been shown that wind turbine energy production is less negatively affected by dry rime icing the larger the turbine is, and indicated that this is the case for other types of icing as well.
- It has been demonstrated that changing the control system of a wind turbine can improve energy production during icing events.
- Modeled results have been compared with observations and thereby given increased confidence in the modeled results.

6.1.1 Icing monitoring

Monitoring of the icing at Nygårdsfjell wind park was described in Chapter 3. In Section 3.3 a HoloOptics T23 icing sensor was used to monitor the icing. In spite of significant icing time indication from the sensor, relatively little production losses could be seen from analysis of the production data. Suspected spontaneous shedding of icing with increasing wind speed was observed in the power production data. Lower sensitivity to icing for larger turbines was proposed as a possible reason for the relatively low production losses.

In Section 3.4 installation of a new HoloOptics sensor together with webcameras was described. The webcameras were planned to allow visual confirmation of icing conditions and were useful in verifying some of the icing events, but due to poor visibility during icing the images could not be used to verify all of the events. An often occurring event called overproduction was defined. This corresponds to a measured power production higher than the measured wind speed should allow and indicates an incorrect wind measurement. In Section 3.5 the power production losses at Nygårdsfjell were compared with two other windparks. A simple method of estimating production losses by using a binning method, taking the median power production for each bin, and using a threshold of 85% of the median was developed. Nygårdsfjell wind park, with the largest turbines of the three sites, appears to have significantly less energy losses due to icing than the other two sites and Aapua, with the smallest turbines, has significantly higher energy losses, though it can not be sure that the differences in turbine size contribute to the differences in energy losses.

6.1.2 Icing parameter sensitivity

In Chapter 4 the results from modeling of icing to analyze the sensitivity of atmospheric icing to different parameters are presented. Variations in icing due to change in turbine size was the primary parameter examined. In Section 4.1 a panel method based ice accretion code, TURBICE, was used to model dry rime ice accretions at -10 °C on four different sized turbines. From these model results it was found that in spite of the larger turbines having a higher relative wind speed near the blade tips, the increased chord of the larger blades caused a lower collection efficiency and thereby ice accretions that were relatively thinner and lighter than on the smaller turbines. Since the ice shapes were found to be similar for the different turbines, it is reasonable to infer that the thinner shapes will have less of an aerodynamic impact on the turbine performance.

In Section 4.2 TURBICE was used to model the same four turbines and a larger pitch controlled turbine at higher temperatures (-10, -7.5, -5, and -2.5 °C). From these results it was found that the ice shapes for the different turbines become dissimilar at higher temperatures. The heat balance of the leading edge was examined and it was found that larger turbines have a higher stagnation line temperature during rime ice accretion than smaller turbines due to the heat transfer coefficient decreasing more than the collection efficiency decreases. Higher relative wind speeds also contribute to the higher temperatures. This means that the ice shapes which typically have the largest drag penalty, horn ice, will occur at lower temperatures for a larger turbine than for a smaller.

In the work described in Section 4.3 a 3-D CFD based solver, FENSAP-ICE, was used to calculate ice accretions at different sections along the blade of a 5 MW pitch controlled wind turbine. The results showed that the outer sections of the turbine blade accrete significantly more ice than the inner sections. This is a result of the outer sections of the blade having both a higher relative wind speed and a higher collection efficiency.

A significant consequence of these results is the knowledge that an activated blade heating system can, in some conditions, result in worse performance than if no heating was used. If a heating system does not have sufficient power to remove the ice forming, activation of the heating system could cause the formation of horn shaped glaze ice instead of a more streamlined rime ice with the result being worse aerodynamic performance than with no heating.

A third icing code LEWICE was also considered for inclusion in this work, but due to restrictions on its use outside the United States it was not possible to include it here.

6.1.3 Icing - effects on aerodynamics and power production

In Chapter 5 the changes in the aerodynamics resulting from icing are described and the resulting effect on power production is calculated. Section 5.1 used a CFD based solver, FLUENT, to calculate the changes in the aerodynamic parameters for rime ice accretions generated by TURBICE on four different sized turbines with ambient temperature of -10 °C. A torque coefficient was calculated for three of the turbines using the CFD calculated lift data together with drag data that was corrected to account for surface roughness of the ice. The torque coefficient was more sensitive to ice for the smaller turbines.

Section 5.2 described the analysis of aerodynamic performance for iced and ice-free profiles from a 5 MW turbine with FLUENT. Variations in both temperature and droplet size were examined and it was found that streamlined rime ice type of shapes caused the least reduction in performance. Starting from a baseline ice shape formed with 17 µm droplets at -2.5 °C, either smaller droplet size or lower temperature resulted in icing that was much less significant in terms of reduced torque coefficient for the wind turbine.

In Section 5.3, FENSAP-ICE was used together with FLUENT to calculate the effect of ice shapes along an entire turbine blade. The aerodynamic performance of five sections along the blade was found for both plain and iced conditions and used to calculate the rotor torque and turbine power curve for both cases. Allowing the

turbine to operate at its design tip speed ratio also when iced, reduced the power loss due to the icing from 27% to 24% for operation in region 2.

In Section 5.4 two icing events at Nygårdsfjell wind park were analyzed and compared with the modeled icing case for the NREL wind turbine. It was found that actual reductions in power production can be greater than those modeled, which is reasonable when the duration of the modeled and actual icing events are compared. The results are deemed to correspond reasonably well with the observed effects and, importantly, give confidence that the modeling methods used can be useful in estimating the effects of icing and exploring methods of reducing the adverse effects of icing. It was seen from the operational data that a pitch controlled turbine can compensate for a partly iced blade in terms of power production, when above rated wind speed, though this will have some effect on the loads the turbine is then subjected to.

While the software used for modeling the ice accretion, calculating the changed aerodynamic coefficients, and calculating the performance reduction all include some error, the actual measured data from the wind turbines also contains significant uncertainties and variations both in the measurements taken and in the atmospheric conditions. This means that in comparisons with actual turbine performance it will likely be unreasonable to expect a better correlation with modeled results than that the results seem reasonable. In this respect the comparison of the model results with operational data from Nygårdsfjell, while not being able to prove that the modeling is correct, does indicate that the modeling gives reasonable results.

6.2 Suggestions for future research

Wind energy is becoming more important and to improve understanding of performance in ice-prone areas further research will be needed. Some of the areas which seem relevant following this work are described below.

Since it was found that icing and icing shapes are dependent on the turbine design parameters, the research work indicates that the ice accretion on wind turbine blades can possibly be controlled by optimizing its geometric design features rather than using anti-icing or de-icing systems. Further research is needed here to investigate both the reduction in icing sensitivity and any performance penalties for plain conditions resulting from the design changes.

Another promising area for further research is investigating the possibility of deicing using modified operation of the wind turbine. This can possibly de-ice the turbine in two ways. First, normal operation induces vibration and flexing of the blades which can accelerate the cracking loose and removal of ice accretions. Second, normal operation causes kinetic heating of the moving wind turbine blades. This kinetic heating may be accelerated by allowing the rotor to spin at high speeds following an icing event until erosion, or sublimation, of the accumulated ice allows a gradual return to normal operation. It has been observed at Nygårsdfjell that ice near the blade tips has been relatively quickly eroded after icing conditions cease. Since it is ice near the blade tips that most affects wind turbine power production, this may be a viable low-cost method of dealing with icing at sites with light to

moderate icing. This method also requires that the turbines are not damaged by operating with the ice on the blades and that potential ice cast from the blades will not cause harm to persons or property.

There is still quite a long way to go with respect to gaining certain knowledge about icing from modeling. One very important item lacking in current numerical models is the ability to include the flexing of the blade and breaking loose of the ice. This is a significant deficit in the current models as observations of operating wind turbines shows that ice does not build up indefinitely, but rather portions break off and the accretion process begins again at those portions. The result of this kind of process can be seen in the image of stepped ice shown in Figure 1.5. To accurately model the effects of long duration icing events that can occur naturally, new models must be developed. For aircraft purposes this has not been an issue as aircraft would not remain in icing conditions for many hours, but as observations here have shown, wind turbines can be subject to icing events lasting over 12 hours, which is far beyond the scope of current models. To address this, coupled models that include both the aeroelastic bending of the blades together with the ice accretion modeling are needed.

As with all studies of this type, verification of the results presented through icing wind tunnel testing or other methods would be interesting and useful to uncover and quantify deficiencies in the models. In this respect automated sensors to monitor the liquid water content and droplet size during icing events would be a significant assistance. And, as the severity of icing for aerodynamics was shown to be dependent on droplet size, a low cost automated sensor for liquid water content and droplet size would also be valuable for estimating the type of icing during a wind resource assessment campaign.

Finally, further studies into how the turbine controller should be redesigned to adaptively deal with ice accretion may allow reduced icing losses. It will also be necessary to ensure that the turbine design will tolerate the modified operation during iced conditions.

Bibliography

[1] J. Jonkman, S. Butterfield, W. Musial, and G. Scott. Definition of a 5-MW reference wind turbine for offshore system development. Technical Report NREL/TP-500-38060, NREL, 2009. URL:http://www.nrel.gov/wind/pdfs/38060.pdf. Accessed: 2010-06-11. (Archived by WebCite at http://www.webcitation.org/5qPatf7uk).

[2] P.J. Musgrove. Wind energy conversion: Recent progress and future prospects. *Solar & wind technology*, 4:37–49, 1987.

[3] H. Seifert. Technical requirements for rotor blades operating in cold climate. In *Proceedings of the 2003 BOREAS VI Conference. Pyhätunturi, Finland.* Finnish Meteorological Institute, 2003.

[4] H. Ganander and G. Ronsten. Design load aspects due to ice loading on wind turbine blades. In *Proceedings of the 2003 BOREAS VI Conference. Pyhätunturi, Finland.* Finnish Meteorological Institute, 2003.

[5] G. Ronsten. Svenska erfarenheter av vindkraft i kallt klimat - nedisning, iskast och avisning. Elforsk rapport 04:13, 2004. (In Swedish).

[6] W.J. Jasinski, S.C. Noe, M.S. Selig, and M.B. Bragg. Wind turbine performance under icing conditions. *Transactions of the ASME, Journal of solar energy engineering*, 120:60–65, 1998.

[7] E. Peltola, T. Laakso, G. Ronsten, L. Tallhaug, R. Horbaty, I. Baring-Gould, and A. Lacroix. Specific recommendations for the development of wind energy projects in cold climates. In *Proceedings of the BOREAS VII conference. Saariselkä, Finland.* Finnish Meteorological Institute, 2005.

[8] A. Dahlqvist. The effects of ice on the aerodynamics of the rotor blades of a wind turbine. Master's thesis, Helsinki University of Technology, Department of Mechanical Engineering, 1997.

[9] H. Seifert and F. Richert. A recipe to estimate aerodynamics and loads on iced rotor blades. In *Proceedings of the BOREAS IV Conference.* Finnish Meteorological Institute, 1998.

[10] R. K. Calay, A. E. Holdo, P. Mayman, and I. Lun. Experimental simulation of runback ice. *Journal of Aircraft*, 34:206–212, 1997.

[11] M.G. Potapczuk and K.M. Al-Khalil. Ice accretion and performance degradation calculations with lewice/ns. Technical report, NASA Technical Memorandum 105972, 1993.

[12] S. Kimura, B. Tammelin, and K. Säntti. Estimation of reduction of power production due to icing from the existing meteorological data. In *Proceedings of the BOREAS V Conference*. Finnish Meteorological Institute, 2000.

[13] B. Tammelin, M. Stuke, H. Seifert, and S. Kimura. Icing effect on power production of wind turbines. In *Proceedings of the BOREAS IV Conference*. Finnish Meteorological Institute, 1998.

[14] M. Marjaniemi and E. Peltola. Blade heating element design and practical experiences. In *Proceedings of the BOREAS IV Conference*. Finnish Meteorological Institute, 1998.

[15] M. Marjaniemi, L. Makkonen, and T. Laakso. TURBICE - The wind turbine blade icing model. In *Proceedings of the BOREAS V conference*. Finnish Meteorological Institute, 2000.

[16] M. C. Homola, P. J. Nicklasson, P. A. Sundsbø, and A. E. Holdo. Experiences from icing at Nygårdsfjell wind park. In *Proceedings of the EWEC 2008*, 2008.

[17] B. Tammelin, M. Cavaliere, H. Holttinen, C. Morgan, H. Seifert, and K. Säntti. Wind energy production in cold climate. In *Meteorological publications*, volume 41. Finnish Meteorological Institute, 2000.

[18] L. Makkonen, P. Lehtonen, and L. Helle. Anemometry in icing conditions. *Journal of atmospheric and oceanic technology*, 18(9):1457–1469, 2001.

[19] G. Fortin, J. Perron, and A. Ilinca. Behaviour and modeling of cup anemometers under icing condtions. In *IWAIS XI*, 2005.

[20] John F. Maissan. Wind power development in sub-arctic conditions with severe rime icing. In *Circumpolar climate change summit and exposition*, 2001.

[21] R. Westerlund. Is på vindkraftverk: Detektering, utbredning, personskaderiskminimering og produksjonsbortfall. Elforsk rapport 09:06, 2009. (In Swedish).

[22] G. Fortin, J. Perron, and A. Ilinca. A study of icing events at Murdochville. In *International Conference Wind Energy and Remote Regions*, 2005.

[23] K. Säntti, B. Tammelin, T. Laakso, and E. Peltola. Experience from measurements of atmospheric icing. In *Proceedings of the 2003 BOREAS VI Conference*. Finnish Meteorological Institute, 2003.

[24] I. Baring-Gould, L. Tallhaug, G. Ronsten, R. Horbaty, R. Cattin, T. Laakso, M. Durstewitz, A. Lacroix, E. Peltola, and T. Wallenius. Wind energy projects in cold climates. IEA Research and Development Wind, Task 19, 2009.

[25] M. C. Homola, P. J. Nicklasson, and P. A. Sundsbø. Ice sensors for wind turbines. *Cold Regions Science and Technology*, 46:125–131, 2006.

[26] M. Durstewich. Results of the new icetools inquiry on operators' experience with turbine icing. In *Proceedings of the BOREAS VII Conference*, 2005.

[27] S.M. Fikke, K. Säntti, and T. Laakso. Detectors for atmospheric icing. In *Proceedings of the 2005 BOREAS VII Conference*. Finnish Meteorological Institute, 2005.

[28] O. Parent and A. Ilinca. Anti-icing and de-icing techniques for wind turbines: Critical review. *Cold Regions Science and Technology*, 2010. doi: 10.1016/j.coldregions.2010.01.005.

[29] W.B. Wright. *User Manual for the NASA Glenn Ice Accretion Code LEWICE*, 2002. URL: http://gltrs.grc.nasa.gov/reports/2002/CR-2002-211793.pdf, Accessed: 2010-08-05. (Archived by WebCite at http://www.webcitation.org/5rsIwxHmU).

[30] J. Shin, B. Berkowitz, H. Chen, and T. Cebeci. Prediction of ice shapes and their effect on airfoil performance. Technical report, NASA Technical Memorandum 103701, 1991.

[31] K. J. Finstad and L. Makkonen. Modelling of rime on turbine blades. In *Wind Energy Production in Cold Climates, BOREAS III Symposium*, pages 281–293. Finnish Meteorological Institute, 1996.

[32] L. Makkonen, T. Laakso, M. Marjaniemi, and K. J. Finstad. Modelling and prevention of ice accretion on wind turbines. *Wind Engineering*, 25:3–21, 2001.

[33] J. Månsson. Why de-icing of wind turbine blades? In *Global WINDPOWER 2004*. URL:http://www.lmwindpower.com/upload/why_de-icing_of_wind_turbine_blades.pdf. Accessed: 2010-08-09. (Archived by WebCiteő at http://www.webcitation.org/5rr9Go79N), 2004.

[34] R. Horbaty. Wind energy in cold climates - The Swiss experience. In *Proceedings of the BOREAS VII conference. Saariselkä, Finland*. Finnish Meteorological Institute, 2005.

[35] G. Botura and K. Fisher. Development of ice protection system for wind turbine applications. In *Proceedings of the 2003 BOREAS VI Conference*. Finnish Meteorological Institute, 2003.

[36] S. Kimura, T. Sato, and K. Kosugi. The effect of anti-icing paint on the adhesion force of ice accretion on a wind turbine blade. In *Proceedings of the 2003 BOREAS VI Conference*. Finnish Meteorological Institute, 2003.

[37] S. Kimura, K. Furumi, T. Sato, and K. Tsuboi. Evaluation of anti-icing coatings on the surface of wind turbine blades for the prevention of ice accretion. In *Proceedings of the 7th international syposium on cold region development*, number 63, 2004.

[38] L. Battisti. Anti-icing system for wind turbines, 2004. World Intellectual Property Organization, International publication number WO 2004/036038 A1.

[39] M. C. Homola, G. Ronsten, and P. J. Nicklasson. Energy production losses due to iced blades and instruments at Nygårdsfjell, Sveg and Aapua. In *IWAIS XIII*. URL:http://ansatte.hin.no/mch/documents/IWAIS2009-Homola-Ronsten-Nicklasson.pdf. Accessed: 2010-08-05. (Archived by WebCite at http://www.webcitation.org/5rkfMidVY), 2009.

[40] M. C. Homola, P. J. Nicklasson, and P. A. Sundsbø. Two years of icing monitoring at Nygårdsfjell wind park. In *IWAIS XIII*. URL:http://ansatte.hin.no/mch/documents/IWAIS2009-Homola-Nicklasson-Sundsb%C3%B8.pdf. Accessed: 2010-08-05. (Archived by WebCite at http://www.webcitation.org/5rkfm4YHg), 2009.

[41] T. Wallenius, M. C. Homola, L. Makkonen, and P. J. Nicklasson. Relationship between chord length and rime icing on wind turbines. In *Winterwind 2008, Dec. 9-10, Norrkjoping, Sweden*, 2008.

[42] M. C. Homola, T. Wallenius, L. Makkonen, G. Beeri, P. J. Nicklasson, and P. A. Sundsbø. Scaling of icing on wind turbines. In *Multiphysics 2008*, 2008.

[43] M. C. Homola, T. Wallenius, L. Makkonen, P. J. Nicklasson, and P. A. Sundsbø. The dependence of icing severity on chord length. In *Proceedings of the EWEC 2009*. URL:http://ansatte.hin.no/mch/documents/ewec_2009-Homola%20etal.pdf. Accessed: 2010-08-05. (Archived by WebCite at http://www.webcitation.org/5rkg301R2), 2009.

[44] G. Ronsten, B.E. Dierer, L. Nygaard, L. Makkonen, and M. C. Homola. Measures needed for the successful development of wind energy in icing climates. In *Proceedings of the EWEC 2009*. URL:http://ansatte.hin.no/mch/documents/EWEC2009_COST727_Paper-Ronsten%20etal.pdf. Accessed: 2010-08-05. (Archived by WebCite at http://www.webcitation.org/5rkgMxAbr), 2009.

[45] M.C. Homola, T. Wallenius, L. Makkonen, P.J. Nicklasson, and P.A. Sundsbø. The relationship between chord length and rime icing on wind turbines. *Wind Energy*, 2009. doi: 10.1002/we.383.

[46] M. C. Homola, T. Wallenius, L. Makkonen, P. J. Nicklasson, and P. A. Sundsbø. Turbine size and temperature dependence of icing on wind turbine blades. *Wind Engineering*, 34(6):615–628, 2010.

[47] M. Virk, M.C. Homola, and P.J. Nicklasson. Effect of rime ice accretion on aerodynamic characteristics of wind turbine blade profiles. *Wind Engineering*, 34(2):207–218, 2010.

[48] M. C. Homola, M. S. Virk, T. Wallenius, P. J. Nicklasson, and P. A. Sundsbø. Effect of atmospheric temperature and droplet size variation on ice accretion

of wind turbine blades. *Journal of Wind Engineering and Industrial Aerodynamics*, 2010. doi: 10.1016/j.jweia.2010.06.007.

[49] M. C. Homola, M. Virk, P. J. Nicklasson, and P. A. Sundsbø. Modelling of ice induced power losses and comparison with observations. In *Winterwind 2011*, 2011.

[50] R. R. Rogers and M. K. Yau. *A Short Course in Cloud Physics*. Elsevier Science, 1989.

[51] L. Makkonen and K. Ahti. Climatic mapping of ice loads based on airport weather observations. *Atmospheric Research*, 36(3-4):185–193, 1995. doi: 10.1016/0169-8095(94)00034-B.

[52] B.E. Nygaard, J.E. Kristjansson, E. Berge, and L. Makkonen. Using NWP models to simulate in-cloud atmospheric icing episodes. In *IWAIS XII*, 2007.

[53] Guy Fortin, Jean-Lous Laforte, and Adrian Ilinca. Heat and mass transfer during ice accretion on aircraft wings with an improved roughness model. *International Journal of Thermal Sciences*, 45:595–606, 2006.

[54] Lasse Makkonen. *Ice and Construction - Rilem Report 13*. Chapman & Hall, London, England, 1994.

[55] ISO 12494. *Atmospheric icing of structures*. ISO copyright office, Geneva, Switzerland, 2001.

[56] L. Makkonen. Models for the growth of rime, glaze, icicles and wet snow on structures. *Philisophical Transactions of The Royal Society A*, 358:2913–2939, 2000.

[57] IEC 61400-12-1. *Wind turbines - Part 12-1: Power performance measurements of electricity producing wind turbines*. International Electrotechnical Commision, 2005.

[58] B. Smith, H. Link, G. Randall, and T. McCoy. Applicability of nacelle anemometer measurements for use in turbine power performance tests. In *To be presented at AWEA Windpower 2002 Conference*. Preprint NREL from http://www.nrel.gov/docs/fy02osti/32494.pdf, 2002.

[59] A. Llombart, J.M. Fandos, D. Llombart, A. Talyero, and S.J. Watson. Power curve characterization: Stochastic methods. In *Proceedings of the EWEC 2006*, 2006.

[60] M. Marjaniemi, H. Holttinen, J. Keinänen, E. Holttinen, L. Makkonen, E. Peltola, T. Mäki, and K.Ö. Petersen. Wind turbines in light icing conditions - Experiences of the Pori 8 MW wind farm. In *Proceedings of the BOREAS V conference*. Finnish Meteorological Institute, 2000.

[61] NRG Systems. NRG IceFree3 Facts. Information flier from NRG Systems, 2007.

[62] F.T. Lynch and A. Khodadoust. Effects of ice accretions on aircraft aerodynamics. *Progress in Aerospace Sciences*, 37:669–767, 2001.

[63] *M22M Camera Manual*. MOBOTIX AG, 2007. URL `www.mobotix.com/other/file/24718/mx_manual_en_200.pdf`.

[64] L. Makkonen. Structure-independent measurement of icing. In *Proceedings of the BOREAS conference*. Finnish Meteorological Institute, 1992.

[65] G. Ronsten. Influence of icing on the power performance of seven NM82-1.5 MW wind turbines in Aapua. Elforsk rapport 09:59, http://www.vindenergi.org/Vindforskrapporter/09_59_rapport.pdf, (Archived by WebCite at http://www.webcitation.org/5rxED8bfe), 2009.

[66] P-E. Persson. Mätningar av nedisning i en hög mast. Elforsk rapport 09:24, http://www.vindenergi.org/Vindforskrapporter/09_24_rapport_medbilagor.pdf, (Archived by WebCite at http://www.webcitation.org/5rxAt74cL), 2009. (In Swedish).

[67] R. W. Gent, N. P. Dart, and J. T. Cansdale. Aircraft icing. *Philisophical Transactions of The Royal Society of London A*, 358:2873–2911, 2000.

[68] L. Makkonen. Heat transfer and icing of a rough cylinder. *Cold Regions Science and Technology*, 10(2):105–116, 1985.

[69] J. Shin. Prediction of ice shapes and their effect on airfoil drag. *Journal of Aircraft*, 31(2):263–270, 1994.

[70] K. J. Finstad, E.P. Lozowski, and L. Makkonen. On the median volume diameter approximation for droplet collision efficiency. *Journal of the Atmospheric Sciences*, 45(24):4008–4012, 1988.

[71] P. Antikainen, S. Peuranen, T. Laakso, and E. Peltola. Modelling, verification and classification of ice loads in wind turbines. In *Proceedings of the BOREAS VI Conference*, 2003.

[72] T. Burton, D. Sharpe, N. Jenkins, and E. Bossanyi. *Wind Energy Handbook*. John Wiley & Sons, 2001.

[73] B. Tammelin, K. Säntti, H. Dobesch, M. Durstewich, H. Ganander, G. Kury, T. Laakso, E. Peltola, and G. Ronsten. Wind turbines in icing environment: Improvement of tools for siting, certification and operation - NEW ICETOOLS. Reports 2005:6, Finnish Meteorological Institute, Helsinki, 2005.

[74] P. S. Veers, T.D. Ashwill, H.J. Sutherland, D.L. Laird, D.W. Lobitz, D.A. Giffin, J.F. Mandell, W.D. Musial, K. Jackson, M. Zuteck, A. Miravete, S.W. Tsai, and J.L. Richmond. Trends in the design, manufacture and evaluation of wind turbine blades. *Wind Energy*, 6:245–259, 2003. doi: 10.1002/we.90.

[75] H. S. Kim and M. B. Bragg. Effects of leading-edge ice accretion geometry on airfoil performance. *AIAA Paper*, 99-0096:379–391, 1999.

[76] P. Antikainen and S. Peuranen. Ice loads, case study. In *Proceedings of the BOREAS V Conference*. Finnish Meteorological Institute, 2000.

[77] Newmerical, 2010. URL:http://www.newmerical.com/index.php/products/fensap-ice-cfd-software/. Accessed: 2010-06-04. (Archived by WebCiteő at http://www.webcitation.org/5qF5VkNJ5).

[78] K. Mortensen. CFD simulations of an airfoil with leading edge ice accretion. Master's thesis, Technical University of Denmark, DTU, 2008. URL: http://www.dtic.dtu.dk/upload/institutter/mek/fm/... eksamensprojekter/kaspermortensen2008.pdf. Accessed: 2010-08-18. (Archived by WebCite at http://www.webcitation.org/5s4cl8FaB).

[79] C. Bak, P. Fuglsang, and N. Sørensen. Airfoil characteristics for wind turbines. Risø R-1065(EN), Risø National Laboratory, 1999.

[80] E. Ferrer and X. Munduate. Wind turbine blade tip comparison using CFD. In *Journal of Physics*, volume Conference Series 75, 2007.

[81] X. Chi, B. Zhu, and H.E. Addy. CFD analysis of the aerodynamics of a business jet airfoil with leading edge ice accretion. In *42nd Aerospace Sciences Meeting and Exhibit*, Reno, Nevada, 2004.

[82] O. Kwon and L.N. Sankar. Numerical simulations of the flow about a swept wing with leading edge ice accretions. *Computers and Fluids*, 26(2):183–192, 1997.

[83] M. Mirzaei, M.A. Ardekani, and M. Doosttalab. Numerical and experimental study of flow field characteristics of an iced airfoil. *Aerospace science and technology*, 13(6):267–276, 2009. doi: 10.1016/j.ast.2009.05.002.

[84] Z. Zhu, X. Wang, J. Liu, and Z. Liu. Comparison of predicting drag methods using computational fluid dynamics in 2d/3d viscous flow. *Science in China series E: Technological Sciences*, 50(5):534–549, 2007. doi: 10.1007/s11431-007-0048-7.

[85] Ansys. Url:http://www.ansys.com/products/fluid-dynamics/fluent/. 2010.

[86] M. Virk and A. E. Holdo. Numerical study of wind loads on a low-rise pitched roof building with spirelet. *International Journal of Computational Fluid Dynamics*, 22(10):687–694, 2008.

[87] J.F. Manwell, J.G. McGowan, and A.L. Rogers. *Wind energy explained*. John Wiley & Sons, 2002.

[88] M. B. Bragg, A.P. Broeren, and L.A. Blumenthal. Ice-airfoil aerodynamics. *Progress in Aerospace Sciences*, 41(5):323–362, 2005. doi: 10.1016/j.paerosci.2005.07.001.

[89] H.J.T. Kooijman, C. Lindenburg, D. Winkelaar, and E.L. van der Hooft. Dowec 6 mw pre-design: Aero-elastic modelling of the dowec 6 mw pre-design in phatas. filename: 10046_009.pdf DOWEC-F1W2-HJK-01-046/9 public version, 2003. URL:http://www.ecn.nl/docs/dowec/10046_009.pdf. Accessed: 2011-01-04. (Archived by WebCite at http://www.webcitation.org/5vU1JUi35).

[90] Ira H. Abbott and A. E. von Doenhoff. *Theory of Wing Sections: Including a Summary of Airfoil Data*. Dover Publications, 1959.

[91] R. Van Rooij and W.A. Timmer. Roughness sensitivity considerations for thick rotor blade airfoils. *Journal of Solar Energy Engineering*, 125:468–478, 2003.

[92] J. Jonkman. https://wind.nrel.gov/forum/wind/viewtopic.php?f=2&t=363, 2010. URL:https://wind.nrel.gov/forum/wind/download/file.php?id=100. Accessed: 2010-06-08. (Archived by WebCite at http://www.webcitation.org/5qKovdSv6).

[93] K.E. Johnson. Adaptive torque control of variable speed wind turbines. Technical Report NREL/TP-500-36265, NREL, 2004. URL:http://www.nrel.gov/docs/fy04osti/36265.pdf. Accessed: 2010-06-11. (Archived by WebCite at http://www.webcitation.org/5qPZcviKt).

[94] S. Barber, Y. Wang, N. Chokani, and R.S. Abhari. The effect of ice shapes on wind turbine performance. In *IWAIS XIII*. URL:http://www.iwais2009.ch/fileadmin/user_upload/pictures/... Session_5_wind_energy.zip. Accessed: 2010-06-05. (Archived by WebCiteő at http://www.webcitation.org/5qFtIvN5U), 2009.

[95] T. Laakso and E. Peltola. Review on blade heating technology and future prospects. In *Proceedings of the BOREAS VII Conference*. Finnish Meteorological Institute, 2005.